UNIVERSITAS INDONESIA

CHARACTERIZATION AND DESIGN OF GALLIUM NITRIDE SEMICONDUCTORS FOR WAVEGUIDING APPLICATIONS

PENELITIAN IV

IRMA SARASWATI
1006803663

PROGRAM DOKTOR TEKNIK ELEKTRO

FAKULTAS TEKNIK UNIVERSITAS INDONESIA

DEPOK 2016

THESE DE DOCTORAT / UNIVERSITE DE LILLE 1

En Cotutelle Internationale avec

UNIVERSITAS INDONESIA, DEPOK INDONESIA

pour le grade de

DOCTEUR DE L'UNIVERSITE DE LILLE 1

Mention : Micro Nano Technologies, Acoustique et Télécommunications
Ecole Doctorale : Ecole Doctorale Régionale des Sciences Pour l'Ingénieur (SPI 072)

Présentée par

IRMA SARASWATI

DESIGN AND CHARACTERIZATION OF GALLIUM NITRIDE FOR WAVEGUIDING APPLICATIONS

Soutenance le 3 Décembre 2015 devant le jury compose de

Prof. Masbah RT SIREGAR	Indonesian Institute of Sciences, Jakarta
Prof Abderrahim RAMDANE	Laboratoire Photonique Nanotech, Marcoussis
Dr Jing-Hua TENG	Institute Materials Research Eng, Singapore
Prof Harry S. SUDIBYO	Universitas Indonesia, Depok
Prof Tuami LASRI	Université de Lille 1
Prof Djoko HARTANTO	Universitas Indonesia, Depok
Prof Nji Raden POESPAWATI	Universitas Indonesia, Depok
Prof Elhadj DOGHECHE	Université de Valenciennes
Dr Retno W. PURNAMANINGSIH	Universitas Indonesia, Depok
Prof Didier DECOSTER	Université de Lille 1

TABLE OF CONTENT

TITLE
TABLE OF CONTENT i
LIST OF FIGURE iii
LIST OF TABLE v
ABSTRACT vi
I. INTRODUCTION..... 1
1.1. Research background 1
1.2. Research Objective 3
1.3. Researc Scope 4
1.4. Research Methodology 4
1.5. Writing Methode..... 4

II. GROUP III-NITRIDE SEMICONDUCTORS 7
2.1. Fundamental of III-Nitride Material Properties..... 7
2.2. Breakthrough and Challenges III-V Nitrides 9
2.3. Suitable Substrates 9
2.4. Basic of Optical Waveguide 10
2.4.1. Equation of Plane Wave 11
2.4.2. Componen of The Electric and Magnetic Fields 13
2.4.3. Guided modes in The Structure 15

III. CHARACTERIZATION OF GALLIUM NITRIDE MICROSTRUCTURE 20
3.1. Experimental Growth Process for Gallium Nitride (GaN) 20
3.1.1. Gallium Nitride on Silicon 20
3.1.2. Gallium Nitride on Sapphire (Al_2O_3)..... 22
3.2. Characterization of GaN Microstructure..... 24
3.2.1. Scanning Electron Microscopy (SEM)..... 25
3.2.2. Transmission Electron Microscopy (TEM)..... 26
3.2.3. Atomic Force Microscopy (AFM) 28
3.2.4. X-ray Diffraction (XRD)..... 32

IV. OPTICAL AND ELECTRO-OPTICAL CHARACTERIZATION OF GALLIUM NITRIDE FILMS..... 36
4.1. Prism Coupling Technique..... 36
4.2. Observation of The Modes..... 39
4.3. Measurement of Refractive Index and Thickness at GaN/Silicon Samples 41
4.3.1. Refractive Index and Thickness at GaN/Si Samples (TE Mode) 42
4.3.2. Refractive Index and Thickness at GaN/Si Samples (TM Mode)..... 44
4.4. Refractive Index and Thickness at GaN/Sapphire Samples 46
4.4.1. Refractive Index and Thickness at GaN/Al_2O_3 Samples-1 46

4.4.2. Refractive Index and Thickness at GaN/$A1_2O_3$ Sample-2 50
4.4.3. Refractive Index and Thickness at GaN/$A1_2O_3$ Sample-3 51
4.4.4. Refractive Index and Thickness at GaN/$A1_2O_3$ Sample-4 and Sample-5 52
4.5. Optical Analysis of GaN Films Surface Roughness 53
4.5.1. Roughness analysis for TE0 Mode Applied to GaN/Sapphire Sample-1 54
4.5.2. Roughness Analysis for Fundamental Mode of GaN/$A1_2O_3$ Samples-2 and Samples-3 56
4.5.3. Roughness analysis for fundamental Mode of GaN/Si Samples..... 57
4.6. Analysis of Tempereture Dependence into GaN Films 58
4.6.1. Tempereture Dependence into GaN Films 58
4.6.2. Evoltion of the Refractive Index Versus Applied Temperatures 59
4.7. Optical Loss Measurement of GaN Films 61
4.7.1. Optical Loss Measurement into GaN/$A1_2O_3$ Films 61
4.7.2. Optical Loss Measurement into GaN/Si Films 63
4.8. Analysis Of Birefringence 64
4.8.1. Refractive Index Dispersion for GaN/Si Sample-1 and Sample-2. 64
4.8.2. Evolution of Refractive Index for TE and TM Modes at GaN/Si ... 66
4.8.3. Comparation TE Modes at GaN on Si and Sapphire 67
4.9. Electrooptical Characterization of Gallium Nitride Film 68
4.9.1. Process of Electrode Manufacturing at GaN Film 68
4.9.2. Static Characterization of Electrooptical Effect 70
4.9.3. Dynamic Characterization of Electrooptical Effect 71

V STRUCTURE DESIGN OF GALLIUM NITRIDE ON SILICON 79
5.2.1. Introduction of optiBPM 79
5.2.2. Structure for Gallium Nitride (GaN) samples 80
5.2.3. Simulation of optical channel waveguide structure 81

VI CONCLUSION 78
REFERENCES 80
APPENDIX
PUBLICATION

LIST OF FIGURE

Figure 2.1.	Zinc-blende (left) and wurtzite (right) crystallographic structures. Large elements represent the cations and small element, the anions..	7
Figure 2.2.	Bandgap energy vs. lattice constant a for III-nitrides at $300^{O}K$	8
Figure 2.3	Principle of light wave propagation in a planar waveguide under direction x, this illustrates the concept of total reflection at interfaces of the guiding layer ï the substrate and the superstrate.....	11
Figure 2.4	Representation of Index in the waveguide structure	15
Figure 2.5	Different confinements as a function of the sign for the propagation constant β	16
Figure 2.6	Evanescent optical wave occurring substrate modes	16
Figure 2.7	optical wave propagating in air and substrate	17
Figure 2.8	Optical wave in the structure	17
Figure 3.1	(a) Schematic depicting the sample structure (Al compound x>y). (b). Photo of sample GaN/Si	22
Figure 3.2	Structure of the GaN/sapphire samples at difference thickness and difference carrier concentration (a) GaN/Sapphire-1, (b) GaN/Sapphire-2, (c) GaN/Sapphire-3, (d) GaN/Sapphire-4, (e) GaN/Sapphire-5	23
Figure 3.3	Cross-section SEM observation (a) GaN/sapphire-1 and (b) GaN/sapphire-4	25
Figure 3.4	SEM of cross-sectiononal of GaN/Si (a) GaN/Si-1 and (b) optical microscopy	26
Figure 3.5	Preparation of samples by FEI Tecnai G2 20, (a) GaN/Sapphire-1 (scale 5µm), (b) GaN/Sapphire-1 (scale 1µm) and (c) GaN/Silicon-1 (scale 1µm)	27
Figure 3.6	TEM by FEI Tecnai G2 20, (a) GaN/sapphire and (b) GaN/silicon ...	28
Figure 3.7	SEM image of an (a) AFM cantilever and (b) AFM tip	29
Figure 3.8	AFM analysis of GaN/sapphire for threading dislocations density ...	30
Figure 3.9	AFM analysis of GaN/Si: scan size (a)[1 µm × 1 µm] and (b) [500 nm × 500 nm]	31
Figure 3.10	Type of dislocation at GaN/Si structure for difference scan size, (a) 2 µm × 2 µm and (b) 500 nm × 500 nm	31
Figure 3.11	The XRD spectrum of the GaN/Si(111) sample	32
Figure 3.12	The XRD rocking curve (x-scan) of a GaN epilayer	33
Figure 4.1	Prism coupling system setup	37
Figure 4.2	Principle component in Metricon 2010	38
Figure 4.3	Principle diagram of prism coupling in Metricon 2010	38
Figure 4.4	Evolution of the prism index with the wavelength for TE/TM modes	40
Figure 4.5	Evolution of the refractive index prism at 633nm with the incident angle (for TE/TM modes)	41
Figure 4.6	TE Mode spectrum of GaN/Si sample-1 at 450 nm and 1539 nm ...	42
Figure 4.7	TE Mode spectrum of GaN/Si sample-2 at 450 nm and 1539 nm ...	43

Figure 4.8a.	The TE mode spectrum of GaN/Si sample-1 and sample-2 comparation at five wavelength, (a) 450 nm, (b) 532 nm, (c) 633nm, (d) 975nm and (e) 1539 nm	44
Figure 4.8b.	Dispersion of the refractive index (TE Mode) for GaN/Si (111) samples	44
Figure 4.9a.	The TM mode spectrum of GaN/Si sample-1 and sample-2 comparation at five wavelength, (a) 450 nm, (b) 532 nm, (c) 633nm, (d) 975nm and (e) 1539 nm	45
Figure 4.9b.	Dispersion of the refractive index (TM Mode) for GaN/Si (111) samples	46
Figure 4.10	TE modes spectrum of GaN/ Al_2O_3 sample-1 at λ = 633 nm and 1550 nm	47
Figure 4.11	TM modes spectrum of GaN/ Al_2O_3 sample-1 at λ = 633 nm and 1550 nm	47
Figure 4.12	TE and TM modes spectrum of GaN/ Al_2O_3 sample-1 at four wavelength, (a) 532 nm, (b) 633nm, (c) 975nm and (d) 1539 nm	48
Figure 4.13	Dispersion of refractive index at GaN/Al_2O_3 sample-1.....	49
Figure 4.14	Thickness for GaN/Al_2O_3 sample-1 from different wavelengths.....	50
Figure 4.15	TE and TM modes spectrum of GaN/Al_2O_3 sample-2 (a) At 633 nm and (b) At 1539 nm	51
Figure 4.16	TE and TM modes spectrum of GaN/Al_2O_3 sample-3 (a) At 633 nm and (b) At 1539 nm	52
Figure 4.17	The TE and TM modes spectrum of GaN/Al_2O_3 at 633 nm (a) sample-4 and (b) sample-5	53
Figure 4.18	(a) Guided-mode spectrum obtained by measuring the reflected intensity versus the angle of indicidence (b) Relationship between the width of dips (***qpd***) and the surface roughness from AFM study ...	53
Figure 4.19	Angular width ***qpd*** of TE mode reported for Sample-1 at different wavelengths (a) 532nm and (b) 633nm	55
Figure 4.20	Angular width ***qpd*** of TE mode reported for Sample-1 at 1550nm.....	55
Figure 4.21	Angular width $\Delta\theta$ of TE0 mode for Sample-2 at (a) 633nm and (b) 1530nm.	56
Figure 4.22	Angular width $\Delta\theta$ of TE0 mode for GaN/Si Sample-1 at λ= 1550nm	57
Figure 4.23	Angular width $\Delta\theta$ of TE0 mode for GaN/Si Sample-2 at λ= 1550nm	57
Figure 4.24	Principle of temperature measurement and experimental set up	58
Figure 4.25	Influence of the refractive index versus temperature (GaN/Al_2O_3 Sample)	60
Figure 4.26	Influence of the refractive index versus temperature (GaN/Si Sample)	60
Figure 4.27	(a) Set up for optical loss characterization and (b) light scattered from the top surface of GaN planar waveguide	61
Figure 4.28	Optical loss in GaN/Sapphire at 633nm (as example for TE mode) ..	62
Figure 4.29	TE Optical loss in GaN/Al_2O_3 at (a) 633nm and (b) 1550nm	62

Figure 4.30	Literature review of waveguide loss for GaN/Sapphire (TE mode) ...	63
Figure 4.31	Optical loss of GaN/Si Sample-1 (TE Mode) at λ = 633nm	64
Figure 4.32	Dispersion of refractive index (TE mode) at GaN/Si samples 1 and 2	65
Figure 4.33	Dispersion of refractive index (TM mode) at GaN/Si samples 1 and 2	65
Figure 4.34	Dispersion of refractive index (TE/TM modes) ï GaN/Si sample 1 .	66
Figure 4.35	Dispersion of refractive index (TE/TM modes) at GaN/Si sample 2	66
Figure 4.36	Dispersion of Refractive index for GaN/Si and GaN/Sapphire	67
Figure 4.37	Top electrode configuration: Argon etching & evaporation-Au 40nm on GaN/Si Thin Film	68
Figure 4.38	Realisation of ohmic contact by RF sputtering	69
Figure 4.39	An Ohmic Contact of GaN/Si	70
Figure 4.40	(a) Application of voltage into GaN film and direction of electric field, (b) photo of sample position in the prism coupling	70
Figure 4.41	The influence of voltage on GaN/Si refractive index	71
Figure 4.42	Fabry-Perot interferometric configuration. The film is sandwich between two Au electrodes	72
Figure 4.43	The simple θ-2θ goniometric setup schematically	72
Figure 4.44	Reflectivities calculated from a measured values at different angles of incidence.....	73
Figure 4.45	Electric-field-induced variation in the reflectivity for TE and TM polarizations.....	74
Figure 5.1	The structure samples, (a). Gallium Nitride on Silicon (GaN/Si), (b). Gallium Nitride on Sapphire (GaN/Al_2O_3).....	80
Figure 5.2	The cross section view of the single mode GaN/Si structure at the input	81
Figure 5.3	Layout of the GaN/Si channel waveguide simulated	82
Figure 5.4	The output field emitted from the simulated channel waveguide when the maximum refractive index is 2.07	82
Figure 5.5	Propagation optical field along the waveguide in the transverse dimension when the maximum refractive index is 2.07.....	82
Figure 5.6	Curves of the optical power vs. the propagation at maximum refractive index	83

LIST OF TABLE

Table 2.1	Parameters for Wurtzite III-nitrides	8
Table 2.2	Properties of GaN, InN and potential substrates	10
Table 3.1	Layer engineering for GaN/silicon samples	22
Table 3.2	List of the studies GaN/sapphire samples at difference thickness and difference carrier concentration	24
Table 4.1	Values of refractive indices for TiO2 rutyl prism	40
Table 4.2	Refractive Index at different wavelength in GaN/Si sample-1	41
Table 4.3	Thickness at different wavelength in GaN/Si sample-1	41
Table 4.4	Refractive Index at different wavelength in GaN/Si sample-2	42
Table 4.5	Thickness at different wavelength in GaN/Si sample-2	43
Table 4.6	Refractive Index at different wavelength in GaN/Al_2O_3 sample-1	49
Table 4.7	Thickness at different wavelength for GaN/Al_2O_3 sample-1	50
Table 4.8	The refractive index of GaN/Al_2O_3 sample-2 at two wavelenghts	51
Table 4.9	The refractive index of GaN/Al_2O_3 sample-3 at two wavelenghts	51
Table 4.10	The refractive index of GaN/Al_2O_3 sample-4 and sample-5	52
Table 4.11	The thickness index of GaN/Al_2O_3 sample-4 and sample-5	52
Table 4.12	Refractive Index at wavelengths 633nm in 5 samples of GaN/Al_2O_3	53
Table 4.13	Synthesis of Measurement at different wavelengths for GaN/sapphire Sample-1	55
Table 4.14	Summary of results for films analyzed at 633nm	56
Table 4.15	Roughness of the GaN/Al_2O_3 films measured by optical tool at 1550nm	57
Table 4.16	Roughness of the GaN/Si film at 1550nm	58
Table 4.17	Refractive index and thickness of GaN/Si at increase temperature	59
Table 4.18	Refractive index and thickness of GaN/Al_2O_3 at increase temperature	59
Table 4.19	Comparison of Index and Optical Loss at 2 wavelengths (GaN/Al_2O_3 sample-3/TE mode)	63
Table 4.20	Comparison of Index and Optical Loss at 2 wavelengths (GaN/Al_2O_3 sample-3/TM mode)	63
Table 4.21	Birefringence Δn calculated for GaN/Si samples 1	67
Table 4.22	Birefringence Δn calculated for GaN/Si sample 2	67

ABSTRACT

A good justification for gallium nitride on silicon is the potential for optoelectronic integrated circuits, and the low cost brings the growth of GaN on a large size wafers. The application interest for GaN/Si is power electronics. This work focused on characterization (optical, electro-optical, and microstructural) and design of GaN/Si channel waveguide. To microstructure characterization of GaN thin film by SEM, TEM, AFM, and XRD. Using the guided wave prism coupling technique, we have fully established the index dispersion and thickness of GaN at room temperature and roughness based on AFM characterization.

Also, the thermal dependence of GaN at ordinary and extraordinary refractive index are determined to be 9.47×10^{-5}/°K and 8.99×10^{-5}/°K, respectively. The thermal dependence of GaN has value better than GaAs in the wavelength range 0.4 µm to 1.5 µm. It has a slightly low-temperature dependence. Results demonstrated excellent waveguide properties of GaN on silicon with an optical propagation loss of GaN/Si at 633 nm is 2.58 dB/cm, this is higher than propagation loss of GaN/sapphire around 1.34 dB/cm. GaN/Sapphire and GaN/Si samples have roughness in the range 1.6 to 5.2 nm and 9.6 to 13 nm respectively. The birefringence of GaN/Si is negative within range - 0.16 $x10^{-2}$ to ï 6.06$x10^{-2}$. The negative value means the polarization of the wave is parallel to the optical axis. Electrooptic constants r_{13} = +1.01 pm/V and r_{33} = +1.67 pm/V are higher than those obtained for III-V GaAs semiconductors.

The input and output of GaN/Si waveguide design are the difference thickness and width. The structure design of GaN/Si has optical power less 50%. We compared the results on Si with those on sapphire. The GaN/Si has opened a real opportunity for a future device using this technology.

Keywords: gallium nitride, silicon, microstructure, refractive index, temperature dependence

CHAPTER 1
INTRODUCTION

1.1. Research Background

The Gallium nitride (GaN) is compound semiconductor at III-V nitrides group that has a wide direct band gap as well crystallizes in a hexagonal wurtzite structure [1]. According to the literature, for many years, the compound GaN, AlN (Aluminium Nitride), and InN (Indium Nitride) is a continuous alloy system. There was direct band gaps of 1.9 eV, 3.42 eV, and 6.2 eV for InN, GaN, and AlN, respectively. A revisit of the InN band gap indicates it to be about 1eV [2] and the same for AlN is about 6 eV in which case the energy range covered would be about 0.7 eV to 6 eV. Thus, the IIIï V nitrides could potentially be used for optical devices application, which active at the wavelengths ranging from the red to the ultraviolet [3]. The band gaps of nitrides, substrates commonly used for nitrides, and other conventional semiconductors are described in litterature by many authors with respect to their lattice constants.

During the past decade, research pertaining to the growth and preparation of metal nitride thin films has culminated in the development of crystalline samples with deposition techniques such as Metal Organic Chemical Vapor Deposition (MOCVD) [4], Molecular Beam Epitaxy (MBE)[5], hybride vapor phase epitaxy (HVPE) [6] and RF Magnetron Sputtering [7].

Much recent work has concentrated on the optical properties of GaN compound in the near-gap region, and on stimulated emission and luminescence. The renewed experimental activity regarding the characterization of this semiconductor nitride material is in part due to the direct band gap of 3.4 eV in undoped GaN, which can be tailored for the production of tunable electro-optical devices in the UV and visible wavelength range of the spectrum when this material is alloyed with either AlN or InN [8]. However, the development of photonic devices such as UV LED's and laser diodes have been hampered by the

inability to produce GaN samples that possess the electronic properties (mobility, etc.) required for commercial applications [9, 10].

AlN/GaN materials are considered as the preferred materials for high performance applications; high density data storage, high power operation, high frequency and high temperature application and high break down voltage. By tuning the composition, the bandgap energy of the AlN/GaN materials can cover the range from deep UV to infrared. It is a good platform material for producing various optoelectronics devices like solid state lighting and the integration of them. For exploring the potential of AlN/GaN materials for photonics applications, the optical properties need to be investigated. For example, the refractive index of thin films and quantum well structures are critical in designing and modelling waveguide based devices, especially in the nanoscale devices. The strong piezoelectric field and the wurtzite crystal structure make the refractive index of AlN/GaN film change with not only the material composition but also the film thickness [11-14].

In this dissertation, the optical properties of the GaN thin films grown on silicon substrates will be investigated at different electrical and thermal conditions. The result will be compared with GaN thin film grown on sapphire (Al_2O_3) because the GaN/Al_2O_3 materials used in the mass production. However, the GaN/Al_2O_3 materials are limited in sized and still more expensive than GaN/Si. The objective of this research is to establish and explore potentialities of this GaN/Si material and also the possibility of this material to answer simultaneously to the whole set of criteria in nanophotonics such as modulation and switching applications.

Both of GaN/Si and GaN/Al_2O_3 samples are provided by Darmstadt Technical University (DTU) in Darmstadt (Germany) and Korea Advanced Institute of Science and Technology (KAIST) in Daejeon (South Korea) using respectively MOCVD and MOVPE for epitaxial growth materials with different AlN/GaN thin films and structures. The structure and optical characterizations of

the AlN/GaN film are investigated at Institute of Electronic, Microelectronic and Nanotechnology (IEMN). While the technology to process nanoscale AlN/GaN structure based on different substrates and novel waveguide devices will be developed and demonstrated by Darmstadt Technical University (DTU), and Korea Advanced Institute of Science and Technology (KAIST). The knowledge and technology developed will be useful for GaN/Si optoelectronic devices development, such as high brightness LEDs, GaN lasers sources and optical switches ï modulators.

The first work undertaken was researching some GaN thin films to determine the GaN/Si and GaN/Al_2O_3 to be studied by characterizing some GaN thin films with team in the optoelectronics group at IEMN. The first result has relation between refractive index and difference doping concentration at some wavelength (450 nm, 532 nm, 633 nm, 975 nm, and 1532 nm). The conclution of the first result was increasing refractive index to decreasing wavelength for difference doping concentration. Based on the first work, the next work is propose to get new GaN/Si this films from KAIST with difference doping concentration and thickness layer. In this work will establish a strong and deep knowledge of GaN/Si, a new semiconductor material, particularly for the growth conditions, and the expected properties. The international scientific community will be sensitive to the suitability of this new material to be applied to the domain of the nanotechnologies. As far as we know, the AlN/GaN material has not yet utilize in a design device; only GaN/Si structure on surface plasmon resonance (SPR) operating at the telecom wavelength [15]. The originality of the work holds the major innovation in terms of materials growth and nano-photonic device process. This work is ambitious as far as on, one hand, it concerns a fundamental scientific domain. Other hand is concern a device applications. It aims at the development and at the implementation of an innovative technology allowing its industrial application such as modulator, Mach-Zender Interferometer, optical switch, etc.

1.2. Research Objective

This dissertation involves characterization, design and optimization of wide band gap semiconductor for optical devices applications.

The objective of this dissertation is to characterize the GaN thin film which very important issues related to GaN-based optoelectronic waveguide devices. In addition, it is also to design and to optimize the GaN/Si Fabry Perot heterostructure to be applied on the optoelectronic devices. Therefore, the microstructure and optical characterization is needed to know to find out the best properties of GaN/Si. Then, the results of characterization will be compared with GaN on sapphire properties.

1.3. Research Scope

Conventional GaN-based epitaxial layers were grown either on sapphire, SiC, GaAs, $LiGaO_2$, and AlN substrates. However, sapphire substrates are insulators with poor thermal conductivity while SiC substrates are much more expensive. Thus, growth of GaN on Si substrate has attracted considerable attention [1]. GaN has a many difference substrate so that in this section, the research scope of dissertation is below:

1. The material structure used in this research are GaN thin film grown on Silicon and GaN on Sapphire.
2. The optical properties of GaN thin film have been analyzed utilize prism coupling technique.
3. The GaN characterization of microstructural properties are carried out using Transmission Electron Microscopy (TEM), Scanning Electron Microscopy (SEM), Atomic Force Microscopy (AFM) and X-Ray diffraction (XRD).
4. The optimization and design of Fabry Perot heterostructure are investigated using Beam Proposagtion Method (BPM) through optiwave/OptiBPM software.

1.4. Research Methodology

The research methodology of dissertation are below:

1. Basic knowledge at physical properties of new III-nitrides semiconductor materials.
2. Characterization of GaN microstuctures using TEM, SEM, AFM and XRD.
3. Electro-optical characterization and investigation of optical properties GaN/Si thin films: refractive index, optical loss, roughness, birefringence, thickness layer and temperature dependence using prism coupling technique.
4. Design of GaN/Si structure devices using Beam Propagation Method simulation.

1.5. Writing Method

This dissertation is composed of 6 chapters, each treating a separate aspect of the issues weôve exposed so far. The dissertation is organized as follows:

Chapter 1 reviews a brief introduction about the basic knowledge of III-nitrides semiconductor materials to understand the state of the art in the global research community up to date.

Chapter 2 discusses some of basic theory of semiconductor period IIIï nitrides, optical waveguide theory and beam propagation mode. In the next chapter is Chapter 3 discusses about the detail of GaN thin films structure and microstructure characterization utilizing Scanning Electron Microscopy (SEM), Transmission Electron Microscopy (TEM), Atomic force microscopy (AFM) and X-ray Diffraction (XRD).

Chapter 4 investigates the optical characterization using prism coupling technique, measurement and analysis of the results for both sample of GaN on Sapphire and Silicon substrates.

Chapter 5 explains about optimalisation thickness layer of GaN/Si structure to design of waveguide structure devices by optiwave/optiBPM software. Finally in Chapter 6, we conclude this manuscript by the synthesis of the main results and the perspectives in terms of devices design using the beam propagation method.

CHAPTER 2
GROUP III-NITRIDES SEMICONDUCTORS

Since more than a decade, III-nitrides-based semiconductors are considered as the leading materials in photonics for the production of blue laser diodes and light emitting diodes LEDs as well as for high-power microelectronics. Since the demonstration of optical pumped stimulated emission in GaN crystals [16] and the first LEDs [17], almost 20 years have been necessary for the investigation of blue laser diodes. New markets have emerged with the demonstration of high brightness blue LEDs based on InGaN/GaN materials, leading to a revolution in LED technology. In this context, the improvement in the growth process and the resulting material quality is one of the major reason that explains the progress realized in this technology, as for example with the use of InGaN/GaN double heterostructures in LEDs in 1997 [18] and the achievement of *p*-doping in GaN demonstrated by *Akasaki et al* [19].

2.1. Fundamental Properties for III-Nitrides Materials

The III-nitrides crystallize into two crystallographic structures: the cubic zinc-blende and the hexagonal wurtzite structures, but the more commonly studied is the wurtzite structure with the thermodynamically stable form under ambient conditions. Nitrogen atoms form hexagonal close packed structure and the group III atoms occupy half of the tetrahedral available sites as shown in Figure 2.1 [20].

The III-V nitride system includes three binary compounds consisting of aluminum nitride (AlN), gallium nitride (GaN), and indium nitride (InN); three ternary compounds of $Al_xGa_{1-x}N$, $In_xGa_{1-x}N$, and $In_xAl_{1-x}N$; and the quaternary compounds $Al_xIn_yGa_{1-x-y}N$. This system is particularly suitable for optoelectronics due to its direct bandgap, the band gap continuously range from 6.2 eV for AlN to 1 eV for InN, which covers the entire visible, near ultraviolet and near infrared portions of the electromagnetic wave spectrum as illustrated in Figure 2.2 [21].

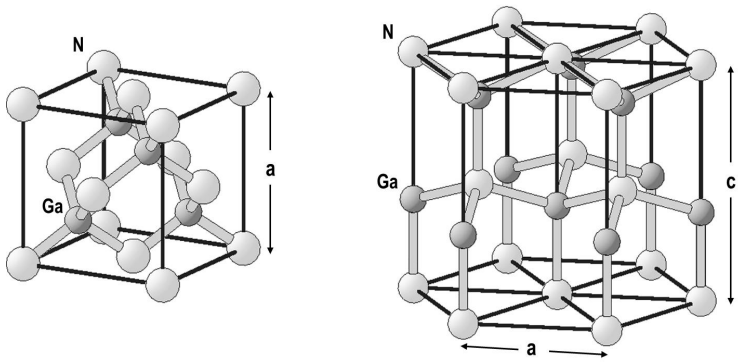

Figure 2.1. Zinc-blende (left) and wurtzite (right) crystallographic structures. Large elements represent the cations and small element, the anions [20]

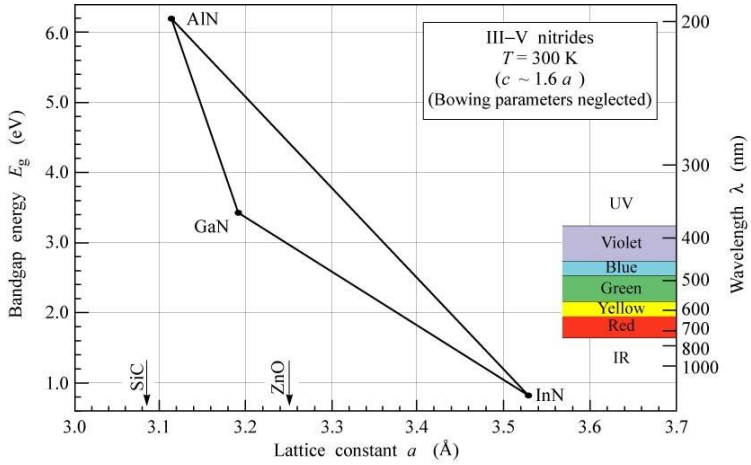

Figure 2.1. Bandgap energy vs. lattice constant a for III-nitrides at 300 ºK [21]

Table 1.1 presents some basic parameters for Wurtzite III-nitride binary compounds at 300 ºK [22-25].

Table 2.1. Parameters for Wurtzite III-nitrides [22-25]

Parameters	**AlN**	**GaN**	**InN**
Lattice constant			
a (Å)	3.112	3.189	3.548
c (Å)	4.982	5.185	5.760
Poisson's ratio ν	0.202	0.205	0.272
Bandgap energy E_g (eV)	6.2	3.4	0.7
Electron mobility μ_e (cm^2/V.s)	300	1100	3200
Dielectric constant ε_r	9.1	8.9	15.3
Electron saturation velocity V_{sat} ($\times 10^7$ cm/s)	1.8	2.7	4.4
Effective electron mass m_e x m_0	0.3	0.22	0.14

2.2. Breakthrough and Challenges of III-V Nitrides

The emergence of photonic devices using III-nitrides materials was limited by many technical challenges related to growth process. During all these years, it was necessary to study the question related to the suitable substrates, to investigate different growth techniques or to achieve doping, especially p-type. Firstly, GaN was synthesized in 1910 [26] and crystals were grown in 1932 by reacting metallic gallium with ammonia gas at 900-1000 °C [27], but the material was polycrystalline and could not be used for semiconductors devices. Later, with the development of sophisticated epitaxial growth techniques, GaN single crystals on sapphire substrate were achieved: by hydride vapor phase epitaxy (HVPE) [28], by metalorganic chemical vapor deposition (MOCVD) [29] and by molecular beam epitaxy (MBE) [30].

2.3. Suitable Substrates

GaN crystals have a high melting temperature, over 2500 °C, which avoid the application of traditional techniques as Czochralski or Bridgeman. The fabrication of homoepitaxy was therefore under investigation during long time. Intensive search of suitable substrates [25, 31] was under investigation in order to obtain the heteroepitaxy of GaN. Existence single crystal substrates as sapphire,

MgO, $SrTiO_3$, etc has different physical properties compared to those of III-nitrides, especially lattice constants and thermal dilatation coefficients. These differences increase the stress of the grown layers and the misfit and threading dislocation densities, causing higher leakage currents and poorer thermal dissipation. Table 2.2 gives the properties of the well known substrates for GaN growth [32].

Sapphire (Al_2O_3) is a good compromise and remains the most popular alternative: it is available in large high-quality wafers, has a hexagonal structure; the lattice mismatch, although not good (16%), is better than silicon and it presents good chemical and thermal stability. Its transparent nature and electrical insulator properties is also an advantage. Silicon substrate is one of the master substrate for microelectronics and it represents one of the major opportunities for the development of III-nitride based optoelectronics, with low cost solution, integrable with different functions. But it has a different crystal structure (diamond cubic). One of the major difficulty lies on the large lattice mismatch with GaN (17%). Silicon carbide (SiC) presents a much closer lattice matching (-3.4%) and already possesses a wurtzite structure, but it is particularly costly, mainly dedicated to high-power applications.

Table 2.2. Properties of GaN, InN and potential substrates [32]

Parameters	**GaN**	**AlN**	**Si (111)**	**6H-SiC (0001)**	**Al_2O_3 (0001)**
Crystal structure	wurtzite	wurtzite	diamond	wurtzite	wurtzite
Lattice constant a (Å)	3.189	3,112	5.431	3.081	4.785
Lattice constant c (Å)	5.185	4.982	-	15.117	12.991
Lattice mismatch with GaN	0%	-2%	+17%	-3.4%	-16%
Thermal dilatation coeff. $\breve{U}_c$ ($\times 10^{-6}$ K^{-1})	3.17	5.27	2.6	4.7	4.3
Approximate price of a 2inches-wafer ($)	3000	1800	30	1000	100

The bandgap energy for GaN is 3.4 eV [18]. Early studies reported values of 1.8 to 2 eV for InN [19] but improvements in epitaxial growth techniques eventually lead to a bandgap around 0.76 eV [20,21]. The bandgap energy of the ternary alloy $In_xGa_{1-x}N$ is calculated as [22,23]:

$$Eg.x = x.Eg.InN + 1 - x.EgGaN - b(x).x.(1-x) \quad (2.1)$$

where the bowing parameter b(x) accounts for the deviation from a linear interpolation between GaN and InN:

$$b.x = (1-x).(11.4 - 11.4.x) \quad (2.2)$$

Equation 2.2 was determined experimentally and provides values for the bowing parameter such as b(0.25) = 4.9, b(0.5) = 0.9 and b(0.75) = -0.8.

One of the main problems consists in growing the high quality materials on the selected substrate. The direct growth of GaN on sapphire results on poor nucleation, causing high dislocation densities. Amano et al have demonstrated that a low-temperature nucleation layer (or ñbuffer layerò) of AlN dramatically improve the quality of GaN-on-sapphire, if grown prior to the actual epilayer [33]. *Nakamura et al* reported that a low temperature GaN nucleation layer improved the epilayer quality [34]. The buffer layer grown at low temperature (450-550 °C) provides high nucleation center density and promotes the lateral growth of the main GaN layer. Same studies are also reported for other substrates (Si for example) with lower efficiencies.

2.4. Basics on Optical Waveguide

This section is dedicated to the fundamentals about the optical waveguiding techniques. In theory, an optical waveguide consists of the core layer with higher refractive index (dimension comparable to wavelength λ) and surrounding cladding layers with lower refractive index. When certain discrete electromagnetic

resonances are confined in the core layer, they correspond to waveguide modes. Each mode has its own propagation constant β (also named effective index Nm), which is the kz vector in the propagation direction. A single mode waveguide can only support one mode known as the fundamental mode. The optogeometric parameters of the waveguide structure, the refractive index and the laser wavelength correspond to key values for determination of the single mode waveguide. The waveguide propagation constants β and profiles of the electric field in the core layer are essential for the design and successful operation of optical devices [35].

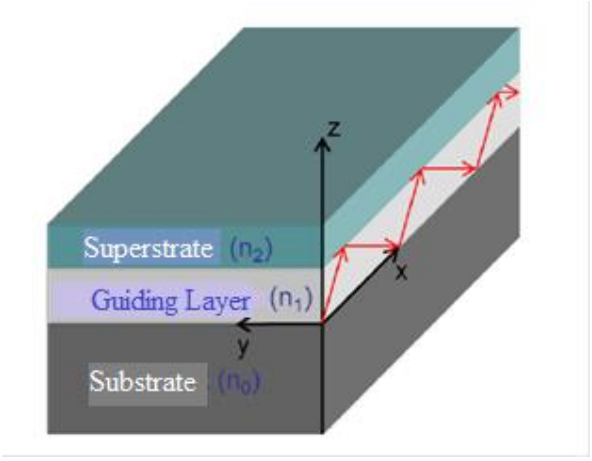

Figure 2.3. Principle of light wave propagation in a planar waveguide under direction x, this illustrates the concept of total reflection at interfaces of the guiding layer ï the substrate and the superstrate [35]

The physics for the light wave propagation is based on the resolution of Maxwellôs equations at the interface of n layers strcuture (Figure 2.3) with differences electromagnetic properties. Before studying the different cases, we recall the notions related to waves equation and the expression of electricï magnetic fields in a medium [35].

2.4.1. Equation of Plane Wave

The electromagnetic configuration of the medium is described by the following Maxwellôs Equations (Equation 2.3) [36]:

$$\begin{aligned}
\vec{\nabla} \wedge \vec{E} &= -\frac{\partial \vec{B}}{\partial t}, \\
\vec{\nabla} \wedge \vec{H} &= \vec{J} + \frac{\partial \vec{D}}{\partial t}, \\
\vec{\nabla} \cdot \vec{D} &= \rho, \\
\vec{\nabla} \cdot \vec{B} &= 0,
\end{aligned} \tag{2.3}$$

Where:

$$E = E_0 \exp(j\omega t + \varphi) \text{ and } H = H_0 \exp(j\omega t + \varphi) \tag{2.4}$$

with

E= the electric field

H= the magnetic field

$B = \mu_0\mu_r$, B: induced magnetic field with μ_r,

μ_0: the relative magnetic permittivity in vacuum.

$D = \varepsilon_0\varepsilon_r$, D: electric displacement with ε_r,

ε_0: the relative dielectric permittivity in vacuum

J= current density

ρ: the electric charge density

In our study, we have considered that our medium is non magnetic ($B=\mu_0 H$) without external charges ($\rho = 0$), linear with an electromagnetic wave propagating (pulsation exp jωt). The medium is homogeneous and isotrope (ε). The Maxwellôs equations (Equation 2.5) are:

$$\begin{aligned}
\vec{\nabla} \wedge \vec{E} &= j\omega\mu_0\vec{H}, \\
\vec{\nabla} \wedge \vec{H} &= j\omega\varepsilon_r\varepsilon_0\vec{E}, \\
\vec{\nabla} \cdot \vec{E} &= \vec{\nabla}\vec{B} = 0,
\end{aligned} \tag{2.5}$$

We decompose the relative permittivity (ε_r) in real and imaginary parts $\varepsilon_r = \varepsilon$ôï j ε_rò. We can therefore write the equation (Equation 2.6):

$$\vec{\nabla} \wedge \vec{\nabla} \wedge \vec{E} = -j\omega\mu_0(\vec{\nabla} \wedge \vec{H}) = -j\omega\mu_0(j\omega\varepsilon_r\varepsilon_0\vec{E}) \\ = \omega^2\mu_0\varepsilon r\varepsilon 0\vec{E} = -\frac{\omega^2}{c^2}\varepsilon_r\vec{E}, \quad (2.6)$$

The left term could be details in Equation 2.7.

$$\vec{\nabla} \wedge \vec{\nabla} \wedge \vec{E} = \vec{\nabla} \wedge (\vec{\nabla} \cdot \vec{E}) - \nabla^2\vec{E}, \quad (2.7)$$

We assume also for a medium considered without charges that

$$\vec{\nabla} \wedge (\vec{\nabla} \cdot \vec{E}) = \vec{0} \quad (2.8)$$

We define the wave vector k_0 in relation with the wavelength λ_0 of the electromagnetic wave propagating in the dielectric medium by:

$$k_0 = \sqrt{\omega^2\mu_0\varepsilon_0} = \frac{2\pi}{\lambda_0} \quad (2.9)$$

Therefore, we obtain the Helmoltz Equation:

$$\vec{\nabla}^2\vec{E} + k_0^2\varepsilon_r\vec{E} = \vec{0}, \quad (2.10)$$

We assumed to solve this equation for each media (air/dielectric layer/substrate), taking into account the conditions at the limit (mainly at the interfaces). One can rely the complex dielectric permittivity to the optical constants of the medium by $\varepsilon_r = (n$ ï $j\ k)^2$, this gives us the real part [$\varepsilon_r = \varepsilon_r\hat{o} = n_2$ ï k_2] and the imaginary part [$\varepsilon_r\grave{o} = -2nk$].

The study of the light propagation in a waveguide consists in solving Equation 2.10, this is the subject of the next section. Generally, the absorption coefficient α is connected to the extinction coefficient k by the relation:

$$\alpha = 2\ \omega\ k\ /\ c \quad (2.11)$$

2.4.2 Component of the Electric and Magnetic Fields

We consider the Cartesian geometric repere and the problem as one-dimensional one. The propagation direction of the wave is under x axis. Any

variation is possible under y axis. The dielectric function only depends on one variable of the space, here $\varepsilon_r = \varepsilon_r(z)$ defined in the repere (O,x,y,z) as illustrated in Figure 2.3. The interface that interests us, matches with the plan corresponding to z = 0 [35]. The expression can be written as:

$$\vec{E}(x,y,z) = \vec{E}(z)e^{i\beta x} \tag{2.12}$$

With $\beta = k_x$, propagation constant of the wave at the interface. This constant corresponds to the component on the wave vector in the direction x. This leads to this novel equation:

$$\frac{\partial^2 \vec{E}(z)}{\partial z^2} + (k_0^2 \varepsilon_r(z) - \beta^2)\vec{E}(z) = \vec{0} \tag{2.13}$$

By analogy, we can consider a similar equation for the magnetic field H. In order to simplify the system, we must select one polarization for the field. Two types of polarization exist:

a. Transverse electric polarization (TE or s) where only components Hx, Hz and Ey ≠ 0
b. Transverse magnetic polarization (TM or p) where only components Ex, Ez and Hy ≠ 0

We obtain in this case of TE polarization, the system of equation as given below:

$$H_x = -i\frac{1}{\omega\mu_0}\frac{\partial E_y}{\partial z}, \quad H_z = -\frac{\beta}{\omega\mu_0}E_y, \tag{2.14}$$

This conducts to equation of the wave for TE polarization:

$$\frac{\partial^2 E_y(z)}{\partial z^2} + (k_0^2 \varepsilon_r(z) - \beta^2)E_y(z) = 0 \tag{2.15}$$

By analogy, we can find a system of equations similar for TM polarization:

$$E_x = i\frac{1}{\omega\varepsilon_0\varepsilon_r(z)}\frac{\partial H_y}{\partial z} \quad E_z = \frac{\beta}{\omega\varepsilon_0\varepsilon_r(z)}H_y \tag{2.16}$$

Leading to the equation:

$$\frac{\partial^2 H_y(z)}{\partial z^2} + (k_0^2 \varepsilon_r(z) - \beta^2) H_y(z) = 0 \qquad (2.17)$$

In this part, we have presented the basic equations that permit to solve the Maxwellôs equations for TE polarization (Equation 2.15) or TM polarization (Equation 2.17). We are now applying these equations to the specific case of the planar dielectric waveguide.

2.4.3 Guided Modes in the Structure

The notion of guided modes does not take into account how the light penetrates in the waveguide. We suppose therefore that the light is already present and we will study the conditions for the propagation. We will consider waveguides with refractive indices as given in Figure 2.4.

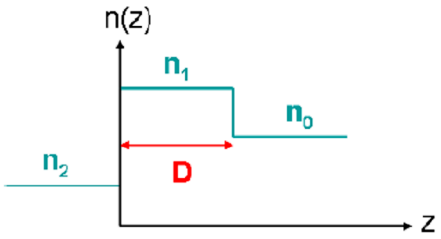

Figure 2.4. Representation of index in the waveguide structure [36]

$$n(z) = \begin{cases} n_2 & \text{for } z < 0, \\ n_1 & \text{for } 0 << z << D, \\ n_0 & \text{for } z > D \end{cases} \qquad (2.18)$$

where n_1 and n_0 are the index of the air and the substrate and n_2, the index of the guide.

The origin of axis is taken at the interface air-guide. In the following part, we will take the case of TE polarization only. The solutions of Equation 2.17 are sinusoidal or exponential as a function of z as a function of the sign for the factor ($k_0^2 n^2 - \beta^2$), as presented in Figure 2.5 [36]. Two forms of solutions are possible as

a function of the sign for this factor. We obtain the following equations of the electric field Ey:

a. For $k_0^2n^2-\beta^2 > 0$

$$E_y = \left[Ae^{ik_o pz} + Be^{-ik_o pz}\right] e^{i\omega t - i\beta z}, \text{avec } p = \sqrt{n^2 - \left(\frac{\beta}{k_o}\right)^2} \quad (2.19)$$

b. For $k_0^2n^2-\beta^2 > 0$

$$E_y = \left[Ce^{k_o qz} + Be^{-k_o qz}\right] e^{i\omega t - i\beta z}, \text{avec } q = \sqrt{\left(\frac{\beta}{k_o}\right)^2 - n^2} \quad (2.20)$$

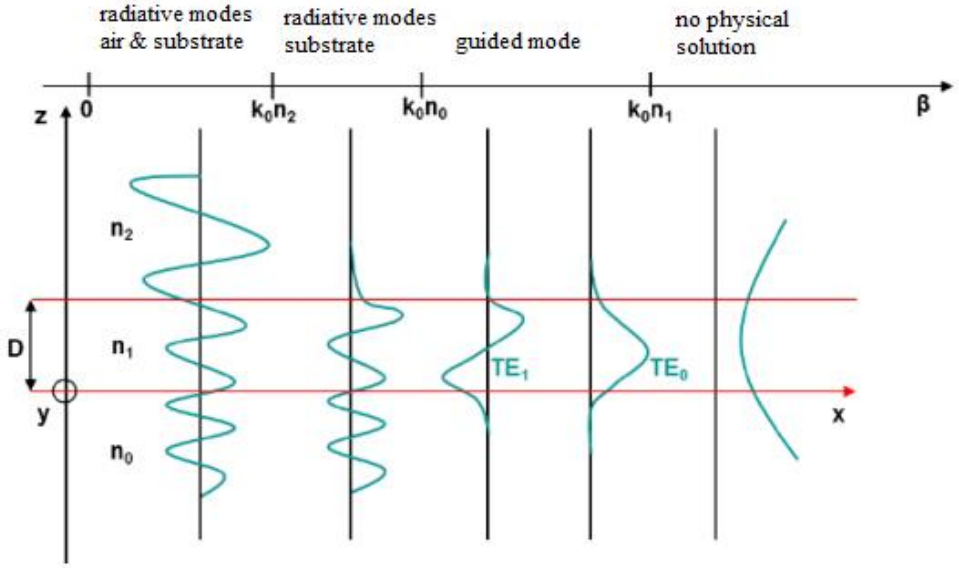

Figure 2.5. Different confinements as a function of the sign for the propagation constant β [36]

As a function of the sign for the propagation constant β, three types of solutions exist as we remind that $n_2 < n_0 < n_1$. Letôs consider the three types of modes that can occur during the light propagation:

a. Mode Substrate

If $n_2 < \beta/k_0 < n_0$, the field can not be attenuated at the interface of the intermediate medium with the substrate, only an evanescent wave exists in the substrate (Figure 2.6)

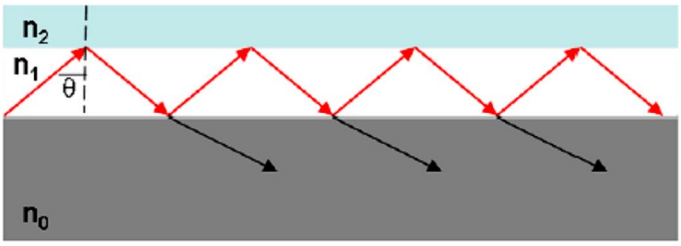

Figure 2.6. Evanescent optical wave occurring substrate modes [36]

b. Mode Air

When we have $\beta/k_0 < n_2$, the solutions for the field are periodic under the direction O_z and the light could be confined in any medium. This type of mode is degenerated for all β values, we can therefore define air mode which is symmetric and air mode asymmetric. (Figure 2.7)

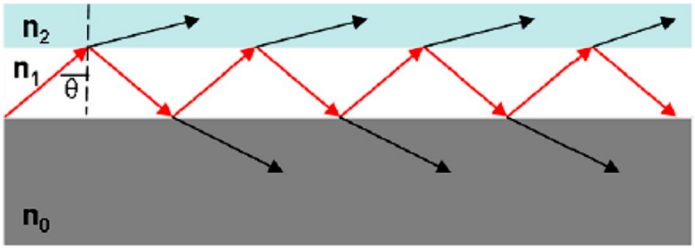

Figure 2.7. Optical wave propagating in air and substrate [36]

c. Guided Mode

If $n_0 < \beta/k_0 < n_1$, the field is evanescent in the two extreme media as well as it is periodic under the direction O_z in the intermediate medium. The light is confined in this unique medium as illustrated in Figure 2.8.

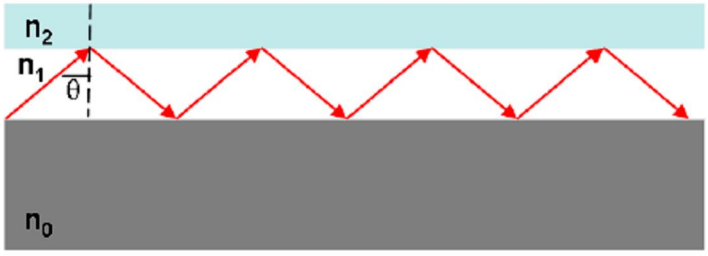

Figure 2.8. Optical wave in the structure [36]

The goal is to obtain guided modes in the core material; we will consider only this last type of modes. It will be necessary to have a material of higher refractive index than the substrate or superstrate (air).

In conclusion, this chapter describes the fundamental properties of III-nitrides semiconductors and the basics knowledge for optical waveguiding. In the next Chapter 3, we will apply this for the strcuture characterizations.

CHAPTER 3
CHARACTERIZATION OF GALLIUM NITRIDE MICROSTRUCTURE

This chapter discusses GaN/Si thin film structures and the characterization of their microstructure. Conventional tools are used to investigation of crystalline quality and morphology. The results will be compared to those obtained with GaN on sapphire. The material characterization of the semiconductor structures is an important part of this work since it is providing essential information to optimize the design of the active layer and technological processes.

3.1. Experimental Growth Process for Gallium Nitride

The structure of GaN thin films deposited on silicon and sapphire substrates investigated in this section. It is important to understand the structure of GaN on both substrates to distinguish which substrate is very suitable for the device application. The microstructure is mainly characterized by the crystallinity of the layers, the homogeneity, the morphology with the surface roughness and the density of dislocations.

3.1.1. Gallium Nitride on Silicon

In this dissertation, the case of GaN on silicon is investigated. The GaN/Si samples have been fabricated in Laboratory of Nanophotonics directed by Prof Yong Hoon Cho at the Korean Advanced Institute of Science and Technology (KAIST- Daejeon), in the frame of the Korean ï French international project PHC Star 21455QB (white LEDs based on GaN and ZnO). These layers have been specific deposited on n+ silicon in order to further applied an electric across the layer. The main issues was to minimize the thickness of AlN and AlGaN buffer

layers in order to maintain a lattice mismatch with GaN and guaranty a correct material quality. Samples used in this experimental study are grown by MOCVD (metal organic chemical vapor deposition). MOCVD has emerged as an efficient technological growth method for the deposition of high quality III-nitrides semiconductors and device structures [37- 40]. Briefly, a home made MOCVD system have been developped at KAIST, KAIST has horizontal reactor with a rotating disk reactor which two inch wafers can be grown simultaneously. Compared to commercial MOCVD equipments, this system has a larger dynamic range for growth temperature, pressure, etc. Growth temperatures can be as high as 1350 ^{o}C, which is highly preferable for the growth of high quality AlN [41,42].

All the details related to the experimental set-up and the process, are given in previous work by *S.M Ko et al* [42]. Inside the reactor, complex reactions of different gas precursors take place. Gases are introduced into the chamber locally and allowed to react on the surface of a heated substrate to grow thin film crystals as well as volatile gas-phase. The column-III precursors are used for growth process: these are trimethylgallium (TMG) and trimethylaluminum (TMA). Ammonia is used as the nitrogen source. A carrier gas, either H_2 or N_2, is bubbled through the metalorganic (MO) sources and carries the MO precursors to the reaction chamber. The ammonia nitrogen source is kept in a separate high-pressure gas cylinder and is brought to the reactor through a separate line. All gases flow rates are controlled by mass flow controller.

For the growth process developped, different steps are necessary:

a) It starts with deposition of a low temperature (LT) AlN and $Al_xGa_{1-x}N$ (Al content noted x) buffer layers on the silicon substrates. The crystalline buffer layer is formed by three-dimensional islands when it is heated at high temperatures. The objective is to eliminate the strain caused by the large lattice mismatch between the GaN material and the Si substrate.

During the growth process, the islands become bigger and coalesce, forming threading dislocations at the interface.

b) A short period superlattice structure (SPS) is deposited on top of the buffer layers: it consists of 24 periods of $Al_yGa_{1-y}N$ with Al content y higher than the one in the AlGaN buffer layer. The temperature is very high, which reduces the dislocations and provides a fully relaxed bulk layer. The challenge is to optimize the quality of AlN and $Al_xGa_{1-x}N$ layer and to control the thickness. This procedure is detailled by authors [39,40].

c) The top Layer (u-GaN) is therefore deposited on the whole template at a temperature of 1040 °C.

The structure of GaN/silicon with Al content x>y was presented in Figure 3.1. Using MOVCD, two GaN samples were grown on silicon that same condition MOCVD but difference temperature presented in Tabel 3.1.

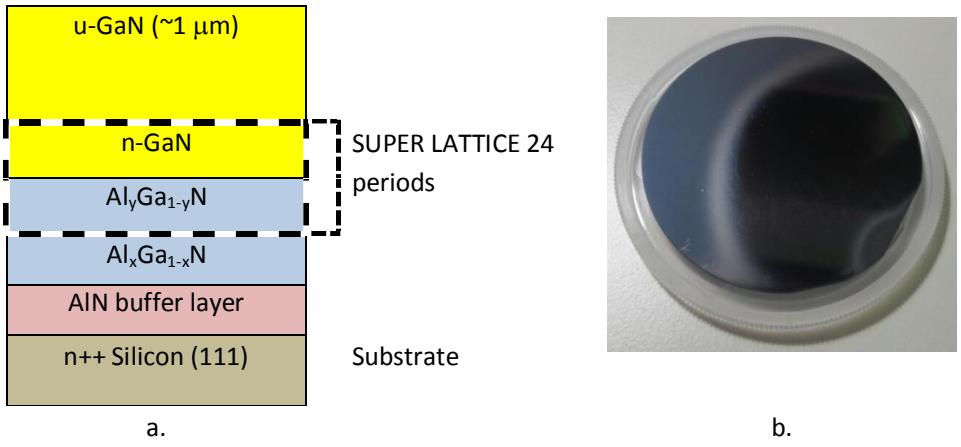

Figure 3.1. (a) Schematic depicting the sample structure (Al compound x > y). (b). Photo of sample GaN/Si

Table 3.1. Layers engineering for GaN/silicon samples

Structure Name	Material	Thickness Estimated
Top Layer	u-GaN	1 µm
SPS	AlGaN/GaN SPS	80 nm
Interlayer	AlGaN	80 nm
Buffer layer	AlN	80 nm
Substrate	Silicon	330 µm

3.1.2. Gallium Nitride on Sapphire (Al_2O_3)

We have also investigated the growth of Galium Nitride on Sapphire (GaN/Al_2O_3) samples for comparation with GaN/Si: GaN have been deposited on sapphire substrates by MOVPE (metal organic vapor phase epitaxy). The samples are provided by Prof Dimitris Pavlidis from Darmstadt Technical University (DTU) in Germany [43]. The structure used in this work is grown by metal organic chemical vapor deposition (MOVPE) on c-plane (001) sapphire substrate (Figure 3.2). Trimethyl aluminium and Trimethyl gallium are used as alkyl sources and ammonia is used as a hydride source. After the cleaning of the substrate at high temperature and the growth of a thin AlN buffer layer (150 nm layer thickness), low temperature (LT) AlN is grown at 950 °C. The temperature is consequently elevated to 1040 °C and the deposition of a 150 nm thick high temperature (HT) grown on plane AlN. Finally, an interlayer consisting of 10 time GaN/AlN layers having a total thickness of 200 nm are carried out under the same HT conditions and 1.5 µm thick GaN is grown on top of the interlayer. The experimental process is described in the litterature [44].

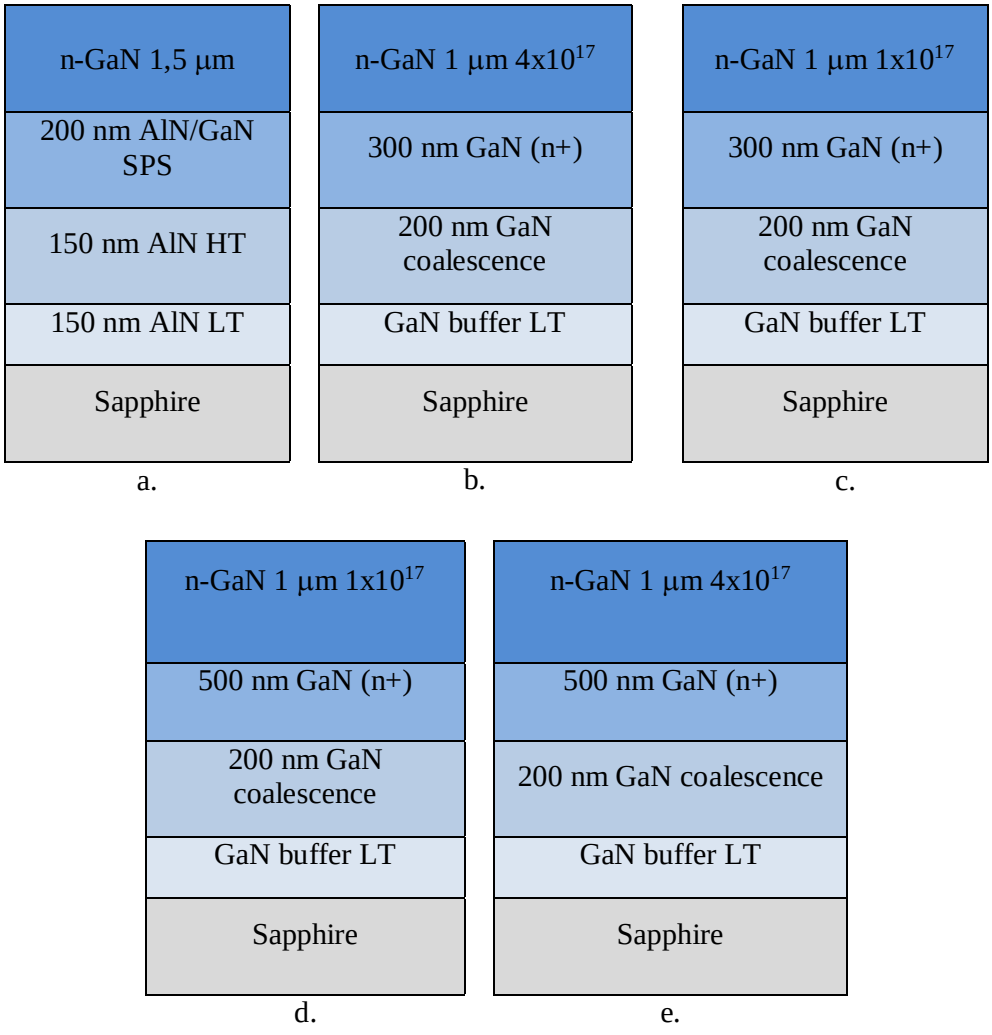

Figure 3.2. Structure of the GaN/sapphire samples at difference thickness and difference carrier concentration (a) GaN/Sapphire-1, (b) GaN/Sapphire-2, (c) GaN/Sapphire-3, (d) GaN/Sapphire-4, (e) GaN/Sapphire-5

Five GaN samples with difference thickness and difference carrier concentration have been grown on sapphire. They are presented in Tabel 3.2. The description of GaN structure on sapphire is presented Figure 3.2.

Table 3.2. List of GaN/sapphire samples for difference thicknesses and carrier concentrations

Sample Name	**Estimation of GaN Thickness (µm)**	**Carrier concentation (cm^{-3})**	
		Top layer	**Buffer Layer** n+
GaN/Sapphire-1	1.5	without n+	without n+
GaN/Sapphire-2	1.3	$4x10^{17}$	$1x10^{18}$
GaN/Sapphire-3	1.3	$1x10^{17}$	$1x10^{18}$
GaN/Sapphire-4	1.5	$1x10^{17}$	$1x10^{18}$
GaN/Sapphire-5	1.5	$4x10^{17}$	$1x10^{18}$

3.2. Characterization of GaN Microstructure

Due to the difficulties to grow III-nitrides, a study of the grown layers is necessary. Several studies on the GaN grown by MOCVD have been focussed on specfic aspects such as the surface morphology, the density of dislocations and the cristalline quality [44]. A close relationship exists between the microstructure and the physical properties of the GaN materials. In order to improve devices performance, a high degree of microstructural perfection is required for the films.

Advancements of GaN-based laser diodes by *Nakamura et al* [45] have been achieved in part due to the introduction of a buffer layer between the films and the sapphire substrates. This technique improved the crystallinity and the surface morphology of the grown layers. Meanwhile, defects always existing at the interfaces of the films are still of concern for the way they affect the epitaxial growth and modify the properties of the devices. Characterization of properties has become an integral part of research for the understanding of the material behaviour and performance under operating conditions [43].

In general terms, microstructural characterization is achieved by allowing

some form of probe to interact with a carefully prepared specimen sample. The most commonly used probe are visible light, X-ray radiation and a high energy electron beam. High resolution X-ray diffraction (XRD), Scanning Electron Microscopy (SEM), Atomic Force Microscopy (AFM) and Transmission Electron Microscopy (TEM), have been employed to characterize the materials.

3.2.1. Scanning Electron Microscopy (SEM)

The scanning electron microscope provides the microscopic images that the depth of field for resolved detail in the scanning electron microscope is very much greater than the spatial resolution in the field of view. The SEM is a type of electron microscope that images a sample by scanning it with a beam of electrons in a raster scan pattern. The electrons interact with the atoms that make up the sample producing signals that contain information about the sample's surface topography, composition, and other properties such as electrical conductivity [46]. The microstructure of the layers can be directly observed using SEM under the cross sectional configuration. In this work, this characterization at the IEMN Lille is realized using SEM JEOL Ultra 55.

a. GaN on Sapphire

In this research, the SEM is one of microstructure characterization to describes the thickness layers of GaN materials. Figure 3.3 shows the result of SEM pictures for two different samples of GaN have been grown on (0001) sapphire (samples 1 and 4). GaN/Al_2O_3 sample-1 in Figure 3.3a with scale 1:200 nm shows the thickness layer at the bottom layer sapphire substrate has 400 nm, the second layer AlN/GaN SPS (short period superlattice) has 200 nm, and the top layer has 1.5 µm.

Figure 3.3b with scale 1:1 µm representation about the thickness layer of GaN/Al_2O_3 sample-4; the bottom layer sapphire substrate has 2 µm, the second layer and the top layer are made of even GaN materials (2 µm thickness). The GaN/Al_2O_3 sample-4 more difficult to observe: the buffer, the doped layer and

the surface layer are made of even GaN material. It shows that the GaN layer is quite homogenous. These images are exhibiting the quite good microstructure obtained when the sapphire substrate is used. Dislocations are clearly propagating from the substrate to the top surface [47]. This structure will be investigated through TEM analysis in the next paragraph.

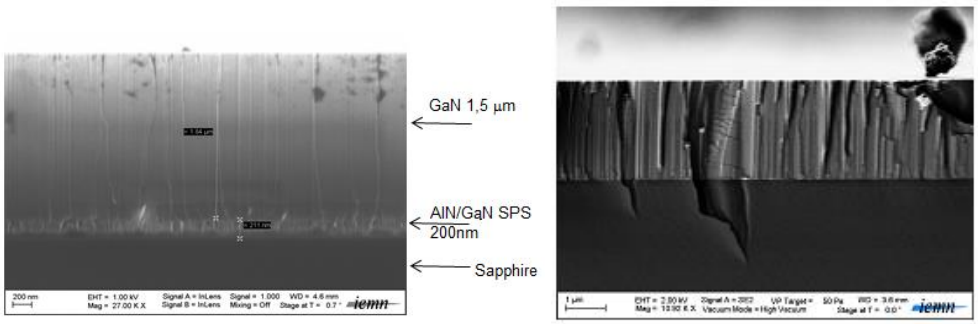

(a) (b)

Figure 3.3: Cross-section SEM observation (a) GaN/sapphire-1 and (b) GaN/sapphire-4

b. GaN on Silicon

In samples developped by KAIST, one process was identified in agreement with reported works [39, 40]. Microstructure of GaN/Si films is presented in Figure 3.4, through SEM cross-section observations.

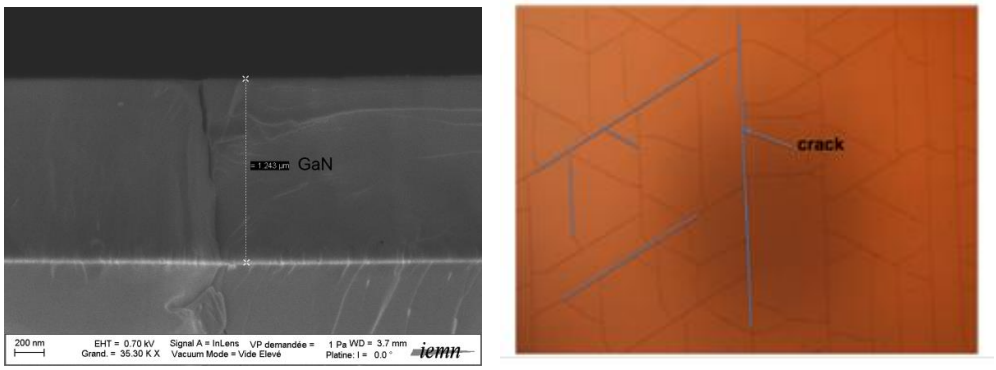

(a) (b)

Figure 3.4: SEM of cross-sectionnal of GaN/Si (a) GaN/Si-1 and (b) optical microscopy

Figure 3.4a shows the top layer of GaN has 1 µm thickness and the buffer layer is measured around 150nm. One can distinguish the silicon substrate, the GaN layer and the whole buffer layers with thickness between 100 and 150nm. The top GaN layer is homogoneus without porosities. The different damages in surface are visible in the images, it shows some cracks in surface (Figure 3.4 b), probably due to the lattice mismatch between the GaN and Si and the severe tensile strain.

3.2.2. Transmission Electron Microscopy (TEM)

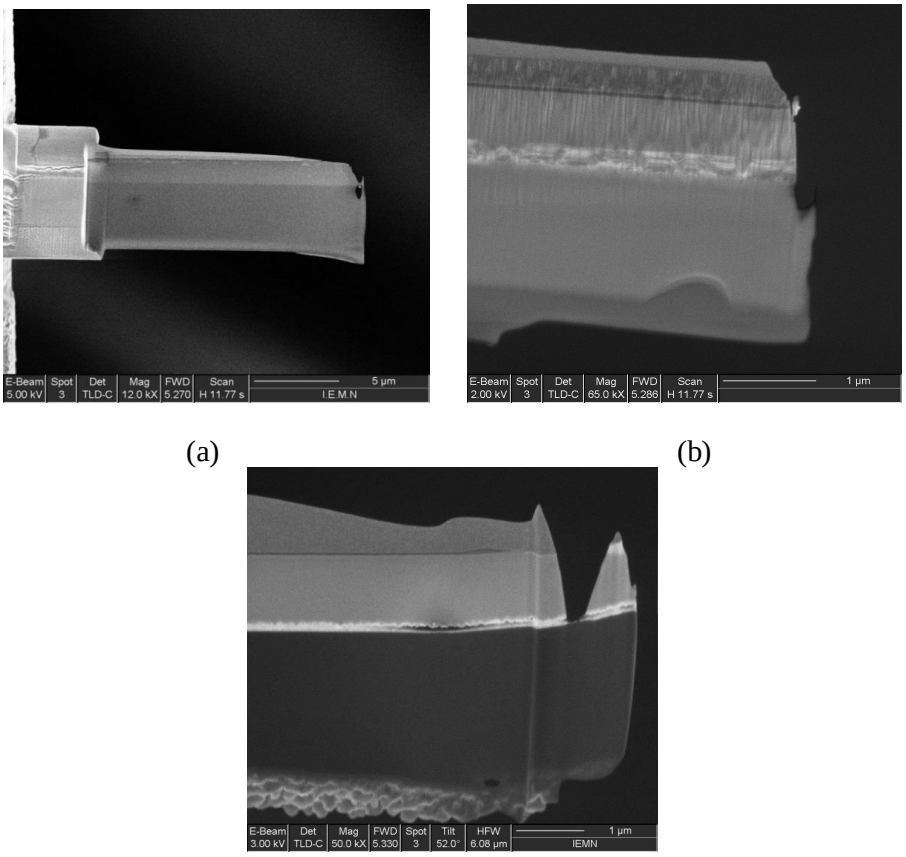

(a) (b)

(c)

Figure 3.5. Preparation of samples by FIB technique, (a) GaN/Sapphire-1 (scale 5µm), (b) GaN/Sapphire-1 (scale 1µm) and (c) GaN/Silicon-1 (scale 1µm)

The TEM is capable of displaying magnified images of a thin specimen, typically with a magnification in the range 10^3 to 10^6. The instrument of TEM can be used to produce electron-diffraction patterns, useful for analyzing the properties and structure of a crystalline specimen. TEM pictures provide informations on the internal structure of the AlN and AlGaN/GaN buffer layers as well as the GaN layer, by showing threading dislocations.

TEM analysis (Tecnai G2-20) is conducted in order to study the microstructural defects existing in the layers. The samples must be prepared by using the Focused Ion Beam (FIB) technique: the equipment at IEMN is FEI Strata DB 235 utilize sample preparation in cross sectional view. A metallic top layer (Chromium-50 nm) is necessary. Figure 3.5 shows TEM preparation in GaN/Sapphire-1 and GaN/Si-1 samples. TEM analysis realized at UMET-CNRS (Unité Matériaux Transformations) is performed using FEI Tecnai G2-20.

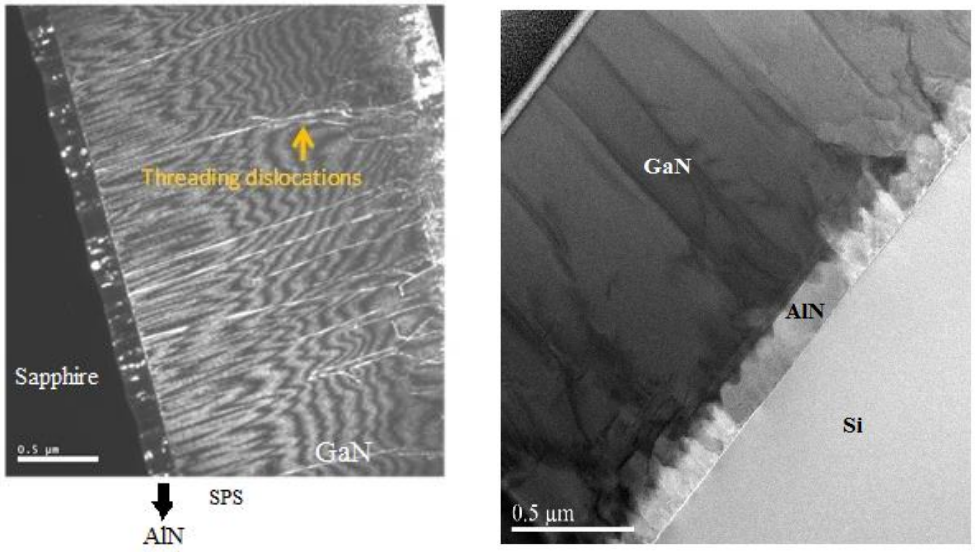

(a) (b)

Figure 3.6. TEM by FEI Tecnai G2 20, (a) GaN/Al_2O_3 and (b) GaN/Si

TEM analysis is conducted in order to study the microstructural defects present in the layers. Figure 3.6 shows a weak beam TEM image of GaN on

sapphire and silicon. Material structure by TEM in Figure 3.6a consist of sapphire substrate, AlN/GaN SPS as buffer layer and the top layer is GaN. Figure 3.6b shows structure material GaN as top layer, silicon substrate, and AlN as buffer layer. This figure presents a large scale cross-sectional weak-beam view of the layers, the images are taken along g=0002 diffraction vector. Threading dislocations are seen to originate in the buffer layers until the top surface. The threading dislocations observed in the images maybe either mixed or pure srew type dislocations [48,49].

Numerous dislocations are generated within the grown layers due to the high stress levels which are present in the structure. The filtering action of the beuufer layer can be confirmed with the confinement of the dislocations away from the GaN active layer and within the AlN and supperlatice layers. In the GaN on sapphire structure, we observe from TEM images that the majority of threading dislocations are stopped by the AlN/GaN SPS superlattice structure. The micrograph in Figure 3.6 reveals the highly defective region, which starts from the top of the substrate, can locally extend to 200nm within the epilayer. Above this defective region, the threading dislocation density is reduced in the GaN epilayer. The average value for the density of dislocations estimated in GaN is relatively low, almost 10^9 cm^{-2} [50, 51]. This finding correlates well to Atomic Force Microscopy analysis given below.

3.2.3. Atomic Force Microscopy (AFM)

In order to analyze the surface morphology and topography, atomic force microscopy (AFM) is applied to GaN thin films. AFM is a powerful imaging tool with high-resolution imaging capability. AFM probes consist of a very sharp tip at the end of a silicon cantilever that can respond to surface artefacts to produce an image of the topography or surface features. They are intrinsically passive devices.

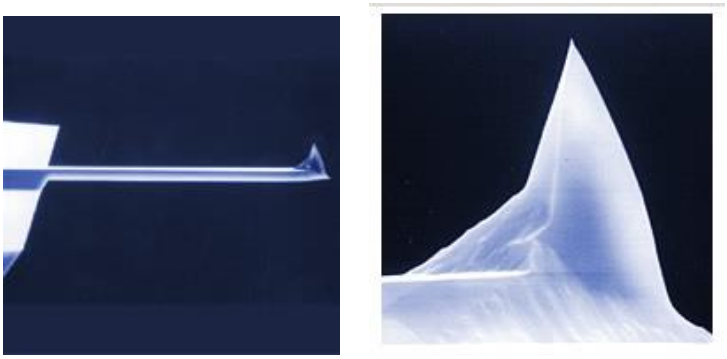

(a) (b)

Figure 3.7. SEM image of an (a) AFM cantilever and (b) AFM tip

The surface quality of the samples is evaluated with Atomic Force Microscopy (AFM) by the Dimension 310 tool (Brucker) in tapping mode in air. Tip is presented in Figure 3.7. Here a non-contact mode is selected. Non-contact AFM can be either static or dynamic, with the cantilever simply moved across the surface at a ýxed distance, or vibrated at or near its resonant frequency. Static imagings will suffer from higher noise due to electrical or thermal noise. Dynamic mode imaging gives access to higher resolution imaging at the expense of simplicity. For image processing, the analyzing can be performed using either Gwyddion software or free software/WsxM software.

The topographical image provides informations about the average dislocation density by counting the V-shaped pits [52] which are correspond to terminating threading dislocations in the epilayer. In this technique gives an underestimated value for dislocations density, it is commonly used to compare the structural quality of semiconductors. The AFM measurements on GaN/Si and sapphire have been realized under the different scan sizes as listed below:

a. $[20 \times 20]\ \mu m^2$
b. $[10 \times 10]\ \mu m^2$
c. $[2 \times 2]\ \mu m^2$
d. $[1 \times 1]\ \mu m^2$
e. $[500 \times 500]\ nm^2$
f. $[200 \times 200]\ nm^2$

a. GaN on Sapphire

AFM analysis on the samples has confirmed the existence of a smooth surface and a density of defects in the same order. V-shape pits caused by the threading dislocation (TD) are observed in GaN on sapphire [47, 52]. Figure 3.8 shows representative area of (500 x 500) nm^2 in AFM topographical images of the GaN layer. It provides also informations from a larger area in the structure compared to TEM. The density of dislocations measured by number of dislocation divided square of scan area, average of dislocation for all samples are $10^9 cm^{-2}$. Average of difference maximum and minimum depth or root mean square (rms) roughness of pits is 5.5 nm.

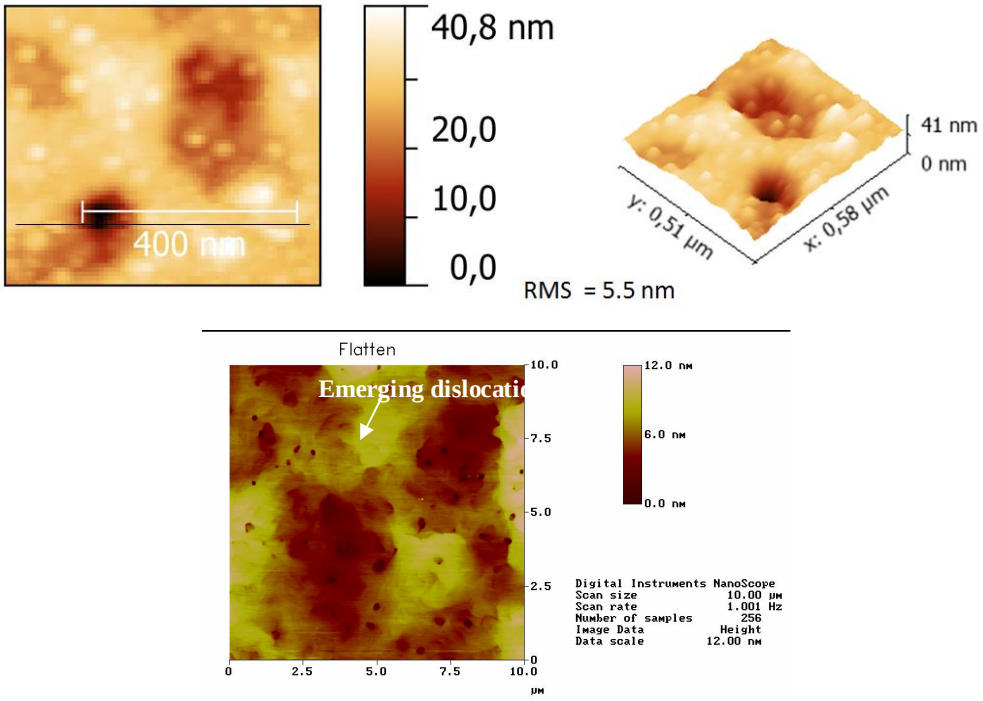

Figure 3.8. AFM analysis of GaN/Sapphire for threading dislocations

The buffer layer has a strong influence on the density of threading dislocations within the 1 µm-thick GaN film. We can see only threading dislocations propagating through the entire GaN layer. In agreement with TEM

analysis, the suppression of dislocation propagation is mainly due to the AlGaN/GaN superlattice period structure (SPS) acting as an absorb of defects, this results only a small presence of these dislocations in the active GaN epilayer [53, 54].

b. GaN on Silicon

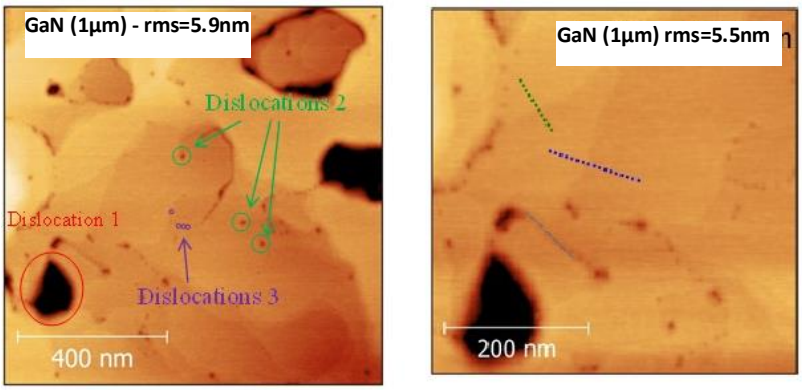

(a) (b)

Figure 3.9. AFM analysis of GaN/Si: scan sizes (a) [1×1] μm^2 and (b) [500×500] nm^2

Figure 3.9 shows AFM analysis of GaN on silicon film with 2 sizes for the surface: (1×1) μm^2 and (500×500) nm^2. AFM analysis shows a small root mean square roughness rms of 5.9 nm for an area of (1x1) μm^2. The existence of threading dislocations is also demonstrated here. The surface morphology of GaN/Si is more damaged compared to GaN on sapphire. Cracks due to lattice mismatch exist along the whole surface.

In the same way, for GaN/Si samples, it has been reported that the strain is a principal cause related to formation of V-pits. The density of dislocations is higher roughly $9.10^9\ cm^{-2}$ (average for all samples) and a root mean square (rms) roughness of 5.9 nm (average for all samples) respectively. This is a consequence of the growth process which still under optimization for silicon technology.

In details, AFM observations show two specific GaN/Si structures: polyatomic steps (thickness of less than 1 nm high) with terrasses of a few

100 nm long and 2 or 3 types of dislocations (400 nm, 100 nm and 5 nm long). Different types of dislocations at 400 nm, 100 nm and 5 nm long are represented in Figure 3.10.

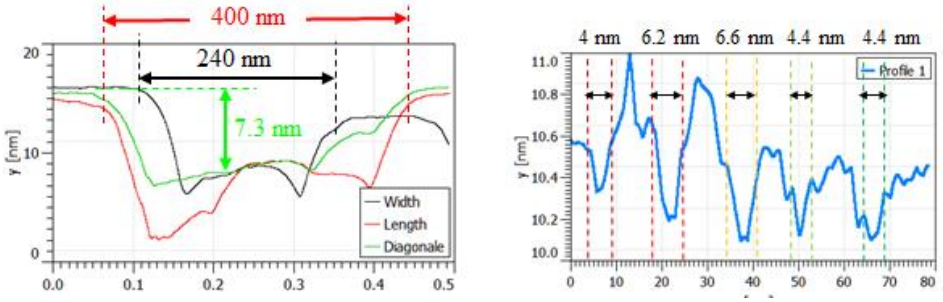

Figure 3.10. Type of dislocation in GaN/Silicon structure for different scan size (a) [2× 2] μm^2 and (b) [500×500] nm^2

These results demonstrate that degradation is usually related to the presence of dislocations on surface. The reason is the poor crystalline quality of the epilayer grown on silicon. Higher quality and improved surface morphology are observed for GaN on sapphire; mainly it is explained by the lower lattice mismatch and the more intensive research to demonstrate the best microstructure. Overall evaluations from TEM and AFM results demonstrate that samples on sapphire have better crystal quality as compared to samples on silicon and improved performance of photonic devices can be expected.

3.2.4. X-ray Diffraction (XRD)

One characterization method for crystalline quality of materials which is commonly used is X-ray Difraction (XRD). This technique is used to identify the crystalline phases in the material by determining the parameters of the lattice structure as well as to get particle size. Each peak appearing in an XRD pattern representing a crystal plane have a particular orientation in three-dimensional axis. Peaks obtained from the measurement data is then matched with a standard X-ray diffraction for almost all types of materials. The structure GaN on sapphire has

been studied by the community since more than 2 decades and epilayers exhibit only single phase in the plane orientation (0002) [41- 44]. In this section, we have only considered the crystalline characterization of GaN films grown on silicon Si(111): they have been characterized through the ω/2θ and phi scan configurations. Figure 3.11 shows the XRD phase analysis scan.

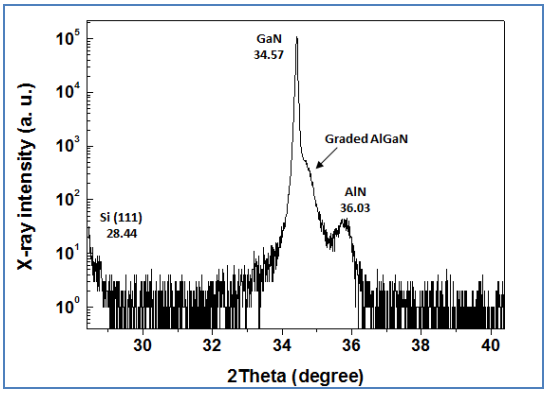

Figure 3.11. XRD spectrum of GaN on silicon Si(111) sample

The intensity data is represented in two dimensions by performing *w* (sample angle)ï 2***d*** (detector angle) scan at a range of different values. XRD spectrum of GaN/Si has peaks which peaks identified at angles 34.57° and 36.03° correspond to (0002) diffraction peak of GaN and AlN films and it indicates complete texture with Si (111). It means GaN and AlN are lattice mismatch with Si.

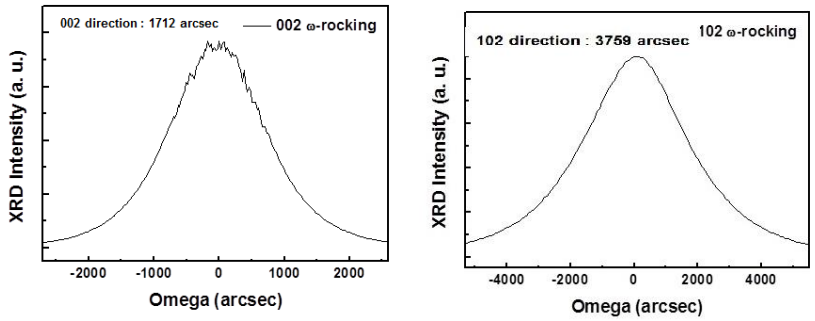

(a) (b)

Figure 3.12. XRD rocking curve (x-scan) of GaN film along (002) and (102) planes

Figure 3.12 shows the XRD rocking curve (x-scan) alond the (0002) plane. The full width at half maximum (FWHM) which indicates the degree of disorientation in the layer is reported here: For the dominant GaN diffraction peak at $\theta = 34.57°$, we have measured it to be as narrow as 1712 arcsec for (002) planes, while it is 3759 arcsec for (102) planes. These values are slightly larger than the ones obtained for sapphire substrates but they are in agreement with those reported recently [55-57].

In summary, we have investigated the materials quality of GaN samples grown on silicon and sapphire by MOCVD. We report experimental XRD, AFM, TEM, SEM study onto GaN samples.We have observed that the microstructure is highly dependent on the substrate and the buffer layers. The knowledge of growth kinetics and its impact on the optical characteristics is essential in order to develop devices with an enhanced performance. The aim of this work is to establish a correlation between the microstructure and the optical properties of GaN which will prove to be highly useful from devices applications point of view.

CHAPTER 4
OPTICAL AND ELECTRO-OPTICAL CHARACTERIZATION OF GALLIUM NITRIDE THIN FILMS

This chapter describes optical characterization by prism coupling technique and electro-optical characterization by goniometric setup. The results of measurement, the analysis and the evaluation of materials properties will be described. These results are obtained from experiments conducted on GaN on Sapphire substrates and GaN on Silicon substrates.

4.1. Prism Coupling Technique

When a non-absorbing dielectric layer with thickness comparable to the wavelength of interest is deposited on a planar substrate, and the thin film has a higher refractive index than the substrate, the structure forms a dielectric waveguide [58]. The film can be deposited by variety of techniques including metal-organic chemical vapor deposition (MOCVD), molecular beam epitaxy (MBE), sputtering, and pulsed laser deposition (PLD). In this dissertation, MOVPE is used to grow thin films such as Gallium Nitride (GaN) on sapphire or silicon substrates. Also MOVCD is used to grow thin films such as GaN on silicon substrate [59, 60].

A dielectric waveguide structure is used in a majority of optical devices including semiconductor lasers [61], optical modulators [62], Mach-Zehnder interferometer [63], splitter and combiner. In our case, GaN materials grown on sapphire constitutes a dielectric waveguide, the refractive index contrast between the GaN and sapphire is much larger than the refractive index difference could provide advantages to make small sized, compact optical devices. Also, the confinement of the mode is strong due to the high refractive index difference between the core (GaN) and cladding layers (buffer layer). This waveguide is also transparent for wavelengths longer than the absorption-edge of GaN layer since

the optical absorption edge is at 3.4 eV (365 nm). This makes the materials suitable for visible and NIR waveguide application [64].

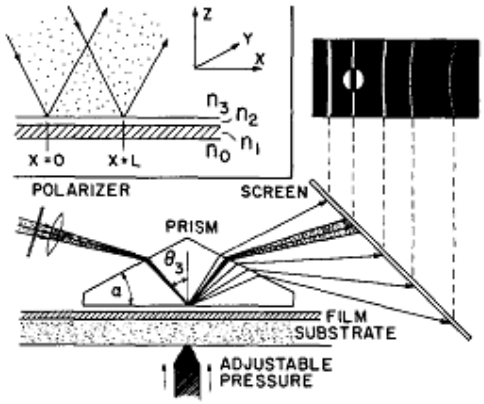

Figure 4.1. Prism coupling system setup [65].

The rutile (TiO2) prism is used to couple light into the air/thin film/sapphire waveguide structure. An air gap less than half of the wavelength of the source light is created between the prism and the sample. At a certain discrete mode angle, when an incident light from the prism is coupled into the thin film layer by the evanescent wave, the sharp drop of reflectivity is detected by the detector and recorded by a computer. The reflectivity changing as a function of rotation angle can be plotted. When a thin film is thick enough to confine two or more modes, the film thickness and the refractive index with high accuracy can be obtained by solving the mode equations [58-60].

Therefore, the waveguide structure can be also applied as a useful structure to determine the refractive index and thickness of the film by prism coupling technique. The refractive index and film thickness are the critical parameters for the design and the fabrication of optical devices. As shown in Figure 4.1, the prism coupling system is composed of a prism placed closely on top of a dielectric thin film mounted on the rotational stage, an air gap formed between them controlled by a pneumatically operated coupling head. The nature of prism (material, base angle) is carefully studied in order to realize the good coupling inside the core layer. The prism coupling is clearly detailled in the literature. The

experimental setup allows the observation of coupling and intermode scattering. This setup also permits the determination of effective mode index or the propagation constants β. In this work, in order to analysis about the effect of the microstructure on the optical properties of GaN epilayer, we used the guided wave technique based on prism coupling. In this work using prim coupling in a Metricon M2010 setup (www.metricon.com), it consists of a rutile (TiO_2) prism. They are presented in Figure 4.2.

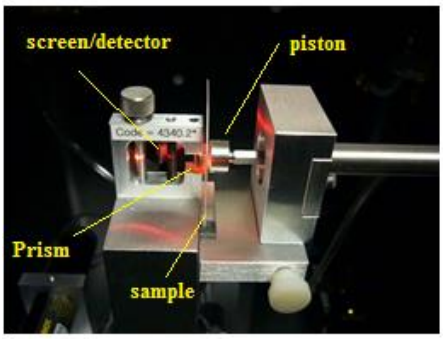

Figure 4.2. Principle of the prism coupling (Metricon 2010)

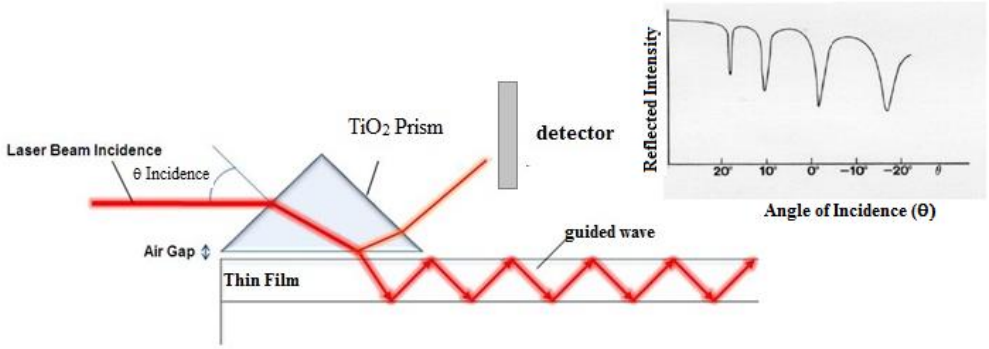

Figure 4.3. Principle diagram of prism coupling in Metricon 2010

Figure 4.3 show the principle of light coupling into the GaN film by the prism coupling technique. By measuring the reflected intensity versus the angle of incidence to the normal of the prism, it is possible to plot the guided-mode spectrum as given in insert of Figure 4.3.

When optical modes propagate in a GaN waveguide, one of the important characteristics is the propagation loss. The loss is generally classified into three different mechanisms: absorption, scattering and radiation. By measuring the scattering loss of the straight waveguide at certain TE or TM modes, it is possible to get knowledge of the roughness of the interface between the waveguide and cladding medium. The scattering loss can be measured using the scattered intensity technique, by moving a probing fiber along the waveguide, and the light is collected by a photo-detector. If the surface imperfections and surface roughness increase, the surface scattering losses increase. We will propose some experiments into GaN on sapphire and Si substrates in the next sections.

4.2. Observation of the Modes

The coupling of the laser beam into the film can be observed in various ways, depending on the characteristics of film and substrate and on the type of prism used. Different configurations of films with small roughness deposited by evaporation or sputtering (e.g., ZnS, ZnO, $A1_20_3$) can be measured with the symmetric prism, especially when they are deposited on low index substrates. In this case, the coupling can usually be observed by the appearance of dip in the recorded intensity spectrum or by the appearance of dark m-lines on the screen in Figure 4.1. By measuring the reþected intensity versus the angle of incidence to the normal of the prism Ŭ, it is possible to plot the guided-mode spectrum of the sample. The reþectivity dips observed at certain angles correspond to the excitation and propagation of guided modes in the ýlm structure. In case of the samples used in this study and with the optical axis normal to the surface, the ordinary and extraordinary modes are excited by using TE and TM polarized light [66-68].

By measuring the reflected intensity versus the angle of incidence ɗ, we draw the guided-mode spectrum of the material. The reflectivity dips observed at certain angles correspond to the excitation of guided modes in the film structure. Sharp and distinguishable mode lines are detected and indicated the optical

quality of this film. From the knowledge of the ɗ angle for modes along different polarization, we can compute the corresponding effective mode indices Nm, according to [66-68]:

$$N_m = n_p \times sin\left[A_p + arcsin\left(\frac{sin\theta}{n_p}\right)\right] \qquad (4.1)$$

where n_p is the refractive index of the prism, θ is the angle of incidence and Ap is the prism angle with respect to the normal. From the experimental values of effective indices N_m and using the calculation procedure reported by Ulrich et al. [62], the refractive indices of the films and the thickness have been determined simultaneously.

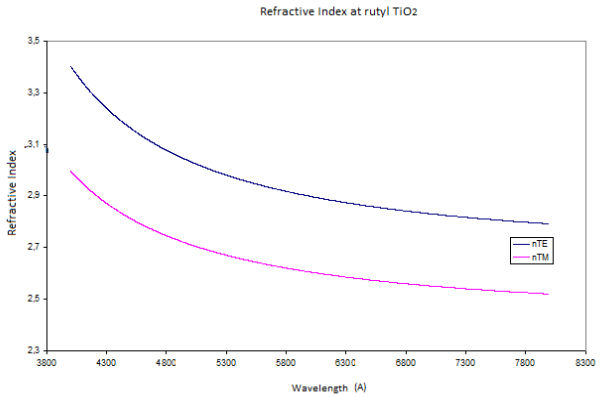

Figure 4.4. Evolution of the prism index with the wavelength for TE/TM modes [69]

For some sample materials, a measure of the refractive index in TE and TM modes was performed for different wavelengths (450 nm, 532 nm, 633 nm, 975 nm and 1550 nm). For sample measurements at different wavelengths, we use the prism P-200-6013.6 2-60 (TiO_2 Rutile) in case of higher wavelength resulting in a lower range of refractive index n_{Prism} for the prism, the relation wavelength and refractive index represented in Figure 4.4 which shows the index range using the TiO2 (rutile) prism: it is from 3.14 at 450 nm to 2.69 at 1550nm in TE mode and 2.8 at 450 nm to 2.44 at 1.5 µm in TM mode. For each sample, a

measurement of the refractive index in TE and TM modes was performed for different wavelength (450, 532, 633, 975, and 1550) nm. For each measurements at different wavelength, we use the rutile prism where values of refractive indices for TiO2 rutile prism (n_{Prism}) represented in Table 4.1.

Table 4.1. Values of refractive indices for TiO2 rutyl prism

λ (nm)	n_{Prism} (TE)	n_{Prism} (TM)
450	3.147	2.808
532	2.967	2.665
633	2.866	2.583
975	2.746	2.487
1550	2.694	2.444

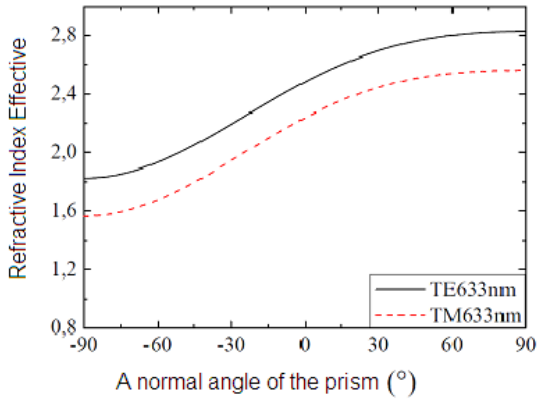

Figure 4.5. Evolution of the refractive index prism at 633nm with the incident angle (for TE/TM modes) [69]

The rutile prism (TiO2) with angle Ap of 60° have index N_m from 1.9 for angle θ = -60° up to N_m= 2.8 for angle θ = +60°. The correlation between angle and refractive index is represented in Figure 4.5.

4.3. Measurement of Refractive Index and Thickness for GaN/Si Samples

In this subchapter, investigation of optical refractive index and thickness will be discussed. The samples studied are two GaN/Si detailed in Chapter 3. The optical measurement technique will be performed using prism coupling method. Therefore, optical measurement for refractive index and thickness at GaN/Si sample-1 film are represented in Table 4.2 and Table 4.3. The samples on silicon are provided by Prof Yong Hoon Cho from Korean Advanced Institute Science and Technology (KAIST). The accuracy of the index is 10^{-3} and the film thickness about 10 nm.

Table 4.2. Refractive Index at different wavelength in GaN/Si sample-1

GaN/Si-1	450 nm	532 nm	633 nm	975 nm	1539 nm
n TE	2.460	2.397	2.357	2.305	2.284
n TM	2.504	2.434	2.359	2.338	2.315

Table 4.3. Thickness at different wavelength in GaN/Si sample-1

GaN/Si-1	450 nm	532 nm	633 nm	975 nm	1532 nm
Thickness TE (μm)	1.245	1.258	1.248	1.271	1.239

4.3.1. Refractive Index and Thickness for GaN/Si Samples (TE Mode)

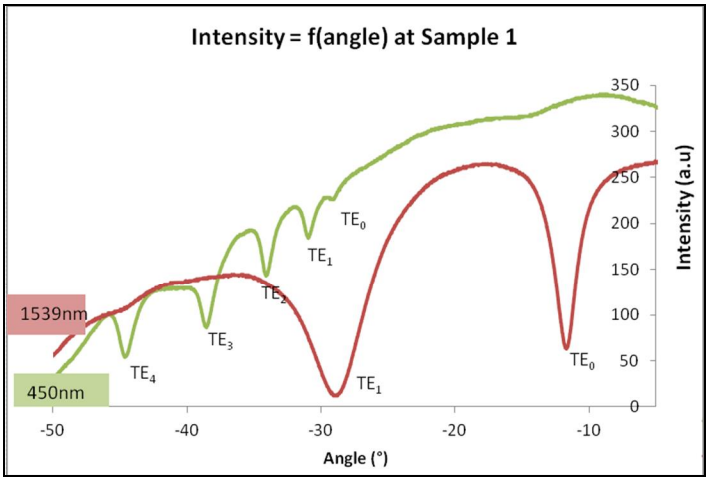

Figure 4.6. TE Mode spectrum of GaN/Si sample-1 at λ = 450 nm and 1539 nm

The result of optical measurement for refractive index and thickness of TE mode at GaN/Si sample-1 are analyzed. Figure 4.6 shows TE mode spectrum of GaN/Si sample-1 at 450 nm and 1539 nm. From Figure 4.6 and Table 4.2, it shows refractive index of GaN/Si sample-1 is n_{TE} = 2.284 at wavelength of 1539 nm and n_{TE} = 2.460 at 450 nm. An increase of the laser wavelength will decreasing the number of modes too. The Figure 4.6 shows 2 modes at 1539 nm and 5 modes at 450 nm.

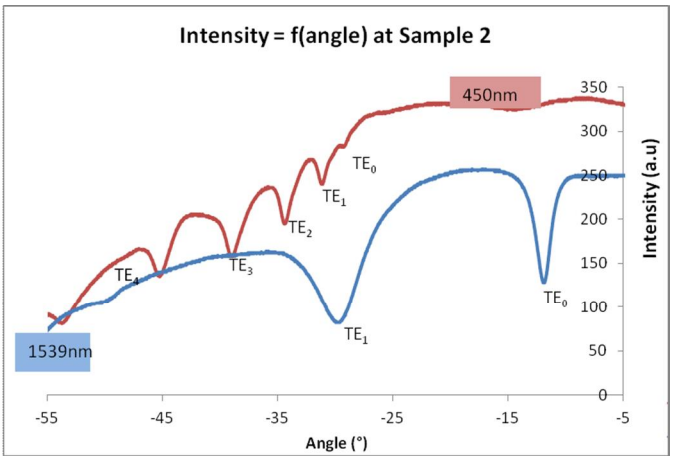

Figure 4.7. TE Mode spectrum of GaN/Si sample-2 at wavelength λ = 450 nm and 1539 nm.

The results of optical measurement for refractive index and thickness at GaN/Si sample-2 film represented are summarized in Table 4.4. and Table 4.5. The dispersion of TE refractive index at GaN/Si sample 2 is plotted in Figure 4.7 at 450 nm and 1539 nm. Because of its plane wave, TM polarization refractive index values are more sensitive to the layer quality.

Table 4.4. Refractive index at different wavelength in GaN/Si sample-2

GaN/Si-2	450 nm	532 nm	633 nm	975 nm	1532 nm
.n TE	2.443	2.396	2.358	2.303	2.277
.n TM	2.503	2.434	2.391	2.339	2.314

The result of measurement in Figure 4.7 and Table 4.4, it shows refractive index of GaN/Si sample-2 were n_{TE} = 2.277 at 1539 nm wavelength and

n_{TE} =2.443 at 450 nm. The optical measurements for TE refractive index at GaN/Si sample-1 and sample-2 are given in Figure 4.8a. Figure 4.8b shows the dispersion of TE refractive index at GaN/Si sample-1 compare with GaN/Si sample-2 at five wavelengths λ = 450 nm, 532 nm, 633 nm, 975 nm, and 1532 nm.

Table 4.5. Thickness at different wavelength in GaN/Si sample-2

GaN/Si-2	450 nm	532 nm	633 nm	975 nm	1532 nm
Thickness TE (μm)	1.281	1.238	1.250	1.253	1.320

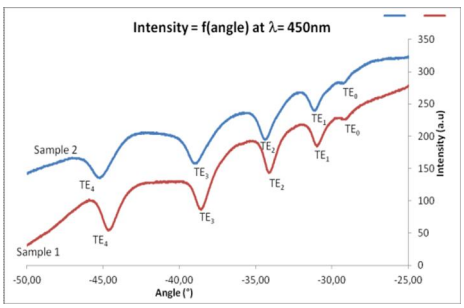

(i)

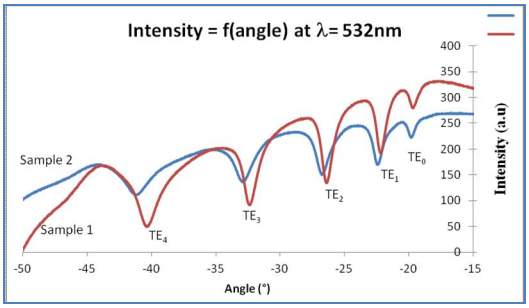

(ii)

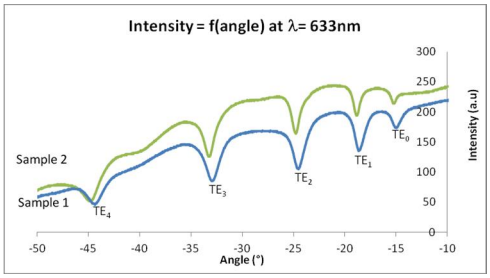

(iii)

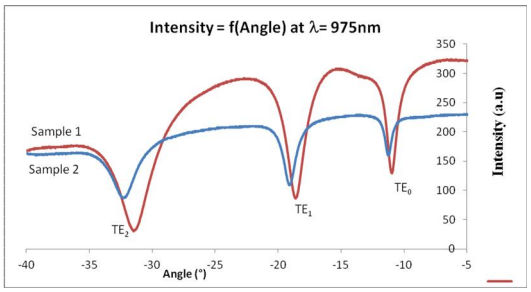

(iv)

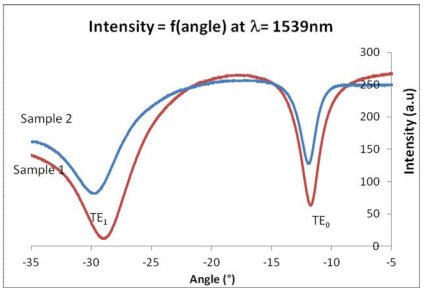

(v)

Figure 4.8 (a). The TE mode spectrum of GaN/Si sample-1 and sample-2 comparation at five wavelengths, (i) λ= 450 nm, (ii) λ= 532 nm, (iii) λ= 633 nm, (iv) λ= 975 nm and (v) λ =1539 nm

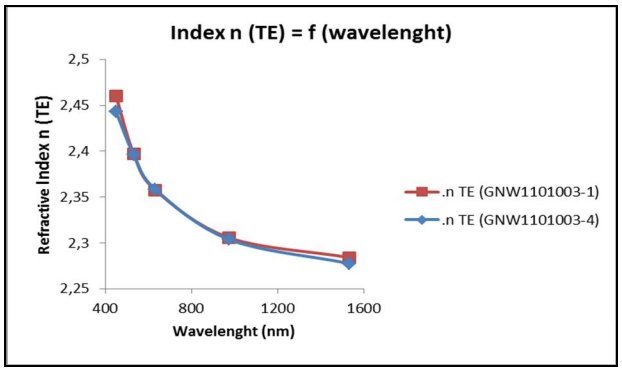

Figure 4.8 (b). Dispersion of the refractive index (TE mode) for GaN/Si (111) samples

4.3.2. Refractive Index and Thickness for GaN/Si Samples (TM Mode)

In the next work, the optical measurement are compared through the recording of the spectra *I(d)*. The refractive indices for TM modes are depending on the wavelengths from 450 to 1532 nm. The optical measurements conducted on GaN/Si sample-2 for TM modes are similar to the ones for GaN/Si sample-1. It is represented in Figure 4.9. The dispersion of refractive index (TE and TM modes) is plotted in Figure 4.9a and Figure 4.9b. Because of its plane wave, TM polarization refractive index are more sensitive to the layer quality.

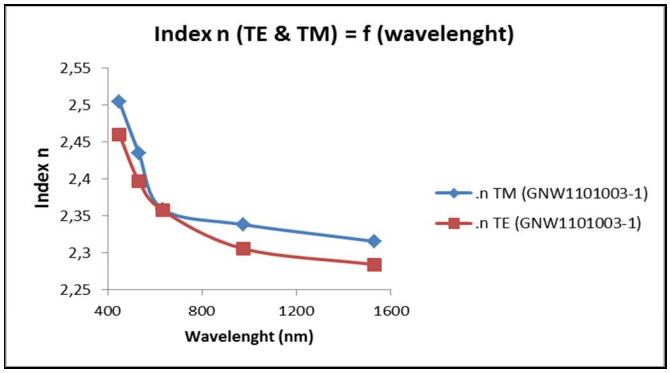

Figure 4.9 a. Dispersion of the refractive index (TM mode) for GaN/Si (111) samples

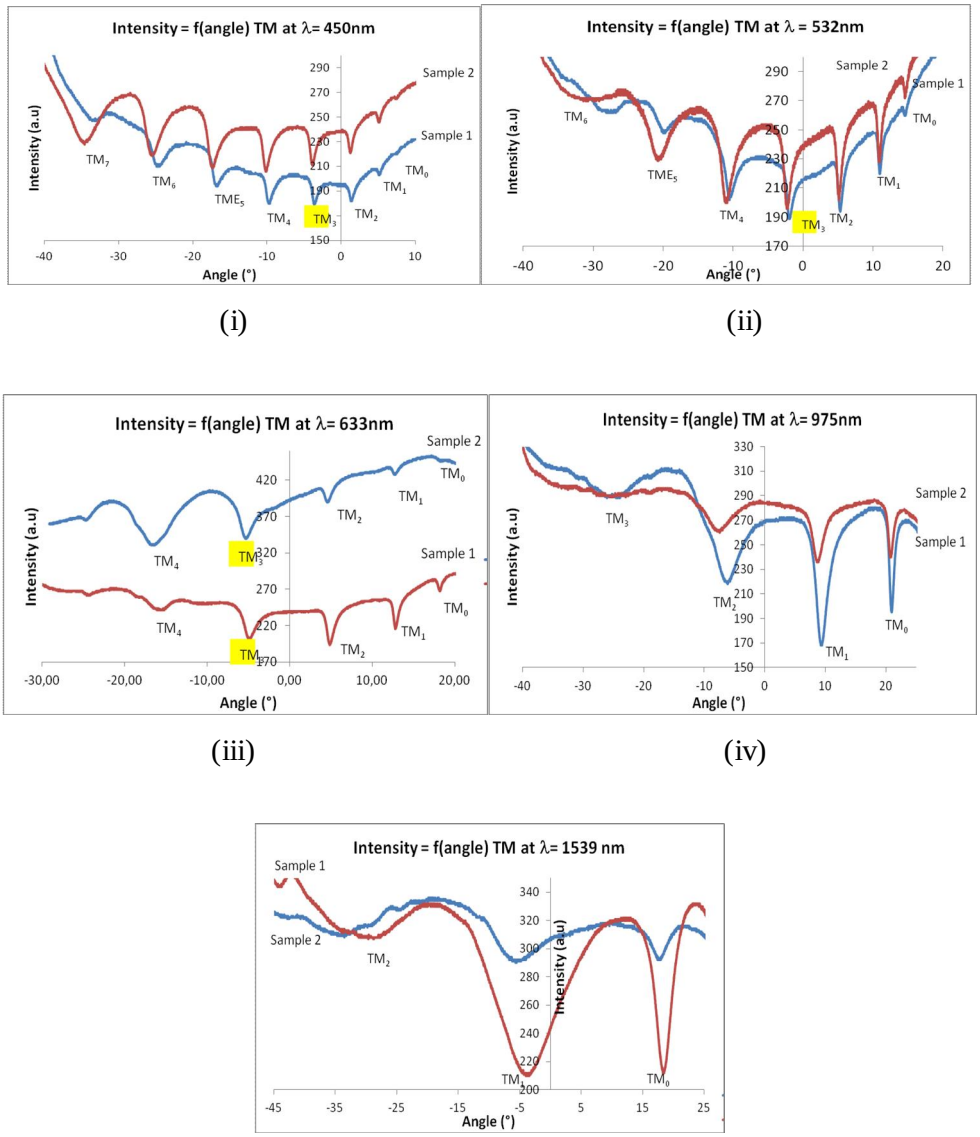

Figure 4.9b. TM mode spectrum of GaN/Si sample-1 and sample-2 comparation at five wavelengths, (i) λ= 450 nm, (ii) λ= 532 nm, (iii) λ= 633 nm, (iv) λ= 975 nm and (v) λ =1539 nm

In the following sections, we propose a detailed optical characterization of the GaN/Si and GaN on sapphire structures using the prism coupling technique. We will consider the refractive index dispersion, the film thickness and we will present additionnal data related to the temperature dependence, the propagation

loss and the birefringence. The comparison of both samples will be interesting in keeping in mind that the Gan/Al_2O_3 is the reference in terms of material quality and optical performance.

4.4. Refractive Index and Thickness for GaN/Sapphire Samples

The refractive index is a key parameter needed to establish a correlation between the optical properties (refractive indices, propagation losses) and the microstructure (morphology, quality of the film/substrate interface). The refractive indices are reported for different wavelengths (532, 633, 975 and 1550) nm, the index accuracy is similar around 10^{-3}. The samples on sapphire are provided by Prof Dimitris Pavlidis from Darmstadt Technical University DTU.

4.4.1. Refractive Index and Thickness for GaN/Al_2O_3 Samples-1

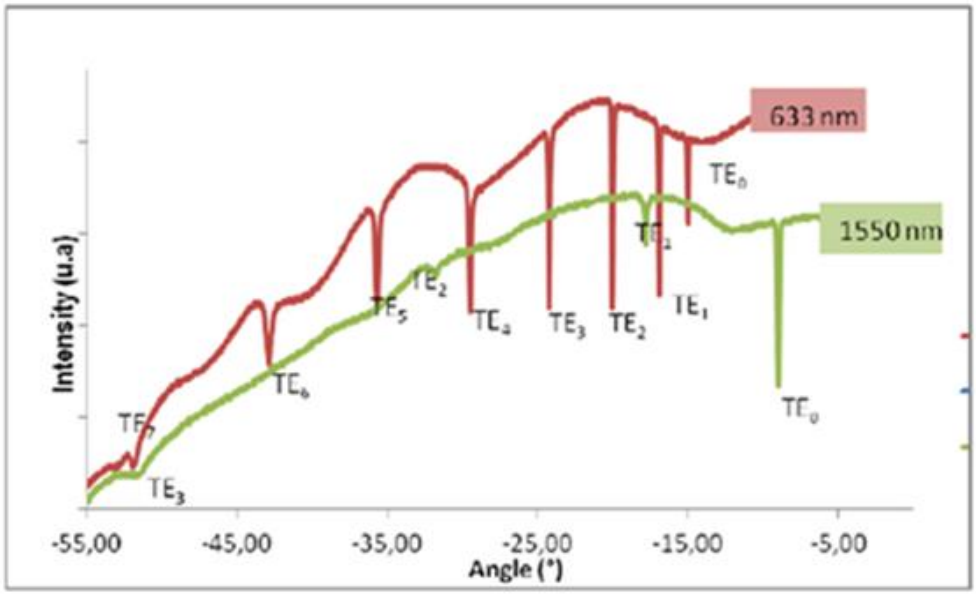

Figure 4.10. TE modes spectrum of GaN/ Al_2O_3 sample-1 at wavelengths λ = 633 nm and 1550 nm

The comparation TE mode spectrum at wavelengths 633 nm and 1550 nm is given in Figure 4.10. At 633 nm has 8 TE modes are excited in the film

with very sharp modes width which is an indication of the film surface morphology. At 1550 nm, the film has 4 TE modes. Figure 4.10 explain about angle and refractive index at fundamental mode for wavelength 633 nm and 1550 nm. Fundamental mode at wavelength λ = 633 nm is 2.352 and λ = 1550 nm is 2.282 respectively.

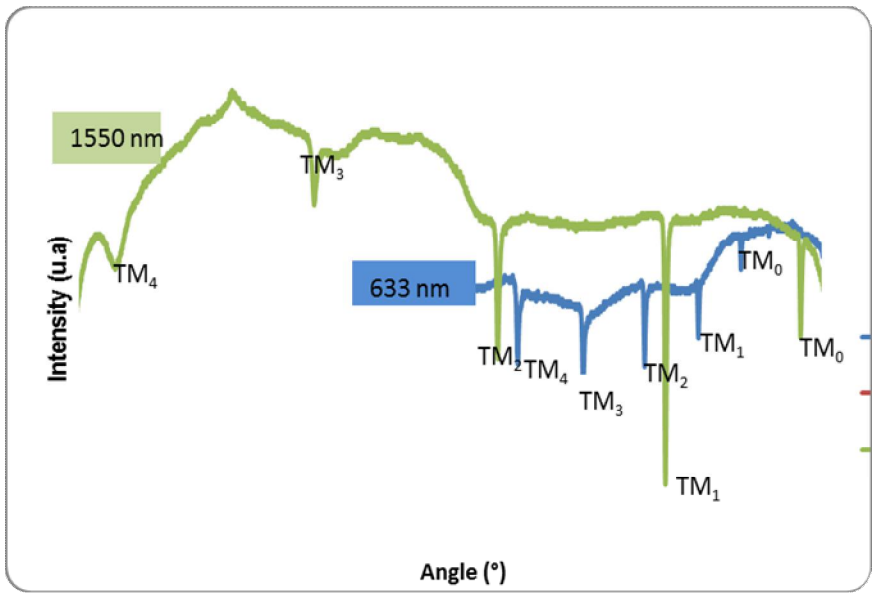

Figure 4.11. TM modes spectrum of GaN/ Al_2O_3 sample-1 at wavelengths λ = 633 nm and 1550 nm

For another polarization, the results for TM modes are given in Figure 4.11. Its shows comparation TM mode spectrum at wavelengths 633 nm and 1550 nm. At wavelength 633 nm, the film has 5 TM modes are excited in the film with very sharp mode width which is an indication of the film surface morphology. At 1550 nm, the film has 5 TM modes. Angle and refractive index at fundamental mode θ_{TM0} = 16.42° and Nm_0 = 2.374 for 633 nm. Also θ_{TM0} = 22.86° and Nm_0 = 2.317 for 1550 nm, respectively.

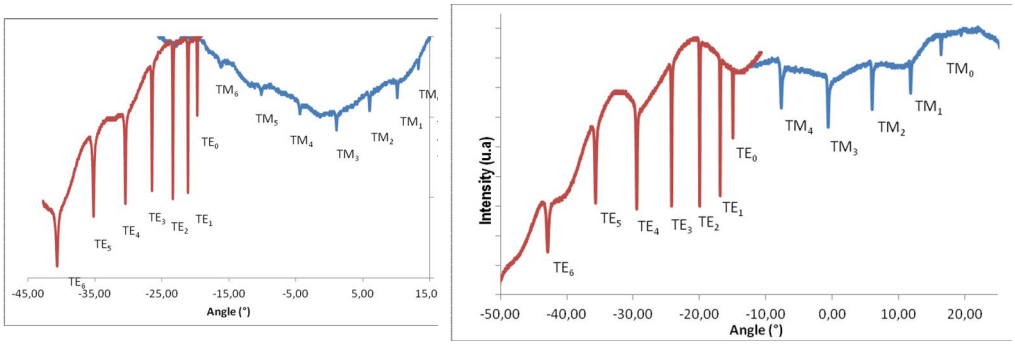

(a) (b)

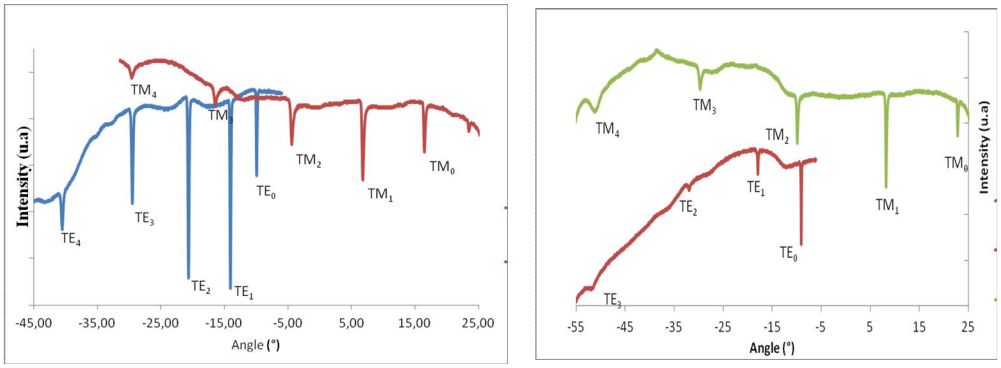

(c) (d)

Figure 4.12. TE and TM modes spectrum of GaN/ Al_2O_3 sample-1 at four wavelengths, (a) λ= 532 nm, (b) λ= 633 nm, (c) λ= 975 nm and (d) λ =1539 nm

The optical analysis using the prism coupling allows us to have the recording of the intensity spectrum as a function of the angle of incidence for wavelengths of 450 nm, 532 nm, 633 nm, 975 nm, and 1539 nm (Figure 4.12.). Two consecutive modes (as TE_0 and TE_1 or TM_0 and TM_1) are required to calculate the refractive index. The associated software automatically calculates the indices corresponding to the modes found with an accuracy of 10^{-3}. For the higher wavelengths, fewer modes are obtained. The wavelength at 532 nm has 7 TE mode and 7 TM mode (Figure 4.12a), at 633 nm has 7 TE mode and 5 TM mode (Figure 4.12b), at 975 nm has 5 TE mode and 5 TM mode (Figure 4.12c.), and at 1550 nm has 4 TE mode and 5 TM mode (Figure 4.12d.). Figure 4.12 shows the optical reflection spectra for different wavelengths, the excited modes are fine and

deep a good indication of the quality of growth material. In literature, the authors [70] have shown that the angular width of the optical excited mode is directly related to the surface roughness of the material. The refractive index measured at GaN/Al_2O_3 sample-1 for the GaN layers are represented in Table 4.6. The layer thickness of GaN/Al_2O_3 sample-1 in TE and TM is plotted with difference wavelengths at Table 4.7.

Table 4.6. Refractive index at different wavelengths for GaN/Al_2O_3 sample-1

GaN/Al_2O_3 sample-1	532 nm	633 nm	975 nm	1550 nm
n TE	2.393	2.352	2.303	2.282
n TM	2.423	2.374	2.340	2.317

Table 4.7. Layer thickness at different wavelengths for GaN/Al_2O_3 sample-1

GaN/Al_2O_3 sample-1	532 nm	633 nm	975 nm	1550 nm
Thickness at TE (µm)	1.760	1.783	1.907	1.943
Thickness at TM (µm)	1.727	1.735	1.869	1.876

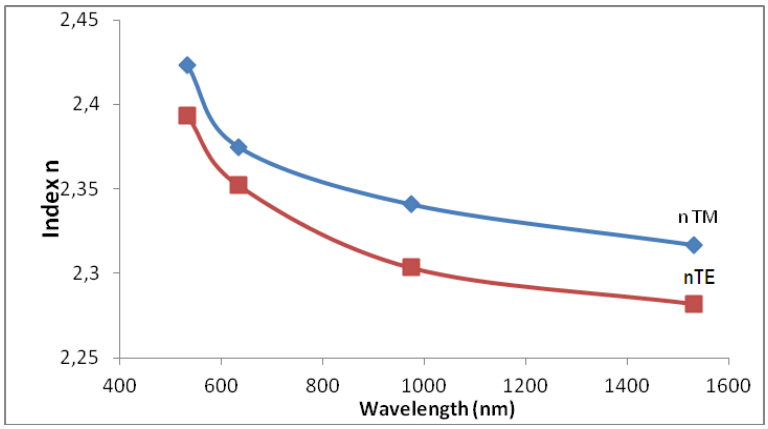

Figure 4.13. Dispersion of refractive index in GaN/Al_2O_3 sample-1.

The dispersion of TE and TM refractive index is plotted in Figure 4.13. A characteristic of the refractive index is its evolution as a function of wavelength,

also called curve dispersion. Figure 4.13, therefore shows the evolution of the refractive index of the GaN layer in TE and TM polarization for different wavelength. Also Figure 4.14 shows the calculation for film thickness in case of GaN/Al_2O_3 sample-1 from optical data. The value reported in Stolz et al [71], the refractive indices for TE mode is n_0= 2.280 and n_e= 2.310 for TM mode. The measurements given in Table 4.6 exhibits value close to the the ones in literature.

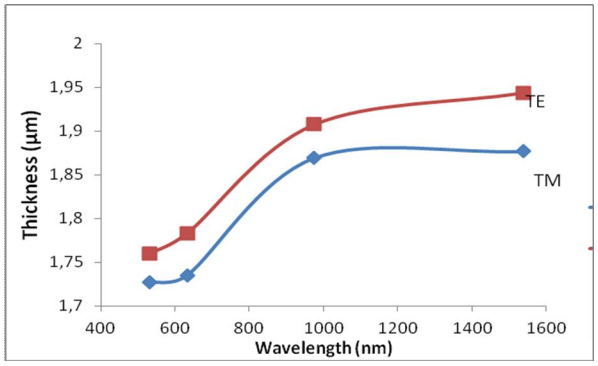

Figure 4.14. Thickness for GaN/Al_2O_3 sample-1 from different wavelengths

It was also possible to investigate optically the film thickness by prism coupling. We have verified the data from the growth process: it is interesting to see that the value is quite changing with the optical laser wavelengths. It is mainly attributed to the interactions of the light with the film/substrate and film/air interfaces.

4.4.2. Refractive Index and Thickness at GaN/Al_2O_3 Samples-2

Table 4.8. The refractive index of GaN/Al_2O_3 sample-2 at two wavelenghts

GaN/Al_2O_3 sample-2	633 nm	1550 nm
n TE	2.338	2.279
n TM	2.378	2.313
Thickness for TE (µm)	1.729	2.083
Thickness at TM (µm)	1.730	2.171

The refractive index measured at GaN/Al_2O_3 sample-2 for the GaN layers are represented in Table 4.8. And it shows thickness of TE/TM mode in GaN/Al_2O_3 sample-2 at 633 nm and 1550 nm wavelengths.

The result of optical measurement has TE/TM mode spectrum of GaN/Al_2O_3 sample-2 at 633 nm and 1539 nm wavelengths represented in Figure 4.15.

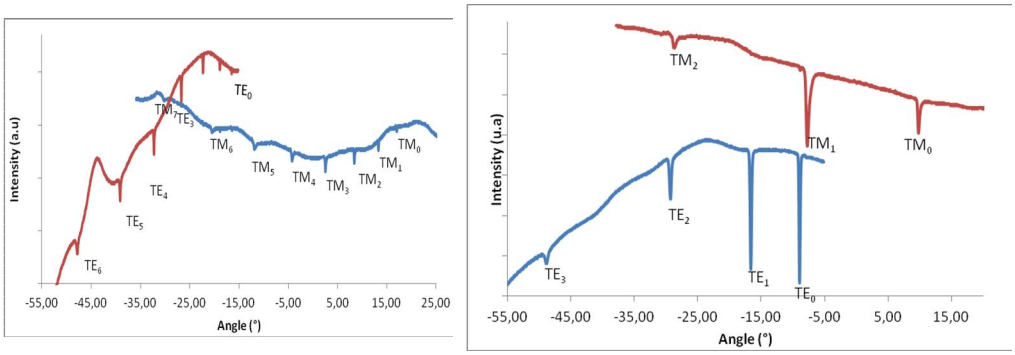

(a) (b)

Figure 4.15. TE and TM modes spectrum of GaN/Al_2O_3 sample-2
(a) At 633 nm and (b) At 1539 nm

4.4.3. Refractive Index and Thickness at GaN/Al_2O_3 Samples-3

In this section, we have considered thickness samples of GaN on sapphire in order to investigate the influence on the optical index. The refractive index measured for GaN/Al_2O_3 sample-3, are represented in Table 4.9. and it shows thickness of TE/TM modes in GaN/Al_2O_3 sample-3 at 633 nm and 1550 nm wavelengths.

Table 4.9. The refractive index of GaN/Al_2O_3 sample-3 at two wavelengths

GaN/Al_2O_3 sample-3	633 nm	1550 nm
n TE	2.351	2.278
n TM	2.392	2.315
Thickness at TE (µm)	2.105	2.184
Thickness at TM (µm)	2.110	2.182

The TE/TM mode spectrum of GaN/Al_2O_3 sample-3 at 633 nm and 1539 nm wavelengths are represented in Figure 4.16.

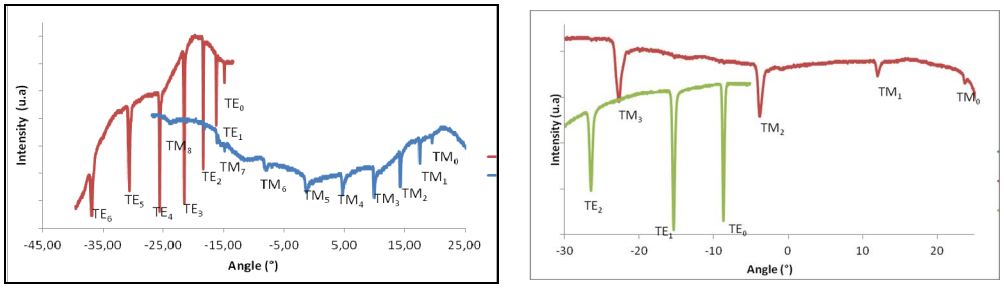

(a) (b)

Figure 4.16. TE and TM modes spectrum of GaN/Al_2O_3 sample-3
(a) At 633 nm and (b) At 1539 nm

4.4.4. Refractive Index and Thickness at GaN/Al_2O_3 Samples-4 and 5

In this work, we have measured the refractive index of GaN/Al_2O_3 sample-4 and sample-5 at the wavelength of 633 nm as shown in Figure 4.17. The result of refractive index are represented in Table 4.10. Table 4.11 gives the thickness measurement of GaN/Al_2O_3 sample-4 and sample-5.

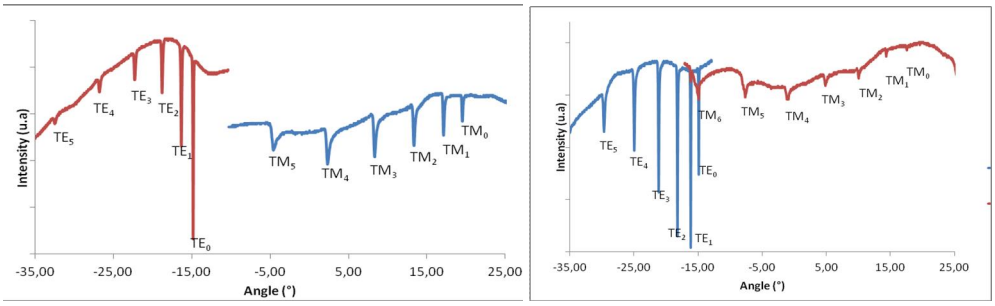

Figure 4.17. TE/TM mode spectrum of GaN/Al_2O_3 at 633 nm
(a) sample-4 and (b) sample-5

Table 4.10. The refractive index of GaN/Al_2O_3 sample-4 and sample-5

Mode of refractive index	GaN/Al_2O_3 sample-4	GaN/Al_2O_3 sample-5
n_{TE}	2.339	2.351
n_{TM}	2.370	2.359

Table 4.11. The thickness index of GaN/Al_2O_3 sample-4 and sample-5

Mode of thickness	GaN/Al_2O_3 sample-4	GaN/Al_2O_3 sample-5
d_{TE}	1.645 µm	2.090 µm
d_{TM}	1.689 µm	2.031 µm

The reflectivity dips observed at certain angles correspond to the excitation and propagation of guided modes in the film structure. These very sharp modes indicate a good film quality of the active GaN epilayer [70-72]. The anisotropy properties of the GaN/Al_2O_3 samples at 633 nm is given in Equation 4.2 and Tabel 4.12 is representation of anisotropy properties of sample 1- sample 5 at wavelength 633 nm.

$$\Delta n = n_{TE} - n_{TM} \quad (4.2)$$

Table 4.12. Refractive Index at wavelengths 633nm in 5 samples of GaN/Al_2O_3

At 633nm wavelenght	n_{TE}	n_{TM}	Δn ($*10^{-2}$)
Sample-1	2.352	2.3001	5.19
Sample-2	2.3383	2.3713	-3.3
Sample-3	2.3521	2.3790	-2.69
Sample-4	2.3517	2.3927	-4.1
Sample-5	2.3516	2.3593	-0.77

4.5. Optical Analysis of GaN Films Surface Roughness

We present here an analysis of optical measurement that can be correlated to the film microstructure. It is possible to evaluate by optical means, the roughness of the surface layer using the spectrum data. In some studies on lithium niobate

[70, 73], authors have correlated the angular half-peak width of the excited mode to surface roughness. From the calculation of the full width at half maximum of TE0 mode ($\Delta\theta$), one can estimate the roughness of layer (r_{ms}) by optical mean. In fact, the prism coupling experiment can be considered as an optical AFM.

$\theta pd = 0.1°$ in correlation with roughness $r_{ms} = 2$ nm [70]

We have applied this result to our GaN structures. By repeating the TE spectrum at various wavelengths (532 nm to 1550 nm) in the Figures 4.18, we have report the angular half-height $\Delta\theta$ of the fundamental modes.

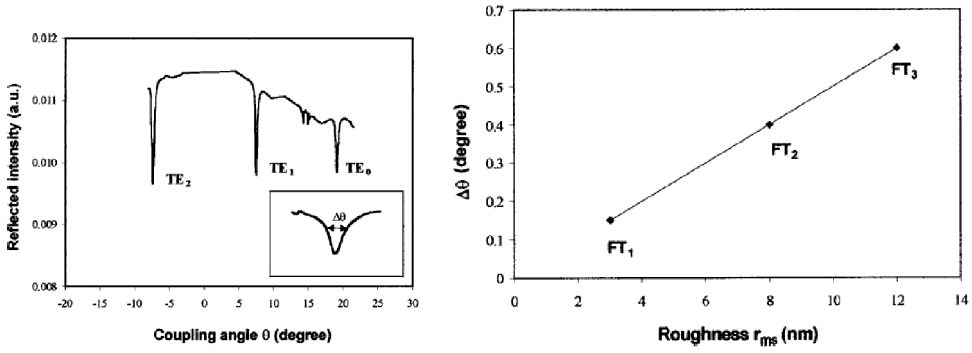

(a) (b)

Figure 4.18. (a) Guided-mode spectrum obtained by measuring the reflected intensity versus the angle of indicidence (b) Relationship between the width of dips (θpd) and the surface roughness from AFM study.

In TM polarization, we have obtained an index value of 2.282 for a thickness of 1.943 µm. It seems that the propagation takes place in GaN planar waveguide. The calculation is not possible at 450 nm since only one mode is found (the minimum is two consecutive modes).

4.5.1. Roughness Analysis for TE0 Mode Applied to GaN/Sapphire Sample-1

Figure 4.19 to Figure 4.20 represents the angular width (FWHM) obtained for the first TE0 mode in the GaN/Al_2O_3 sample-1. We have repeated this

operation at different wavelengths 532 nm, 633 nm, 975 nm and 1550 nm in order to investigate the influence of interaction light ï matter on the results . Reflectivity dips indicate the excitation of specific guided modes in the GaN film and we can see their sharpness. This is a good indication of light confinement in the waveguide. As example, the result in Figure 4.19 (a) gives qpd around 0.107° and the extrapoled roughness r of 2.14 nm.

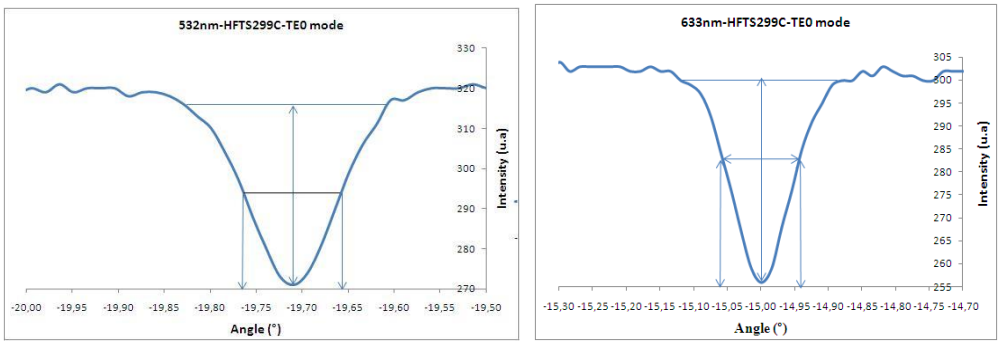

(a) (b)

Figure 4.19. Angular width Δθ of TE0 mode reported for sample-1 at different wavelengths (a) λ = 532 nm and (b) λ = 633 nm

Results obtained in Figure 4.20 for a wavelength of 1539 nm show an angular width qpd= 0.126° and roughness r = 2.52 nm. We can state that the average roughness of the GaN/Sapphire Sample-1 film measured by optical tool is around 2.1-2.6 nm for differents wavelengths.

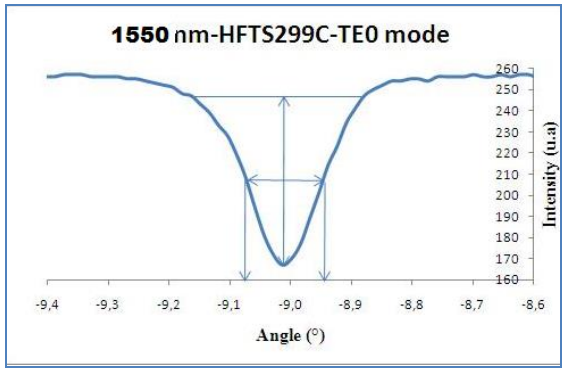

Figure 4.20. Angular width qpd of TE0 mode reported for sample-1 at wavelegth λ = 1550 nm.

Table 4.13. Synthesis of measurements at different wavelengths for GaN/Al_2O_3 sample-1

Wavelength (nm)	532	633	975	1550
TE mode width qpd	0.107°	0.108°	0.132°	0.126°
Roughness rms (nm)	2.14	2.16	2.64	2.52

4.5.2. Roughness Analysis for GaN/Al_2O_3 Sample-2 and Sample-3

In this section, a similar study will be reported for different thickness samples (2 µm for Sample-2 and Sample-3) in order to compare the influence of thickness on the reported data.

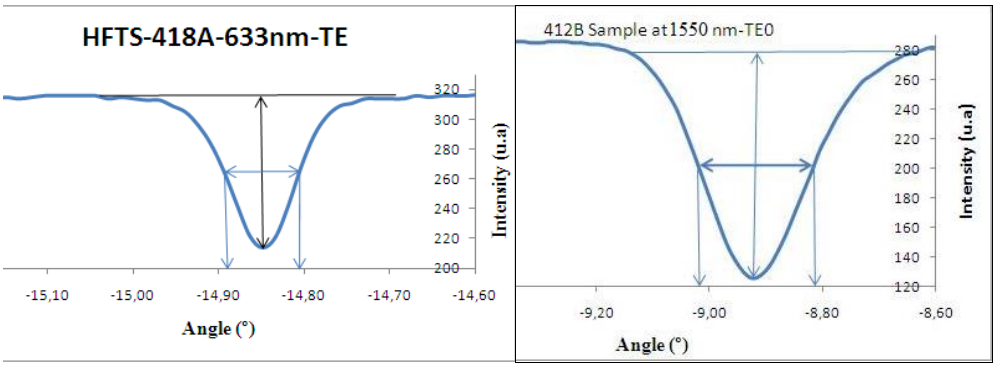

(a) (b)

Figure 4.21. Angular width Δθ of TE0 mode for sample-2 at wavelength (a) λ= 633 nm and (b) λ= 1530 nm

Results in Figure 4.21 for 2 µm thick GaN show qpd = 0.103° and the estimated roughness r = 2.06 nm (λ = 633 nm). When the wavelength is shifted to 1530 nm, qpd increases significantly (Δθ = 0.19°) and the correlated roughness r is 3.8 nm. We can observe the thicker samples present more inhomogenities and defect at the interface and the interaction with the laser beam induces more changes in the optical response. All investigated samples give a similar information for the correlation between optics and the microstructure of GaN. Results summarized in Table 4.14, it show same values qpd in the range around 0.08 to 0.1° and roughness r between 1.6 to 2 nm.

Table 4.14. Summary of results for films analyzed at wavelegth λ = 633 nm

	Sample-2	Sample-3	Sample-4	Sample-5
TE mode width (Δθ)	0.103°	0.09°	0.08°	0.08°
Roughness rms (nm)	2.06	1.8	1.6	1.6

Results obtained at 1530 nm are quite different as shown in Table 4.15 and the roughness of GaN/Al_2O_3 films is around 3.8 - 5.2 nm. The reflectivity dips is more large indicating a worst material quality for a thicker layer.

Table 4.15. Roughness of the GaN/Al_2O_3 films measured by optical tool at wavelegth λ =1550 nm

GaN/Al_2O_3	Sample-2	Sample-3
TE mode width (qpd)	0.19°	0.26°
Roughness rms (nm)	3.8	5.2

4.5.3. Roughness Analysis for Fundamental Mode of GaN/Si Samples

As already written, GaN on sapphire is the best material structure and we propsoe to compare with the GaN/Si structure. Fundamental modes of GaN/Si samples at 1550 nm are represented in Figure 4.22 (sample 1) and Figure 4.23 (sample 2). Result indicates a dependance on the material quality with a higher angular width qpd of 1.3 and 1.8 corresponding to a surface roughness in the range 26 nm and 38 nm respectively, The results are summarized in Table 4.16. The GaN/Si films has roughness more large than GaN/Al_2O_3 films, it is means Ga/Si less light confinement in the waveguide.

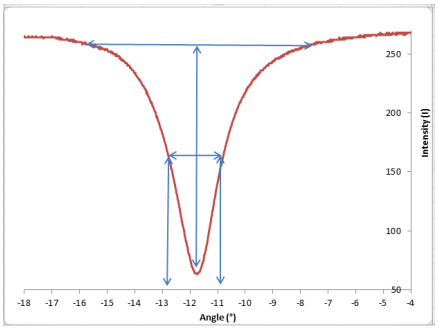

Figure 4.22. Angular width Δθ of TE0 mode for GaN/Si sample-1 at wavelegth λ= 1550 nm.

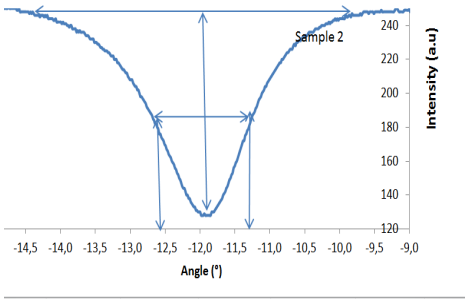

Figure 4.23. Angular width Δθ of TE0 mode for GaN/Si sample-2 at wavelegth λ= 1550 nm.

Table 4.16. Roughness of the GaN/Si film at wavelegth λ = 1550 nm

GaN/Si films	Sample-1	Sample-2
TE mode width (Δθ)	1.3°	1.9°
Roughness rms (nm)	26	38

There is a big difference surface roughness between an AFM and optical measurement by equation. In optical prism coupling measurement, the light is reflected at air - film interface and substrate - film interface. The interaction light - matter is only limited at these two interface and the interaction is very sensitive to quality of the interface as well as to the film quality. The optical signal is correlated to the film microstructure. We have considered that the width of the TE0 mode in the spectrum is correlated to the surface morphology.

In GaN deposited on sapphire, the lattice mismatch is small, the density of dislocations is very limited. The global microstructure is good with the benefit of the buffer layer as studied during two decades by researchers in the community. The global quality of the GaN layer shows a very small width in the optical spectrum. The optical analysis of roughness is in agreement with the direct AFM measurement ($\Delta\theta = 0.1°$ for roughness of 2 nm)

In GaN on Silicon, the lattice mismatch is very important and cracks appear in the top surface and many dislocations are observed at the interface and in the film volume. The interaction of the light with the matter is different here: many diffusion of the light exists in the dislocations and at the interface. This is the reason why the width of the TE0 mode is more important. In that case, this relation (($\Delta\theta = 0.1°$ for roughness of 2 nm) is not valide because of the number of defect inside the GaN layer due to Silicon. We have obtained more important surface roughness by optics compared to direct AFM analysis. We can conclude that this relation (($\Delta\theta = 0.1°$ for roughness of 2 nm) is mainly valid for homogenous film without cracks or internal defects.

4.6. Analysis of Temperature Dependence into GaN Films

The influence of the temperature on the refractive index is measured in this section. For these measurements, we have used a temperature system (thermo-coupler) associated to the prism coupling set-up as shown in Figure 4.24, the temperature range is between 20 - 150 °C. The prism P-200-6013.6 2-60 (TiO2 Rutile) is maintained. In the experiment, we have limited to a value around 100 °C in order to avoid prism set-up degradation.

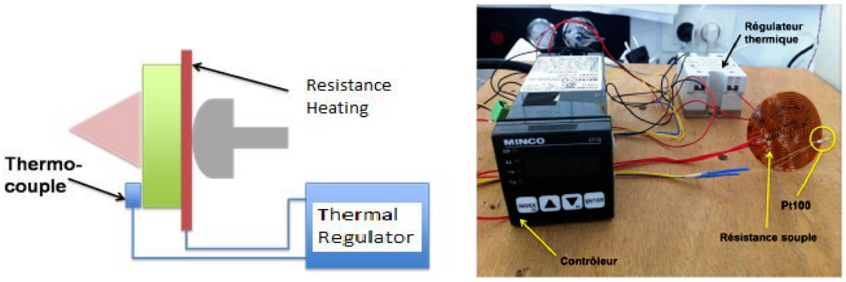

Figure 4.24. Principle of temperature measurement and experimental set up

4.6.1. Temperature Dependence into at GaN films

The effect of temperature on GaN films (GaN/Al_2O_3 and GaN/Si) is evaluated through the change refractive index and the thickness. This effect represented in Table 4.17 (GaN/Si) and Table 4.18 (GaN/Al_2O_3).

Table 4.17. Refractive index of GaN/Si at different temperatures

T (°C)	T (°K)	Index (TE)	ThicknessTE (µm)	Index (TM)	ThicknessTM (µm)
30	303	2.355	1.307	2.400	1.375
36	309	2.356	1.304	2.391	1.371
42	315	2.357	1.299	2.389	1.394
52	325	2.357	1.302	2.390	1.380
57	330	2.358	1.303	2.388	1.367
63	336	2.359	1.301	2.389	1.380
68	341	2.359	1.299	2.389	1.371
73	346	2.360	1.301	2.393	1.387
78	351	2.361	1.300	2.395	1.382
83	356	2.361	1.302	2.395	1.383
88	361	2.362	1.303	2.396	1.377
94	367	2.363	1.301	2.397	1.375
100	373	2.363	1.304	2.398	1.378

Table 4.18. Refractive index of GaN/Al_2O_3 at different temperatures

T (°C)	T (°K)	Index (TE)	ThicknessTE (µm)	Index (TM)	ThicknessTM (µm)
23	296	2.351	2.174	2.361	2.174
24	297	2.351	2.172	2.392	2.177
26	299	2.351	2.169	2.392	2.173
27	300	2.351	2.351	2.360	1.793
30	303	2.351	2.163	2.392	2.163
32	305	2.351	2.166	2.392	2.176
34	307	2.351	2.167	2.386	1.439
40	313	2.352	2.173	2.382	1.82
50	323	2.353	2.174	2.382	1.808
60	333	2.3538	2.174	2.363	1.561
65	338	2.354	2.176	2.383	1.831
70	343	2.354	2.170	2.383	1.826
75	348	2.355	2.170	2.384	1.825
80	353	2.355	2.178	2.384	1.850
85	358	2.356	2.169	2.385	1.801
90	363	2.356	2.356	2.385	1.823
95	368	2.356	2.174	2.385	1.783
100	373	2.356	2.174	2.365	1.524

4.6.2. Evolution of the Refractive Index versus Applied Temperature

Test of stability in temperature of the refractive index at GaN/Al_2O_3 is realized on the layer and are presented in Figure 4.25. The influence of the refractive index is given in the Equation 4.2 - 4.5:

1. Index TE graphic is; $y = 7.55.10^{-5}x + 2.329$ (4. 1)

   It means slope $\frac{\Delta n\,(TE)}{\Delta T} = 7.55.10^{-5}/^{o}K$ (4. 2)

2. Index TM graphic is; $y = 6.525.10^{-5}x + 2.362$ (4. 3)

   It means slope $\frac{\Delta n\,(TM)}{\Delta T} = 6.525.10^{-5}/^{o}K$ (4. 4)

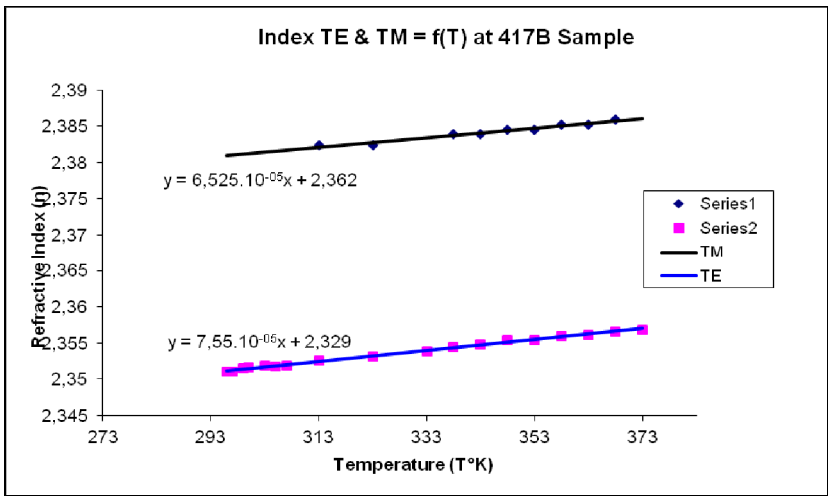

Figure 4.25. Influence of the refractive index versus temperature (GaN/Al_2O_3 Sample)

Figure 4.26 gives an indication of stability in temperature for the refractive index, thus for GaN/Si film. Based on Figure 4.26, stability in temperature of GaN/Si samples is $(1.227 - 1.77)10^{-4}/°K$

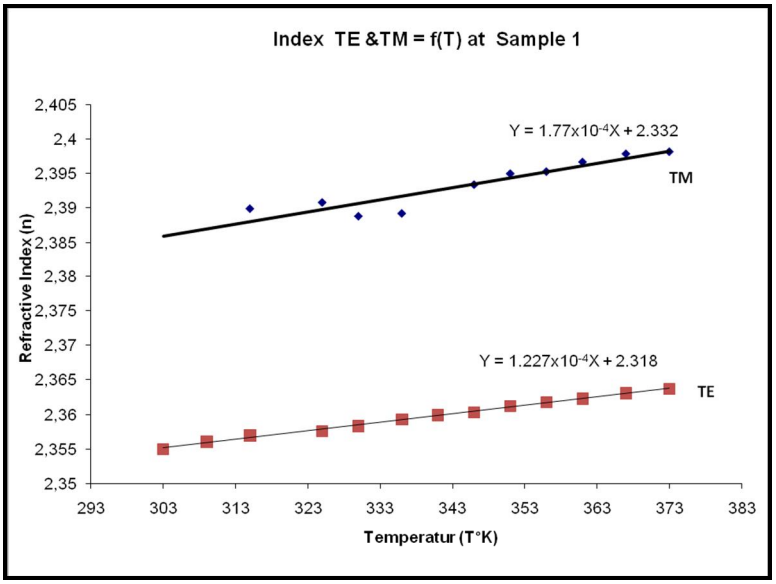

Figure 4.26. Influence of the refractive index versus temperature (GaN/Si Sample)

In the temperature range 20°C - 100°C, the evolution of the index as a function of temperature is about (6.525 - 7.55).10^{-5}/°K on the GaN/Al_2O_3 and (1.227 - 1.77).10^{-4}/°K on GaN/Si film respectively. This value is almost independent of the optical polarization. In these two modes, the variation index is the same order of magnitude (1-10).10^{-5}/°K. The value same with reference in stolz et al for GaN/sapphire [71].

4.7. Optical Loss Measurement of GaN films

The optical transmission loss is one the main parameter for the device study and fabrication. The measurements of optical loss for in TE and TM modes are performed for different wavelengths. For each measurements, we have used the prism P-200-6013.6 2-60 (TiO2 Rutile) as shown in

(a) (b)

Figure 4.27. The prism coupling set-up calculates the optical loss from the scattered light collected on top of the surface as shown below.

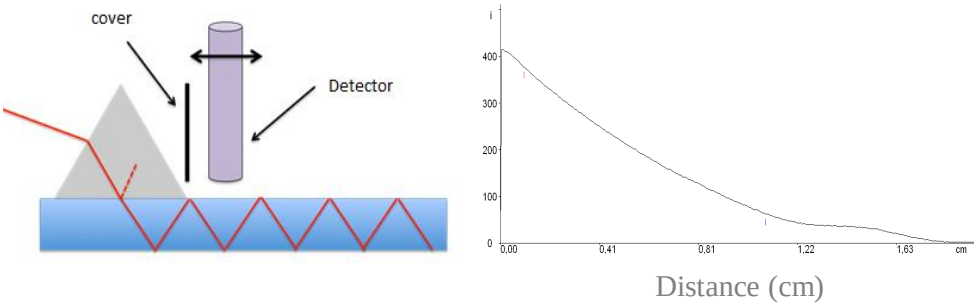

(a) (b)

Figure 4.27. (a) Set up for optical loss characterization and (b) light scattered from the top surface of GaN planar waveguide

4.7.1. Optical Loss Measurement into GaN/Al_2O_3 Films

The description of sample structure provided by Darmstadt Technical University (DTU), is shown at Figure 3.2 (c). The evolution of the recorded intensity is following this equation :

$$Ln (I) = A - B*x \quad \text{for TE and TM modes}$$

with I: Intensity measured, x: the propagation distance, A and B: constants.

Results of optical loss measurement obtained at different wavelengths for GaN/Al_2O_3 samples are given below:

a. At 633 nm (for Modes TE and TM):

At wavelength 633 nm, the measurement indicates an optical loss of 1.34 dB/cm for TE Mode and 3.10 dB/cm for TM mode. We have extrapoled the slope for the curve in Figure 4.28 in agreement with the following equation:

Ln (I) = 5.198 - 0.308x (TE Mode) and Ln (I) = 5.129 - 0.713x (TM Mode)

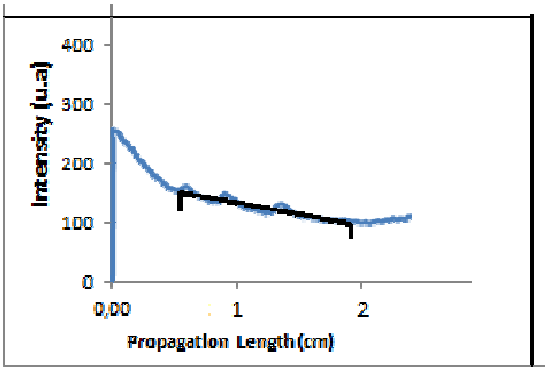

Figure 4.28. Optical loss in GaN/Sapphire at 633 nm (for TE mode)

Taking a value x in centimeter in Figure 4.28 and Figure 4.29, we can calculate the optical losses are around 1.34 - 5.34 dB/cm, this is relatively consistent with literature values: 4.8 dB/cm for GaN or 1.8 dB/cm for AlGaN to 633 nm represented in Figure 4.27Figure b [71]. Value for x in optical loss measurement can be seen in Table 4.19 and Tabel 4.20.

b. At 1550 nm (TE and TM)

Figure 4.29 shows the optical loss experiments at λ = 633 nm and 1550 nm (for TE Mode). The measurement indicates an optical loss of 1.07 dB/cm for TE Mode and 0.98 dB/cm for TM mode. We have extrapoled the slope for the curve in Figure 4.29

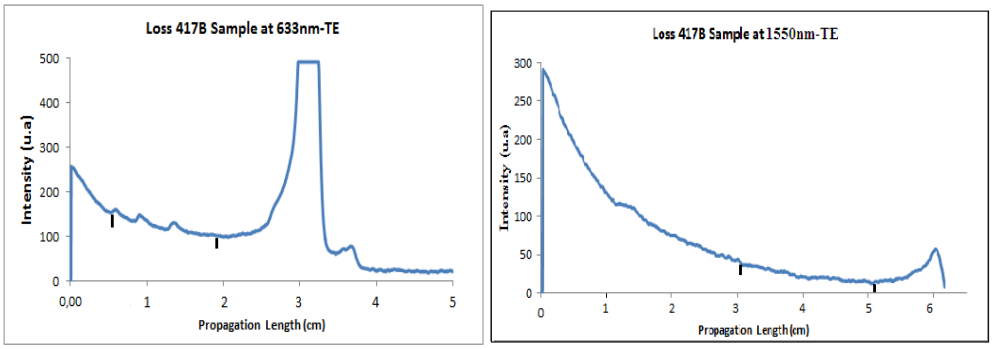

(a) (b)

Figure 4.29. TE Optical loss in GaN/Al_2O_3 at (a) 633 nm and (b) 1550 nm

In the litterature, similar values are reported in the same film configuration [71]. The Figure 4.30 reported a detailled study giving the evolution of optical losses with l. At 1.55 µm, the target wavelength for our future application, the losses are small enough, around 1 dB/cm which is sufficient for device development.

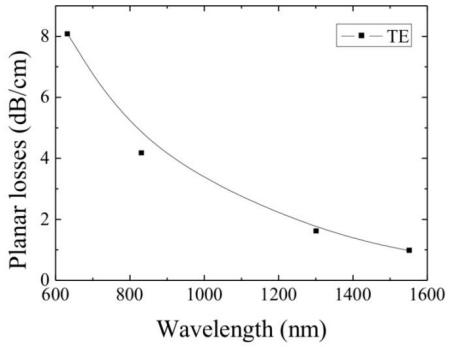

Figure 4.30. Literature review of waveguide loss for GaN/Sapphire (TE mode) [71]

Table 4.19. Comparison of refractive index and optical loss at two wavelengths (GaN/ Al_2O_3 sample-3 at TE mode)

Wavelength (nm)	633	1550
Refractive Index	2.346	2.278
Loss dB/cm	5.34	1.07

Table 4.20. Comparison of refractive index and optical loss at two wavelengths (GaN/ Al_2O_3 sample-3 at TM mode)

Wavelength (nm)	633	1550
Refractive index	2.387	2.315
Loss (dB/cm)	5.10	0.98

These loss values are indicative; we can always observe lower values for TM polarizations.

4.7.2. Optical Loss Measurement into GaN/Si Films

We have also considered the case of GaN/Si films structure: we have already explained that this structure is worst different in terms of material quality and this could be determined with the lower optical properties. The first attempts showed optical loss greater that 2.58 dB/cm at 633 nm as shown in Figure 4.31. This value can give indication about the further progress. For a better microstructure, one can imagine optical loss in the range 1 - 2 dB/cm, therefore GaN/Si could be good material for waveguiding applications.

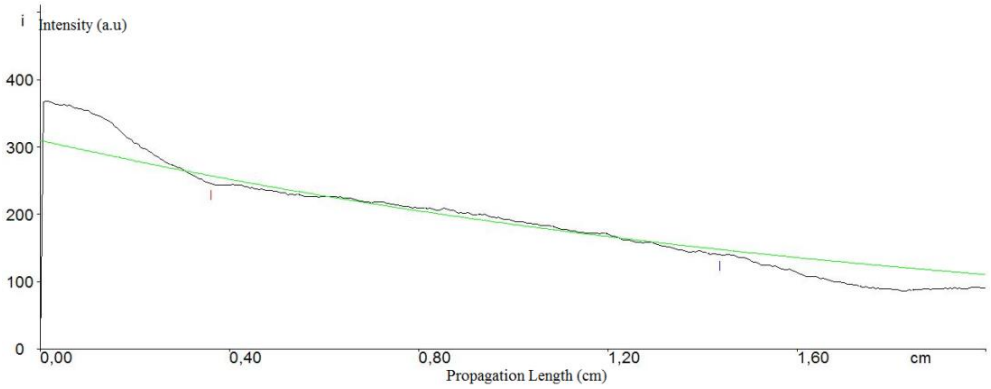

Figure 4.31. Optical loss of GaN/Si Sample-1 (TE Mode) at λ = 633 nm

4.8. Analysis of Birefringence

In theory, the birefringence is the decomposition of a ray of light into two rays when it passes through anisotropic materials. The effect was described by Rasmus Bartholin in 1669, who saw it in calcite [74]. The effect is now known also to exist in various materials as magnetics or non-crystalline materials [75]. The structure of the material has an axis of symmetry with no equivalent axis in the plane perpendicular to it. This axis is known as the optical axis of the material. Therefore, the light with linear polarizations parallel and perpendicular to to this axis has different refractive indices, the extraordinary index n_e and the ordinary index n_o. In case of non polarized light is entering the material at a non-zero angle to the optical axis, the component with polarization perpendicular to this axis will be refracted in agreement with the standard law of refraction, while the complementary polarization component will refract at a nonstandard angle determined by the angle of entry and the difference between the indices of refraction, it is known as the birefringence magnitude [76]. The light will split into two linearly polarized beams, known as ordinary and extraordinary.

4.8.1. Refractive Index Dispersion for GaN/Si Sample-1 and Sample-2

By measuring the reþected intensity I versus the angle of incidence to the normal of the prism θ, it is possible to plot the guided-mode spectrum of the sample. The reþectivity dips observed at certain angles correspond to the excitation and propagation of TE/TM guided modes in the ýlm structure [70-72]. These very sharp modes indicate a good film quality of the active GaN epilayer. In case of the samples used in this study and with the optical axis normal to the surface, the ordinary and extraordinary modes are excited by using TE and TM polarized light. The Figure 4.32 and Figure 4.33 shows the refractive index dispersion curves for GaN/Si. The thickness of GaN allow us to visualize number of guided modes for wavelength ranging from 450 to 1539 nm, indicating that the optical beam propagates in the high index film deposited on top of low index substrate. We note that the refractive index decrease witht the the wavelength

increase. The refractive index from the different configuration of GaN/Si samples (thick or thin) is quite similar.

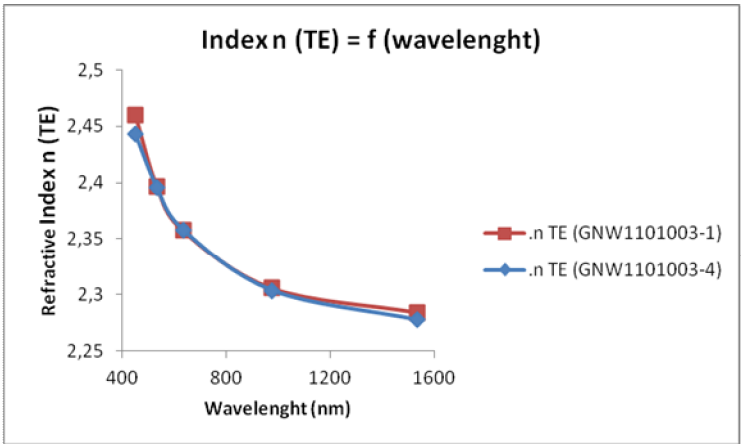

Figure 4.32. Dispersion of refractive index (TE mode) at GaN/Si sample 1 and 2

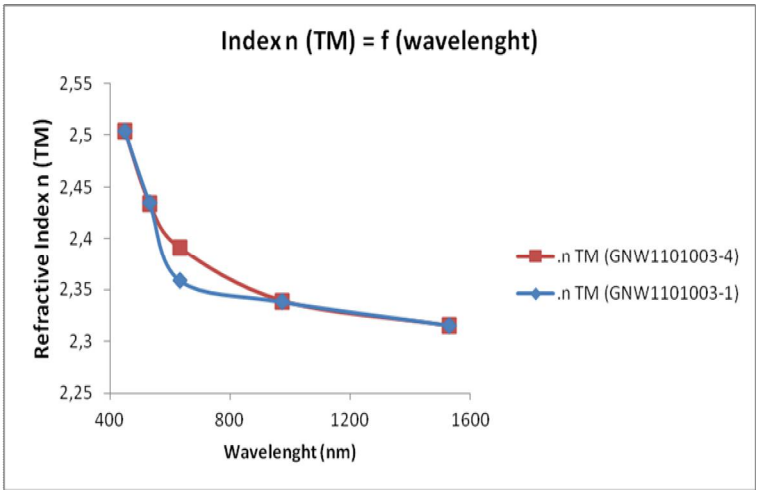

Figure 4.33. Dispersion of refractive index (TM mode) at GaN/Si sample-1 and sample-2

4.8.2. Evolution of Refractive Index for TE and TM Modes for GaN/Si

We report here the comparison of index for two type of GaN/Si structure (sample-1 and 2). The index dispersion (for TE and TM modes) are reported in Figure 4.34 and Figure 4.35 and the calculated birefringence is given in Table 4.21 and Table 4.22.

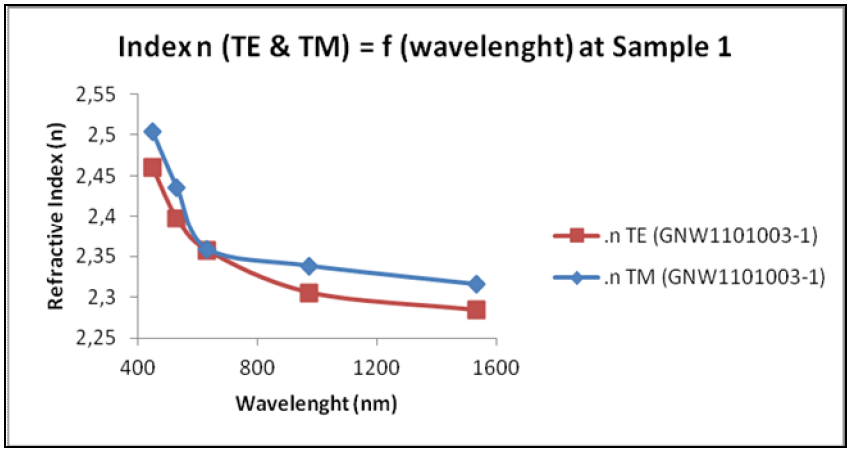

Figure 4.34. Dispersion of refractive index (TE/TM modes) ï GaN/Si sample 1

One can oberve that the birefringence is negative for GaN/Si structure as result in Table 4.21 and Table 4.22. As well know, materials are classified under positively or negatively birefringence. When the light with having parallel and perpendicular components, enters directly to the optic axis, the refractive index of light polarized parallel to the optic axis is greater (or smaller, respectively) than light polarized perpendicularly to the optic axis [74].

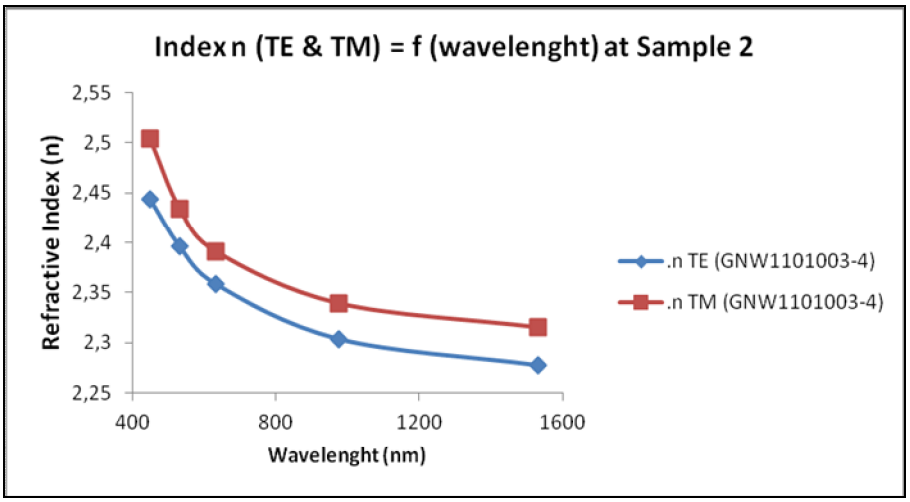

Figure 4.35. Dispersion of refractive index (TE/TM modes) at GaN/Si sample 2

Table 4.21. Birefringence Δn calculated for GaN/Si samples 1

λ (nm)	n_{TE1}	n_{TM1}	$\Delta n = n_{TE1} - n_{TM1}$
450	2.4601	2.5043	-0.0442
532	2.397	2.4349	-0.0379
633	2.3575	2.3591	-0.0016
975	2.3056	2.3382	-0.0326
1539	2.2841	2.3155	-0.0314

Table 4.22. Birefringence Δn calculated for GaN/Si sample 2

λ (nm)	n_{TE2}	n_{TM2}	$\Delta n = n_{TE2} - n_{TM2}$
450	2.4433	2.5039	-0.0606
532	2.3961	2.4342	-0.0381
633	2.3583	2.391	-0.0327
975	2.3037	2.339	-0.0353
1539	2.2776	2.3149	-0.0373

4.8.3. Comparation TE modes for GaN on Silicon and Sapphire

The analysis of samples GaN/Si and GaN/Al_2O_3 in terms of index dispersion is reported in Figure 4.36. The index ranges from 2.48 at 454 nm (blue) to 2.28 at 1539 nm (near IR).

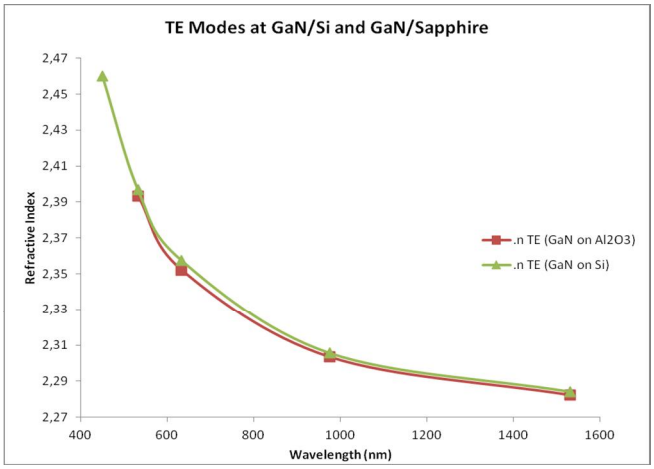

Figure 4.36. Dispersion of Refractive index for GaN/Si and GaN/Sapphire

We can observe a close behavior between GaN/Si and GaN/Al_2O_3, its mean GaN/Si, whatever the material quality is better on sapphire. Locally, the defects have less influence on the refractive index value while for propagation loss along the film ï substrate interface, the difference is greater between Si and Al_2O_3 substrates. This point should be more studied with different configuration of samples deposited in silicon substrates.

4.9. Electro-Optical Characterization of Gallium Nitride Film

In this part, we will introduce the optical properties that are influenced by the electrical signal. In particular, certain materials change their refractive index when an electric field is applied thorugh the layer. This effect is caused by the forces distorting the orientation and the positions of the elements constituting the material. This effect is called the electrooptic effect: this is the change in the refractive index resulting from the application of a DC or AC low-frequency electric field [76]. For electrooptic characterization of thin film, the well known techniques are based on interferometric, polarimetric and prism-coupling [77- 80]. We have identified the prism coupling technique that requires a GaN/Si planar waveguide configuration with a top metallic electrode.

4.9.1. Process of Electrode Manufacturing at GaN film

The top metallic electrode is deposited on GaN layer using the technological process. In order to clean the GaN films sample, a solution remover 'pirahna' is applied to remove organic compounds and then deoxidation GaN by a water/hydrochloric acid (H_2O/HCl 37%) with 1: 1 ratio.

In order to evaluate the properties of the continuous electric field structure, the sizes electrode is large (of the order of 1 cm square). It is possible to use both optival lithography or metallic shadow masks. These masks are mechanically cut from a brass plate of a few hundred microns thick. Then, we have simply attached

masks to the samples during the deposition of metal. The metallization edges by using Argon etching and Evaporation of gold (Au) for a total thickness of 40 nm as show in Figure 4.37.

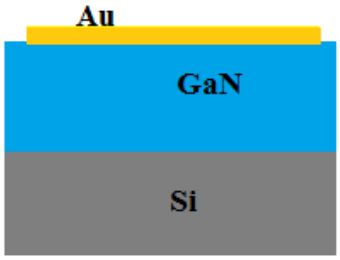

Figure 4.37. Top electrode configuration: Argon etching and evaporation-Au 40 nm on GaN/Si thin film

In the past, we have investigated the static electro-optic effects using GaN/Si configuration: the pockels effect was demonstrated showing an index variation Δn of 10^{-2} in a 1 µm thick GaN layer [71]. We consider here the case of dynamic effect when AC signal is applied thorugh the film.

In our experimental, Si substrate is doped in order to behave as a bottom electrode. To finalize this GaN/Si structure in a diode configuration, it is necessary to form an ohmic contact. Position ohmic contact on the rear face of the sample in the case of a conductive substrate, or on the highly doped layer on sapphire substrate. The choice of a silicon substrate doped n^+ ohmic contact induces a Ti/Au (Titanium/Gold). A Ti (20 nm)/Au(200 nm) ohmic contact was deposited by RF sputtering directly on the doped silicon substrate to form a back electrode. This contact made by RF sputtering since the thickness of the contact is not critical as shown in Figure 4.38. The RF sputtering Ti using power (P) 250 W, etching Ar 30 sccm, time (t) 45 s, and Ti thickness 20 nm. Then, RF Sputtering Au use power (P) 250 W, etching Ar 30 sccm, during time (t) 140 s, and Au thickness 200 nm.

In order to apply an electric ýeld through the GaN ýlm, a transparent 40 nm -Au top electrode was deposited as Schottky contact by e-beam evaporation after an Ar etching [81].

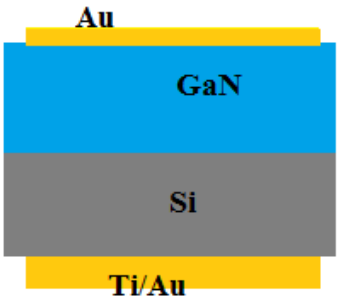

Figure 4.38. Realisation of ohmic contact by RF sputtering

This contact made by the RF sputtering Ti using power (P) 250 W, etching Ar 30 sccm, time (t) 45 s, and Ti thickness 20 nm. And then, RF Sputtering Au use power (P) 250 W, etching Ar 30 sccm, during time (t) 140 s, and Au thickness 200 nm. Platinum wires are then pasted to these electrodes using a thermo-conductive resist. Realisation of ohmic contact by RF sputtering as shown in Figure 4.38 and Figure 4.39 show the picture of GaN/Si sample with Au electrode size of 25 mm^2.

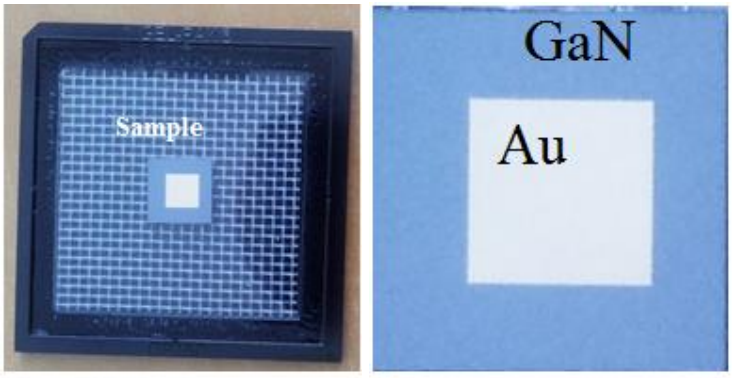

Figure 4.39. An ohmic contact deposted into GaN/Si

4.9.2. Static Characterization of the Electro-Optic Effect

In this section, we report the electrooptic effect in GaN films grown on doped silicon, the DC voltage is used here. Prism-coupling is used to measure the optical properties and we have applied this technique to measure the electro-optic effect. By analyzing the variation of refractive index into the GaN thin film when applying an transversal electric field, one can extract the electro-optic properties. The experimental procedure is given in Figure 4.40.

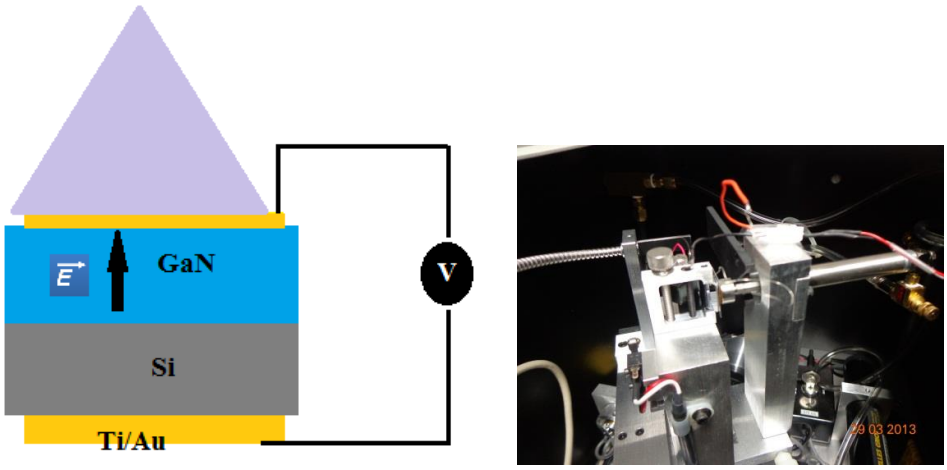

Figure 4.40. (a) Application of voltage into GaN film and direction of electric field, (b) Photo of sample position in the prism coupling.

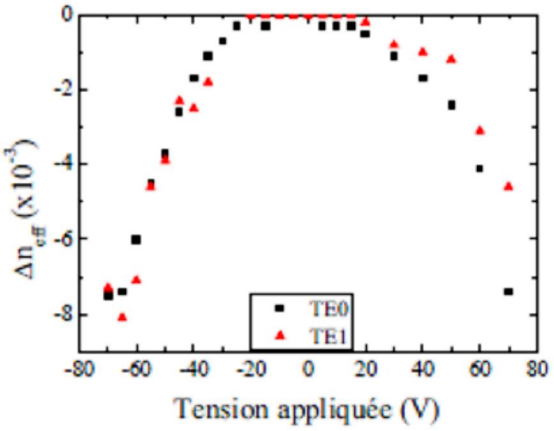

Figure 4.41. The influence of voltage on GaN/Si refractive index

Figure 4.41 is presents the refractive index variation when a static voltage bias is applied through the GaN/Si thin film. Because of the structure geometry, we consider a vertical DC electric field perpendicular to the interfaces. Due to the higher resistivity of the buffer layer, most of the electric field is applied into the top layer because of the electrical conduction of n-doped GaN.

4.9.3. Dynamic Characterization of the Electrooptic Effect

This part is dedicated to the electrooptic effect under dynamic signals. Beyong all the techniques, we have used Fabry-Perot interferometric configuration developed in the literature (Figure 4.42). The collaboration with Dr Cuniot-Ponsard from the Institute of Optics permits us to determine these effects into our GaN films. This method is based on the reflectometry technique: the output reflected intensity I and derivative $\partial I/\partial n_o$ (n_o is the ordinary refractive index of active film) have been rigorously calculated versus incident angle for transverse electric polarization TE without using any simplifying approximation [79]. This technique is largely described in the references 80 and 82.

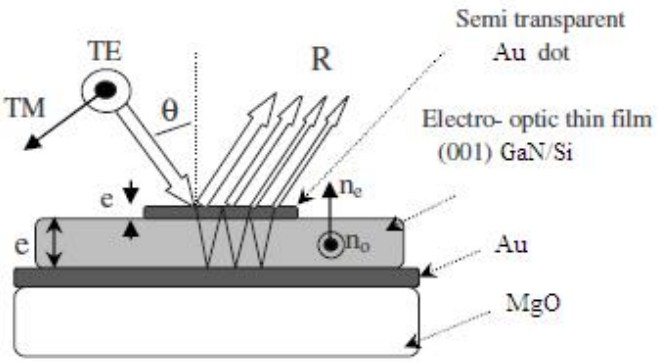

Figure 4.42. Fabry-Perot interferometric configuration. The film is sandwich between two Au electrodes.

Measurements of reflectivity R_{TE} (θ), R_{TM} (θ), ΔR_{TE} (θ),ΔR_{TM} (θ) are performed from reflectivity technique by using the simple θ-2θ goniometric setup [80], it is represented in Figure 4.43. The GaN/Si sample is ýxed on the central rotating part so that the plane of incidence is horizontal and the position of the light spot, centered on a platinum dot, is independent of incident angle. Heï Ne laser laser beam operating at 633 nm is used as source together a polarized either perpendicular (TE) or parallel (TM) to the sample plane of incidence, then split in two perpendicular beams. Intensities of the beams reþected by the beam splitter and by the sample are measured simultaneously by two silicon photodiodes and the absolute value of sample reþectivity is inferred. Electric ýeld applied to GaN ýlm is constituted of both a DC part, which allows a constant poling, and an AC part, which modulates reþectivity at a low frequency around 230 Hz [80].

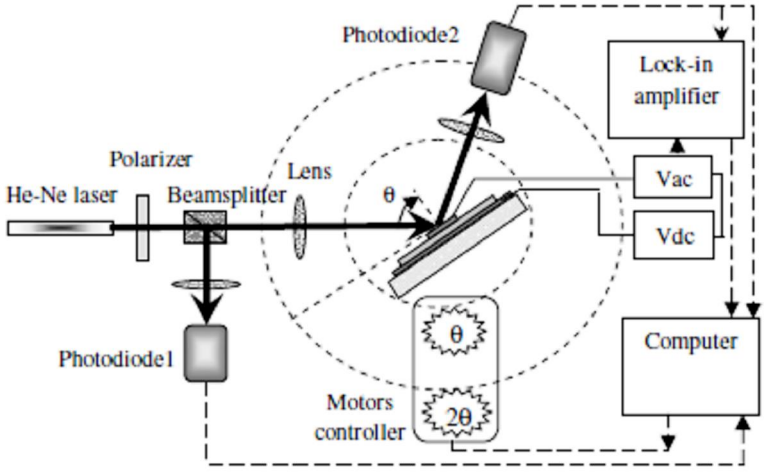

Figure 4.43. The simple θ-2θ goniometric setup schematically [80]

The procedure is carefully described in reference [82]. Reflectivity (R) and variation in reflectivity (qR) induced by an AC voltage are plotted versus incident angle d, successively for transverse electric TE and transverse magnetic (TM) polarizations. According to the above expression:

$$\Delta R_{TE,\theta} = \left(\frac{\partial R}{\partial n_o}\right)_{TE,\theta} \Delta n_0 + \left(\frac{\partial R}{\partial e}\right)_{TE,\theta} \Delta e + \left(\frac{\partial R}{\partial k_o}\right)_{TE,\theta} \Delta k_o \qquad 4.5$$

$$\Delta R_{TM,\theta} = \left(\frac{\partial R}{\partial n_\theta}\right)_{TM,\theta} \Delta n_\theta + \left(\frac{\partial R}{\partial e}\right)_{TM,\theta} \Delta e + \left(\frac{\partial R}{\partial k_o}\right)_{TM,\theta} \Delta k_o \qquad 4.6$$

where qe, qn_o, and qk_o are the electric field-induced variations in, respectively, the GaN active film thickness e, its ordinary refractive index n_o, and its ordinary extinction coefficient k_o. The reflectivity R is calculated from performed from Fresnel formula by taking into account all of the multi-reflection effects in the structure. The parameters (thickness and complex index) of each medium are refined thanks to the measurement of R(θ). The dependence of the ΔR_{TE} and ΔR_{TM} responses on the applied electric field amplitude (ΔE) is measured perfectly linear in the range 0 - 8.3 kV/cm.

In Figure 4.44, we have plotted the reflected intensity as a function of the incident angle: the comparison for TM polarization should allow eliminating some of the ýtting solutions provided large values of incident angle 70° are considered. Note that the pics at around θ = 35°, measurements are shadowed by an electric wire.

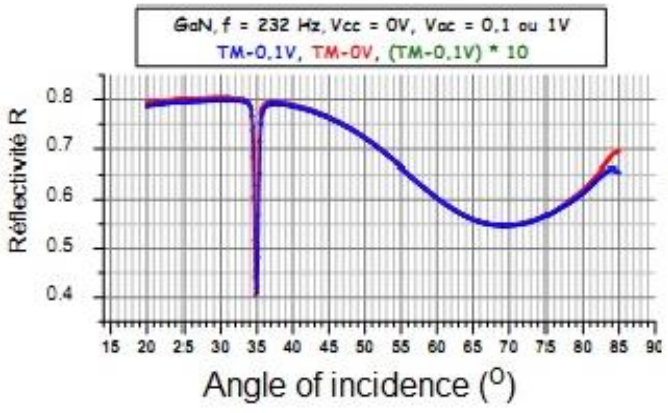

Figure 4.44. Reflectivities calculated from measured values at different angles of incidence.

Figure 4.45 compares the experimental and calculated $|\Delta R(\theta)|$ for both TE and TM polarizations. The agreement is very good except at angles larger than 65°, where the spot size on the sample exceeds that of the gold electrode so that the above model cannot account for the experimental data.

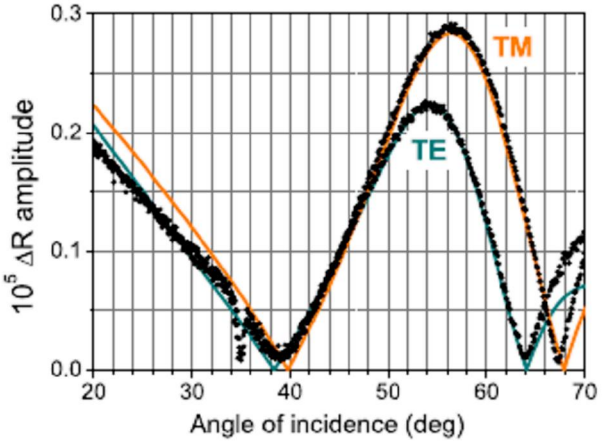

Figure 4.45. Electric-field-induced variation in the reflectivity for TE and TM polarizations.

The electrooptic Pockels coefficients r_{13} and r_{33} of the GaN layer can be deduced using the following expressions:

$$r_{13} = \frac{-2}{n_o^3}\frac{\Delta n_o}{\Delta E}, \qquad r_{33} = \frac{-2}{n_e^3 \sin^2\theta_r}\frac{\Delta n_e}{\Delta E} - r_{13}\cot^2\theta_r, \qquad 4.9$$

where θr is the refracting angle of the light wave in GaN.

We have evaluated an r_{13} and r_{33} electrooptic constants from these experiments. The values found for these coefficients when using a modulation frequency of 230 Hz are r_{13} = +1.01 pm/V, r_{33} = +1.67 pm/V at 633 nm [82]. The values found here for r_{13} and r_{33} may be compared with the values r_{13} = 0.57±0.11 pm/V and r_{33} = 1.91±0.35 pm/V at 633 nm reported in the literature for GaN grown on sapphire and determined from Mach Zehnder measurements at 45 kHz [26].

In summary, single crystalline GaN epitaxial layers grown on silicon (111) substrates have been optically characterized. To investigate the optical properties, the guided wave technique based on prism coupling has been used [70-71]: using a rutile prism (TiO_2) on Metricon M2010 setup. The measurement of the refractive index in Transverse Electric (TE) and Transverse Magnetic (TM) modes have been performed for different wavelengths from ultraviolet to near infrared wavelength ranges (from 450 to 1539 nm) together with the film thickness. We have compared the optical properties of GaN/Sapphire and GaN/Si: the refractive indices are quite close for TE/TM conditions. Electrooptic measurements are then performed using a different technique. A semi-transparent gold electrode is deposited on the top of the GaN layer and an alternating voltage is applied between top and bottom electrodes. The electrooptic coefficients of the GaN layer are simultaneously determined from the measurement of the electric field induced variation $\Delta R(\theta)$ in the reflectivity of the Au/GaN/buffer/Si stack versus incident angle. The results obtained for a GaN layer when using a modulation frequency of 230 Hz are for the electrooptic coefficients r_{13} = +1.01 pm/V, r_{33} = +1.67 pm/V at 633 nm. To our knowledge, this is the first experimentation providing such information onto III-nitrides materials. This indicates that GaN can be applied as active materials in some device configuration.

CHAPTER 5
STRUCTURE DESIGN OF GALLIUM NITRIDE ON SILICON

The future works are related to the design of GaN-based waveguide configurations using the beam propagation method (BPM) for the design. To validate qualitatively, the properties of the waveguide structures fabricated by different techniques as MOCVD or MBE, the simulations of various waveguide structures can be conducted. Waveguide optics modeling software is produced by Optiwave Corporation; OptiBPM is applied to simulate the performance of these waveguide structures; the particular to determine the opto-geometrical configuration for TE/TM modes excitation. This sections will present the first simulation has resulted in different waveguide structures, including some planar waveguide, a channel waveguide, and Fabry-Perot heterostructure. This simulation is a perspective for future research work that could permit the design and the fabrication of devices.

5.1. Introduction of OptiBPM

The finite difference beam propagating method (BPM) is one of the most powerful techniques to investigate linear and nonlinear lightwave propagation phenomena in axially varying waveguides. BPM solves Maxwellôs equations by using finite differences in place of partial derivatives. BPM is computationally intensive and can to model a very wide range of devices accurately. BPM program simulates light propagation in two-dimensional (2-D) and three-dimensional (3-D) waveguide devices. One of the three dimensions is the transverse dimension, recognized as the X-direction. The second dimension is the dimension of propagation, recognized as the Z-direction. For 3-D simulations, the third dimension is the Y direction, identified as depth. The simulated devices have a step-like effective refractive index distribution in the transverse dimensions. The

processing environment of OptiBPM contains the Beam Propagation Method as its core element and mode solvers that are compatible with the BPM algorithms. The Beam Propagation Method is based on a numerical solution of equations that govern light propagation in dielectric media. The BPM considers monochromatic signals and is related to solving the Helmholtz equation. However, to simplify the simulations, reduce the processing time, and have a better computer memory management, models of propagation based on an approximation of the Helmholtz equation are used in simulations.

5.2. Structure for Galium Nitride (GaN) Samples

In the beginning, we will introduce some theory for the general case of a multilayered plane waveguide, the scheme that can be seen in Figure 2.3 and Figure 2.4 (Chapter 2). The assume that different layers have different physical properties, specifically different refractive index. In the modeling, the wave propagation is considered the uniaxial materials, exhibiting then GaN with extraordinary and ordinary refractive index. The optical loss mechanism is also related to the absorption in Si layer. Therefore, it is sufficient to consider a simple layer model (air/GaN/AlN) for an analytical solution. In multilayer models, there is one material that must be considered which will include Silicon dioxide (SiO_2) on Silicon (Si) substrate.

The structure samples are Gallium Nitride on Sapphire (GaN/Al_2O_3) and Gallium Nitride on Silicon (GaN/Si) for simulations by optiBPM software in this section. Both of the samples represented in Figure 5.1. Figure 5.1a consist of a top waveguiding layer of GaN (n=2.31), buffer layer of Aluminium Gallium Nitride (AlGaN; n=2.12) and Aluminium Nitride (AlN; n=2.12), SiO_2 (n=1.47) layer that acts as the cladding, and Si (n=3.4) substrate.

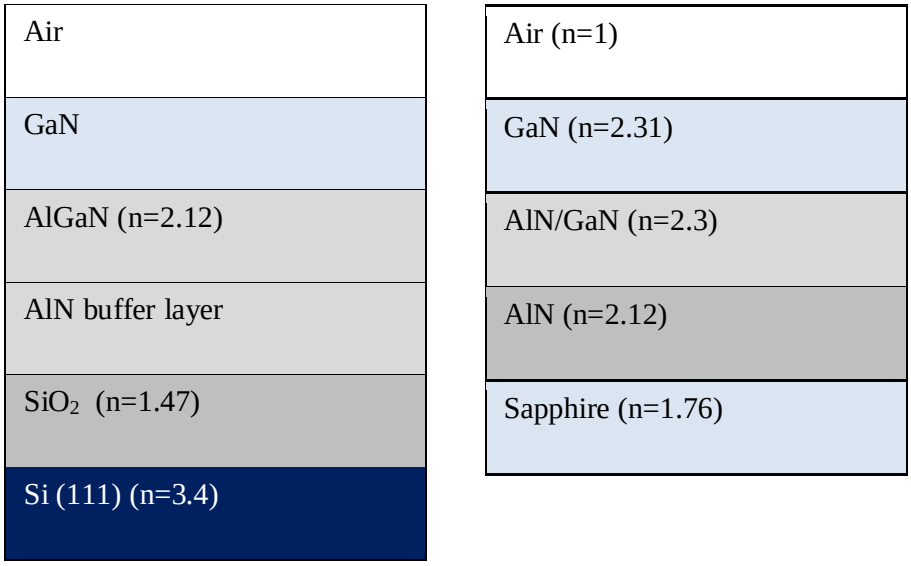

(a) (b)

Figure 5.1. The structure samples, (a). Gallium Nitride on Silicon (GaN/Si), (b). Gallium Nitride on Sapphire (GaN/Al_2O_3)

The silicon technology has some distinct advantages over the other commonly used platforms such as the III-V semiconductor compounds and polymers. First, the high refractive index contrast between the silicon cladding the silica and the gallium nitride facilitates the confinement and guiding of light in GaN structures within submicron dimensions. Besides, the mature silicon microfabrication technology establishes a firm foundation for making low-cost and compact integrated photonic devices. Furthermore, Si technology offers tremendous potential for monolithic integration of electronic and photonic devices on the same substrate.

5.3. Simulation of Optical Channel Waveguide Structure

The first discussion will explain the simulation model that is the base of the sequent simulation analysis. Because the waveguide structures in this project are different from those widely used waveguides, it is difficult to find a model from

the OptiBPM catalog the same as the actual one. While considering 1) all the waveguides simulated and studied in this project has silicon substrates and 2) the refractive index is gradually changed from the center to the bottom, GaN waveguides can be used as a reasonable approximation of the channel waveguides and other structures as well.

To obtain the optimal channel design, there are some parameters to be varied to see the impact on power loss, uniformity of light distribution and light propagation mode. The parameters are the position of the waveguides, the width waveguides, waveguide thickness, refractive index and thickness of the material cladding as well as the thickness of the buffer layer. In designing GaN waveguide, the steps taken are as follows:

i. specifies the width of the waveguide; display to determine the width of waveguide can be seen in the Appendix.
ii. determine the width and long wafer; varying length of wafer dimension (1000 μm, 0.2 cm, 0.5 cm and 1 cm) and varying width (10 μm and 20 μm). The display to determine the length and width of wafer dimension can be seen in the Appendix.
iii. defining the materials used in modeling
iv. determine the wafer material
v. determine the structure of the substrate
vi. determine the waveguide structure
vii. varying the position, width, and thickness of the waveguides
viii. varying refractive index and the thickness of the cladding material
ix. varying the thickness of the material buffer layer

Figure 5.2 shows the cross-section view of the single mode GaN/Si structure at the input. It consists of GaN (thickness layer 0.2 µm and width 4 µm)/ GaN (thickness layer 0.8 µm)/ SiO_2(thickness layer 1 µm)/ Silicon substrate with wafer dimension length 1000µm and width 10µm.

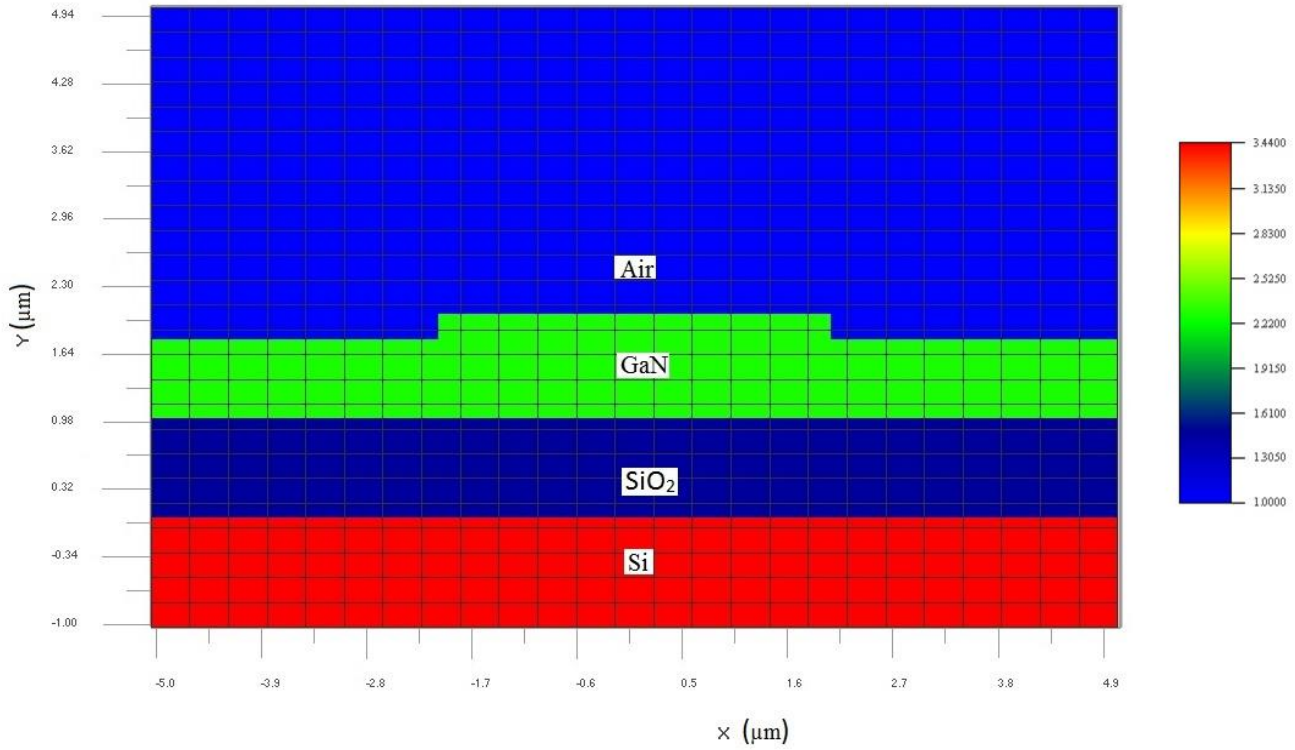

Figure 5.2. The cross section view of the single mode GaN/Si structure at the input.

This structure design (Figure 5.2) is optimum channel design from varying some parameter because design has single mode input and output even if mode is spreading.

A Gaussian field (which was shown as the red edge on the left of Figure 5.3 with the half width is injected from the left to the end of the channel waveguide. The simulation results are presented in Figure 5.4 (input), Figure 5.5 (output), Figure 5.6 (propagation) and Figure 5.7 (optical power).

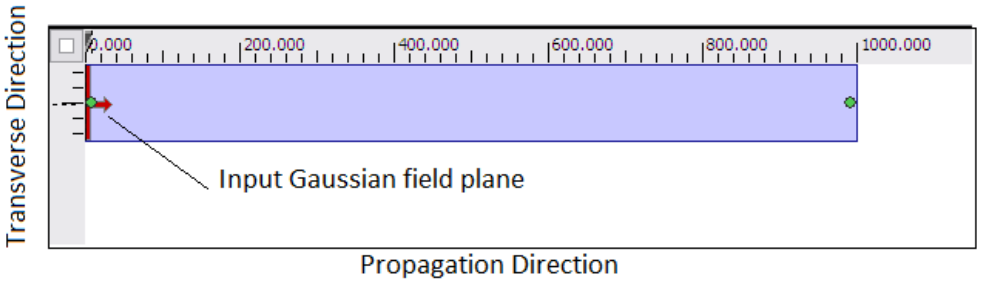

Figure 5.3. Layout of the GaN/Si channel waveguide simulated

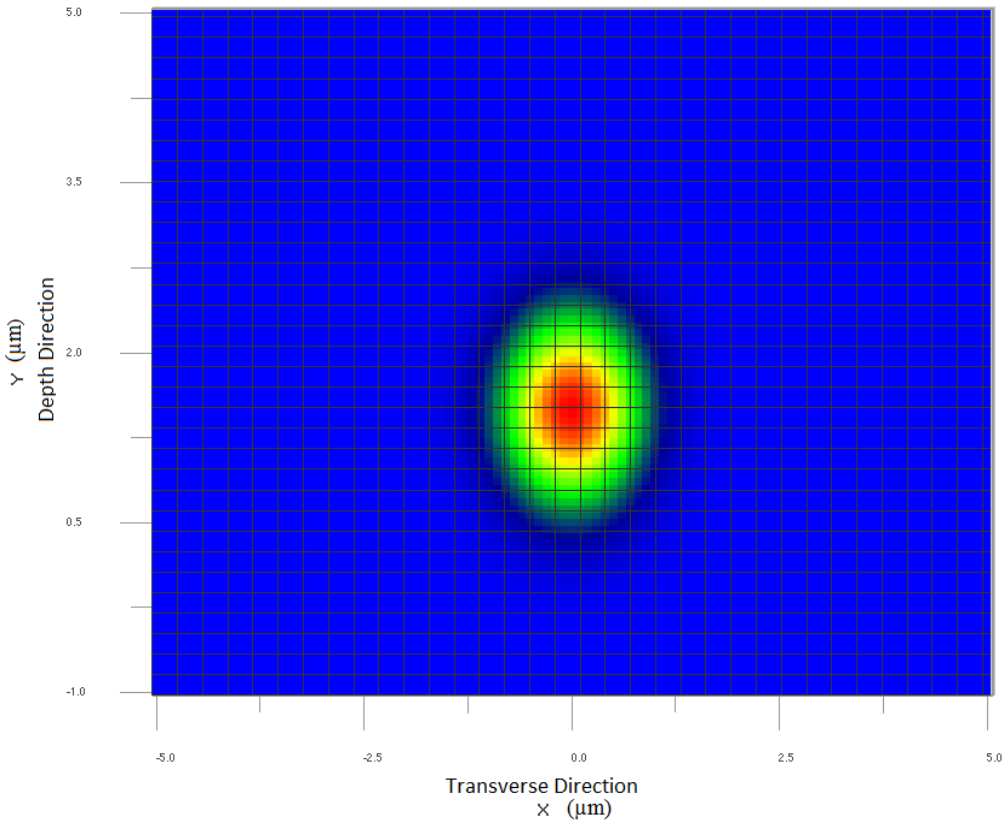

Figure 5.4. The input field emitted from the simulated channel waveguide.

The input field emitted has width and thickness are 2 εm and 2 εm respectively. The input thickness was spreading present in Figure 5.4. The calculated results show that the optimum parameter for the device are as follow: the width and thickness of output linear waveguides are 5 εm and single mode propagation.

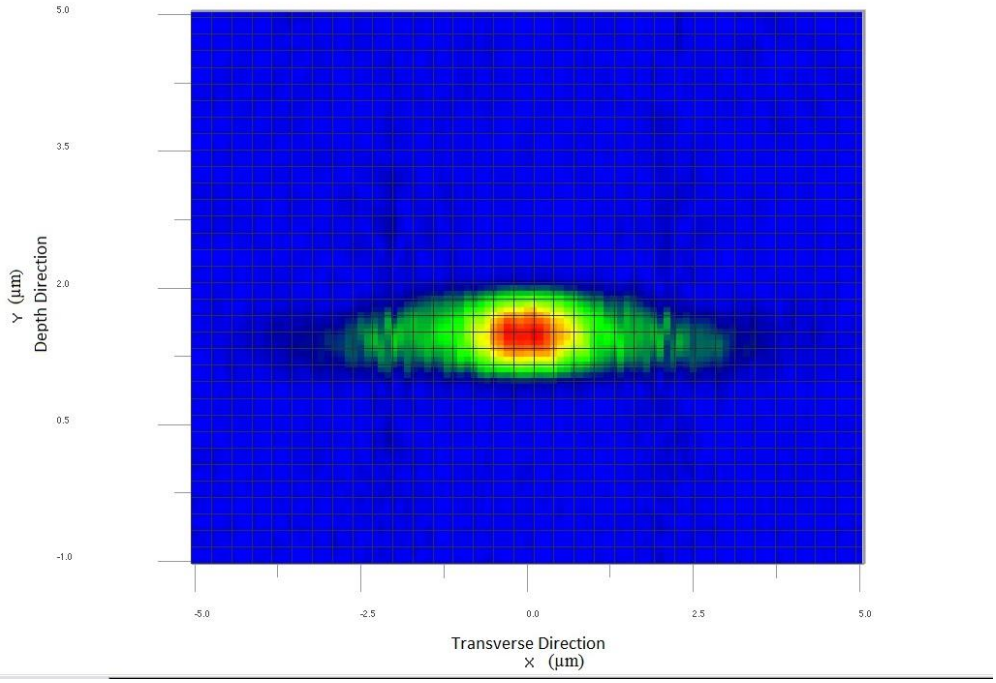

Figure 5.5. The output field emitted from the simulated channel waveguide when the refractive index effective is 2.07

Figure 5.5 shows the output optical field emitted from the end of the channel waveguide. Naturally, the output field shows a single mode shape, because the cross-sectional structure of this waveguide (as shown in Fig.5.1) is approximately single mode.

Using beam propagation method analysis, the optical field propagation of GaN waveguide is presented in Figure 5.6. The red color in straight input waveguide of design indicates that the relative power is maximum. Decreasing of relative power indicated in the green color.

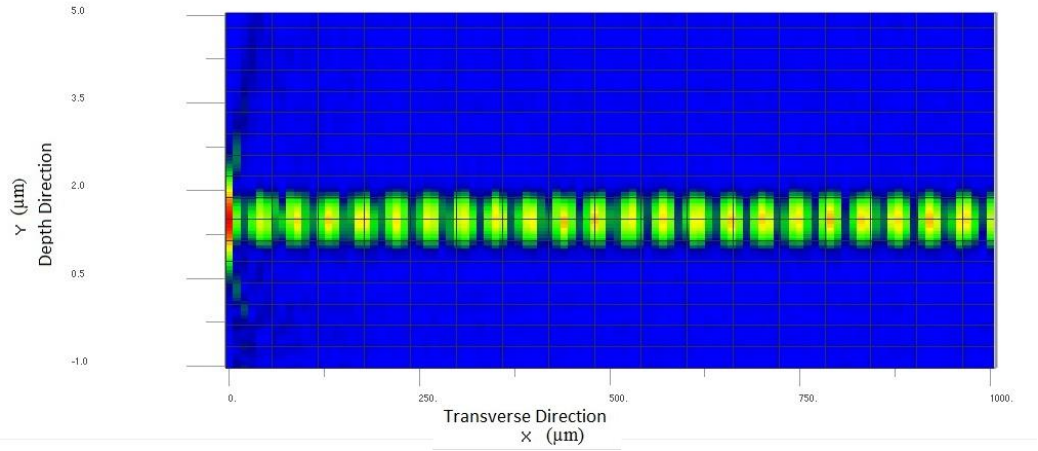

Figure 5.6. The optical field propagation of GaN waveguide

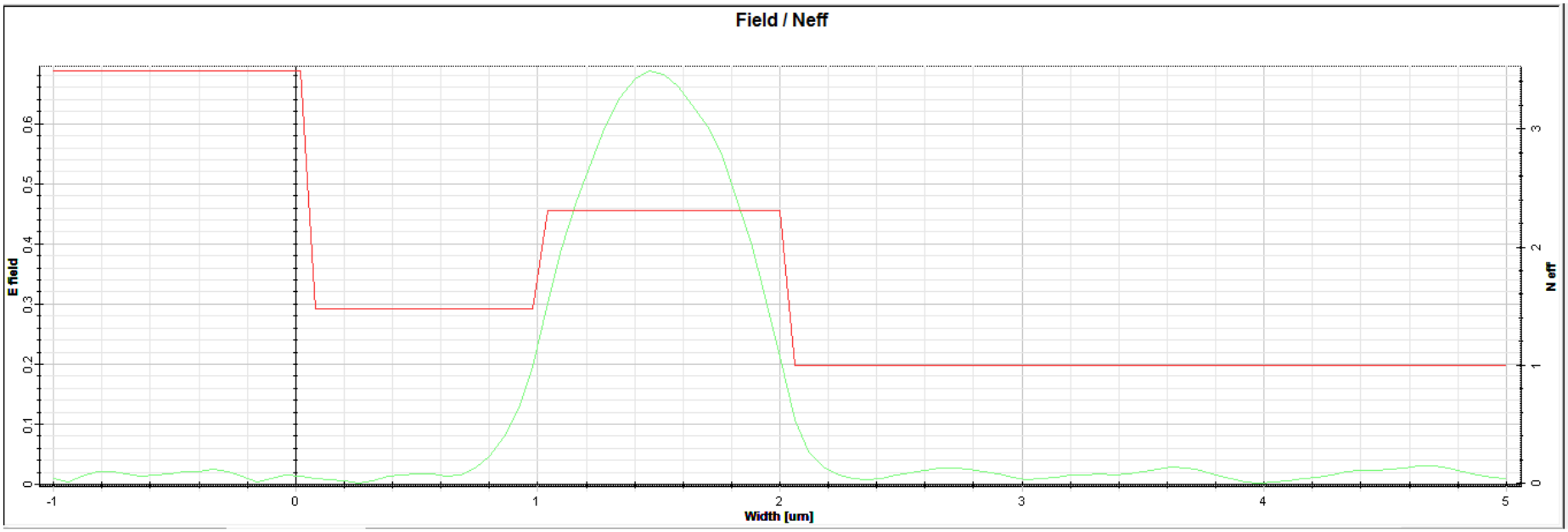

Figure 5.7. Propagation optical field along the waveguide in the transverse dimension when the maximum refractive index is 2.07.

The normalized optical fields propagating along the channel in transverse direction and depth direction are presented in Figure 5.7. Because of the symmetric cross-sectional shape of the waveguide and the very small refractive index change, the optical field attenuates very fast into the waveguide, and a large part of the optical energy is leaked into the substrate and the cladding.

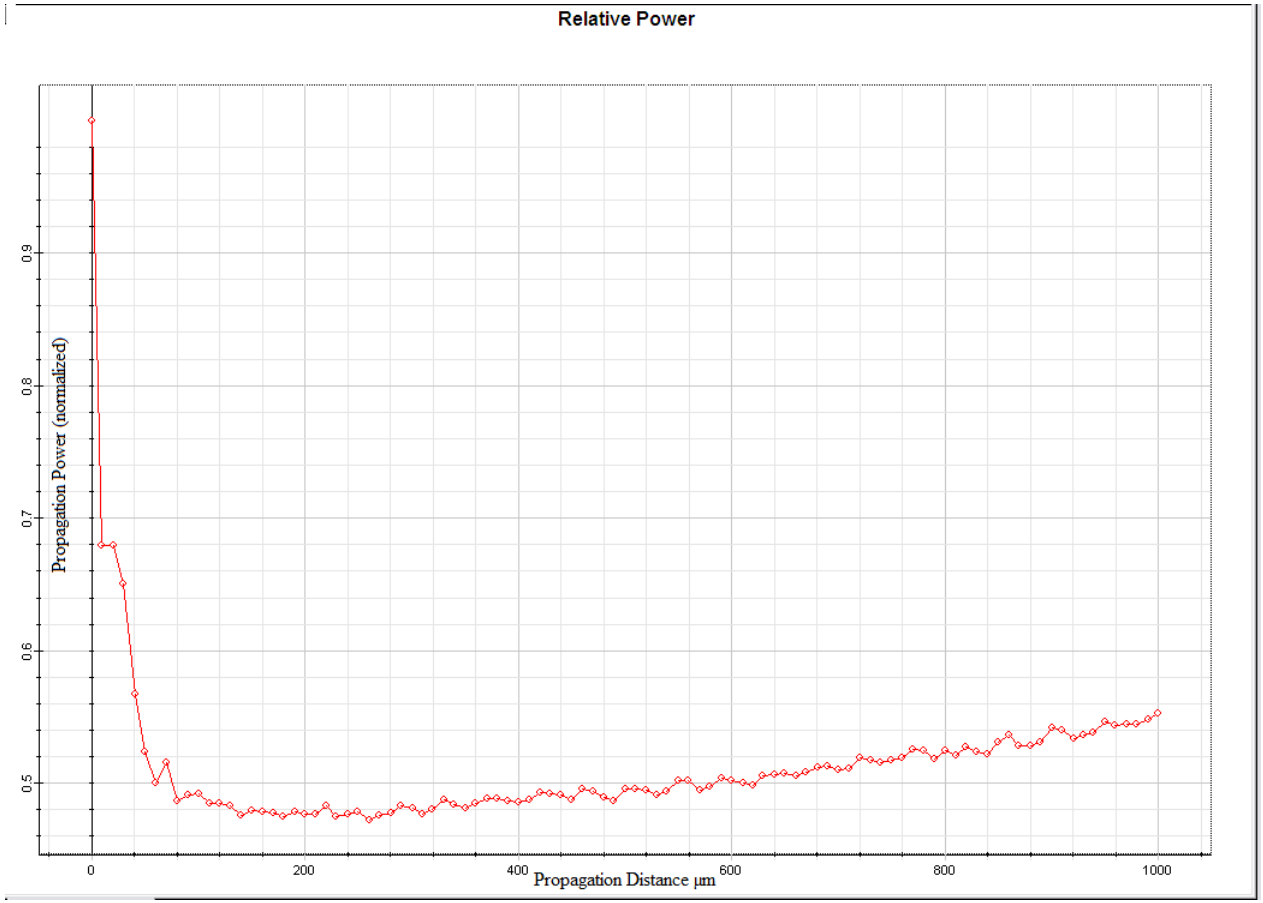

Figure 5.8. Curves of the optical power vs. the propagation at maximum refractive index

The curves in Figure 5.8 are propagation power attenuates quickly when the input Gaussian field enters the waveguide channel in the beginning. With the optical field propagating along the channel, it becomes more and more stable. The optical field reaches stabilizing after propagating in a certain length.

The mode profile of the input at the design with SiO_2 buffer layer represented in Figure 5.7 and the structure has optical power less 50% represented in Figure 5.8.

CHAPTER 6

CONCLUSION

In this research, we have presented a complete analysis of Gallium Nitride-based structures with very promising characteristics for future optical waveguide devices, such as modulators. This work is dedicated to a full knowledge of GaN fundamental properties, a new semiconductor material. We have analyzed two structures for GaN materials: GaN on sapphire and silicon. We have observed the microstructure by SEM, TEM, and AFM analysis. One can summarize the results of characterizations (optical, electro-optical, and microstructural) and design of GaN/Si channel waveguide as below:

a. Optical characterization of GaN/Si and GaN/Sapphire shows a decreasing refractive index with the increasing wavelength.

b. GaN/Sapphire and GaN/Si samples have roughness respectively in the range 1.6 to 5.2 nm and 9.6 to 13 nm.

c. The ordinary and extraordinary refractive indices of GaN/Si have been measured as a function of temperature and wavelength within the ranges 20ï 100 °C by using a prism coupling setup. The thermal dependencies of ordinary and extraordinary refractive indices are determined to be 9.47×10^{-5}/°K and 8.99×10^{-5}/°K, respectively. The thermal dependence has value better than GaAs [1]

d. Optical loss of GaN/Si at 633 nm is 9.4 dB/cm; this is higher than loss around 1.34 dB/cm into GaN/sapphire.

e. The birefringence of GaN/Si is negative within range $0.16x10^{-2}$ to $6.06x10^{-2}$. The negative value means the polarization of the wave is parallel to the optical axis.

f. Electrooptic constants r_{13} = +1.01 pm/V and r_{33} = +1.67 pm/V are higher than those obtained for III-V GaAs semiconductors.

g. The input and output of GaN waveguide design are the difference thickness and width. The width of GaN/Si input and output much greater than the waveguide thickness. The structure design of GaN/Si has optical power less 50%.

The quality of GaN material is higher on sapphire with small dislocations density and defects in the layers, compared to a silicon substrate. From the optical analysis, we found the index of refractive is close on both substrates. Optical measurements demonstrate excellent waveguide properties regarding terms of refractive index and temperature dependence while planar propagation losses are in the order of 1 dB/cm.

REFERENCES

[1] L. Liu, J.H. Edgar, Substrates for gallium nitride epitaxy, Materials Science and Engineering R., 37, 61-127 (2002).

[2] Hadis Morkoç,Handbook of Nitride Semiconductors and Devices: Materials Properties, Physics and Growth, Volume 1, (2009).

[3] J. Wu, W. Walukiewicz, K.M. Yu, J.W. Ager, E.E. Haller, H. Lu, W.J. Schaff, Y. Saito, Y. Nanishi, Unusual properties of the fundamental band gap of InN, Applied Physics Letters, 80, 3967 (2003).

[4] K. Hoshino, Y. Arakawa, Formation of high-density GaNself-assembled quantum dots by MOCVD, Journal of Crystal Growth 272, 161ï 166 (2004).

[5] T.H. Yang, J.T. Ku, J.R. Chang, S.G. Shen, Y-C. Chen, Y.Y. Wong, W.C Chou, C.Y. Chen, C.Y Chang,Growth of free-stan ding GaN layer on Si (111) substrate, Journal of Crystal Growth 311, 1997 ï 2001 (2009).

[6] J. Jasinski, W. Swider, Z. Liliental-Weber, P. Visconti, K. M. Jones, M. A. Reshchikov, F. Yun, H. Morkoç, S. S. Park, K. Y. Lee, Characterization of free-standing hydride vapor phase epitaxy GaN, Applied Physics Letters 78, 2297 (2001).

[7] N Elkashef, R.S. Srinivasa, S. Major, S.C. Sabharwal, K.P. Muthe, Sputter deposition of gallium nitride ýlms using GaAs target, Thin Solid Films 333, 9-12 (1998).

[8] J. Miragliotta, D.K. Wickenden, T.J. Kistenmacher, W.A. Bryden, Linear and nonlinear-optical properties of GaN films, J. Opt. Soc. Am. B, Vol. 10, No. 8, 1447 (1993).

[9] S. Strite, H. Morkoc, GaN, AlN and InN: a review, J. Vac. Sci. Tech. B 10, 1238 (1992).

[10] S. Nakamura, N. Iwasa, M. Senoh, T. Mukai, Hole compensation of p-type GaN films, Jpn. J. Appl. Phys. 31, 107 (1992).

[11] N. Ikeda , J. Li, H. Takehara, T. Wada, S. Yoshida, High-performance normally off FET using an AlGaN/GaN heterostructure on Si substrate, J. Crystal Growth 275 1019-1095 (2005).

[12] S. Kato, Y. Satoh, H. Sasaki, I. Masayuki, S. Yoshida, C-doped GaN buffer layers with high breakdown voltages for high-power operation AlGaN/GaN HFETs on 4-in Si substrates by MOVPE, J. Crystal Growth 298, 831-834 (2007).

[13] C. Jin, D. Pavlidis, L. Considine, A Novel GaN-Based High Frequency Varactor Diode, Proceedings of the 5th European Microwave IC Conference, Paris, France, 27-28 Sept (2010).

[14] A. Cai, Wide band gap semiconductor optical waveguide, Thesis of Philisophy, Electrical Eng. Dept., North Carolina State University, Raleigh NC, (2005).

[15] A. Stolz, L. Considine, S. Faci, E. Dogheche, C. Tripon-Canseliet, B. Loiseaux, D. Pavlidis, D. Decoster, J. Chazelas, Gallium-nitride-based plasmonic multilayer operating at 1.55εm, Optics Letters Vol. 37, No. 15, 3039 (2012).

[16] J.I. Pankove, E.A. Miller, J.E. Berkeyheiser: RCA Rev. 32:383. MRS Internet, J. Nitride Semiconductor Res. 3:3, 1971.

[17] D. Dingle, K.L. Shaklee, R.F. Leheny, R.B. Zetterstrom, Cleaved cavity stimulated emission from an optically pumped laser, Applied Physics Letter Vol. 64 No. 1377, (1994).

[18] S. Nakamura, G. Fasol, The Blue Laser Diode: GaN Based Light Emitters

and Lasers, Berlin: Springer-Verlag, (1997).

[19] H. Amano, M. Kito, K. Hiramatsu, I. Akasaki, p-type Conduction in Mg-Doped GaN Treated with Low-Energy Electron Beam Irradiation (LEEBI), Japanese Journal of Applied Physics, 28, pp.L2112-L2114, (1989).

[20] C. Stampfl, C.G. Van de Walle, density-functionnal calculation for III-nitrides using the local-density approximation and the generalized gradient approxiamtion, Phys. Review B59, 5521 (1999).

[21] E.F. Schubert, Light Emitting Diodes, nd Edition, Fig 12.12, Cambridge University Press, Cambridge (2006).

[22] V.Yu. Davydov, A.A. Klochikhin, R.P. Seisyan, V.V. Emtsev, S.V. Ivanov, F. Bechstedt, J. Furthmuller, H. Harima, A.V. Murdryi, J. Aderhold, O. Semchinova, J. Graul, Absorption and Emission of Hexagonal InN. Evidence of Narrow fundamental band gap, Physica Status Solidi (b) 229, R1-R3 (2002).

[23] T. Matsuka, H. Okamato, N. Nakao, E. Kurimoto, Optical bandgap energy of wurtite InN, Applied Physics Letter, 81, 1246 (2002).

[24] I. Wurgafman, J.R. Meyer, Band parameters for nitrogen-containing semiconductors, J. Applied Physics 94, 3675-3696 (2003)

[25] S. Strite, H. Morkoc, GaN , AlN and InN/ A review, J. Vaccum Sciences and Technology B10 (4) 1237-1266 (1992).

[26] F. Fisher, F. Schroter, Uber neue Matell-Stickstoff Verbindungen and ihre stabilitat an der Hand des periodischen systems, Berichte der Deutschen Chemischen Gesellschaft 43, 1465-1479 (1910).

[27] V.C. Johnson, J.B. Parsons, M.C. MC Crew, Nitrogen compounds of gallium, J. Physics Chem. 36, 2588 (1932).

[28] H.P. Maruska, J.J. Tietjen, The preparation and properties of vapor-deposited single crystal line GaN, Applied Physics Letter, 15, 327 (1969).

[29] H. Manasevit, F.M. Erdmann, W.I. Simpson, The use of Metalorganics in the preparation of semiconductor materials, J. Electrochem. Soc. 118,

1864 (1971).

[30] I. Akasaki, I. Hayashi, Research on blue emitting devices, Ind. Sci. Techn. 17, 48 (1976).

[31] S. Nakamura, S. Pearton, G. Fasol, The blue Laser Diode: The complete Story, Ch 6.3, Springer, Berlin (2000).

[32] D.R. Lide, CRC Handbook of Chemistry and Physics, 78th Edition CRCPress, Boca Raton, New York (1997).

[33] H. Amano, N. Sawaki, I. Akasaki, Y. Toyoda, Metalorganic vapor phase epitaxial growth of a high quality GaN film using AlN buffer layer, Appl. Physics Lett. 48, 353 (1986).

[34] S. Nakamura, GaN growth using GaN buffer layer, Jpn. J. Appl. Phys. 30, L1705 (1991).

[35] J.D. Jackson, R. Fox, Classical electrodynamics, 3rd edition, vol 67, n°9, 841-842 (1999).

[36] J. Cardin, Elaboration et caracterisation de couches minces pour des applications optiques, PhD thesis, Université de Nantes, (2004).

[37] R.P. Dahal, Fabrication and characterization of III-nitride nanophotonic devices, Thesis of Philosophy, Texas Tech University (2009).

[38] J.X. Zhang, H. Cheng, Y.Z. Chen, A. Uddin, Shu Yuan, S.J. Geng, S. Zhang, Growth of AlN films on Si (100) and Si (111) substrates by reactive magnetron sputtering, Surface & Coatings Technology 198, 68-73, 2005.

[39] S.H. Jang, C.R Lee, High-quality GaN/Si (111) epitaxial layers grown with various $Al_{0.3}Ga_{0.7}N$/GaN superlattices as intermediate layer by MOCVD, Journal of Crystal Growth 253, 64ï 70 (2003).

[40] C.C. Huang, S.J. Chang, R.W. Chuang, J.C. Lin, Y.C. Cheng, W.J. Lin, GaN grown on Si (111) with step-graded AlGaN intermediate layers, Applied Surface Science 256, 6367ï 6370 (2010).

[41] H.M Kim, D.S. Kim, D.Y. Kim, T.W. Kang, Y.H Cho, K. S. Chung, Growth and characterization of single-crystal GaN nanorods by hydride vapor phase epitaxy, Appl. Phys. Lett. 81, 2193 (2002).

[42] Suk-Min Ko, Novel photonic devices using core-shell nanostructures, Thesis Korean Advanced Institute of Sciences and Technology, (2014).

[43] E. Cho, GaN based heterostructure growth and application to electronic devices and sensors, Thesis of Philosophy, University of Michigan (2009).

[44] A. Stolz, E. Cho, E. Dogheche,Y. Androussi, D. Troadec, D. Pavlidis, D. Decoster, Optical waveguide loss minimized into gallium nitride based structures grown by metal organic vapor phase epitaxy, Applied Physics Letters, 98, 1 (2011).

[45] S. Nakamura, G. Fasol, The Blue Laser Diode: GaN Based Light Emitters and Lasers, Springer (1997).

[46] D. Brandon and W. D. Kaplan, ñMicrostructural Characterization of Materialsò, 2nd Edition, Technion, Israel Institute of Technology, John Wiley & Sons Ltd, England (2008).

[47] A. Vilalta-Clemente, G.R. Mutta, M.P. Chauva, M. Morales, J.L. Doualan, P. Ruterana, MA.A Sanchez-Garcia, F. Callé, E. Valcheva, K. Kirilov, Investigation of InN layers grown by molecular beam epitaxy on GaN templates, Physica Status Solidi A, 207(5) 1079-1082 (2010).

[48] A. Strittmatter; A. Krost, M. Strabburg, Applied Physics Letter, 74, 1242 (1999).

[49] J.W. Yang, C.J. Sun, Q. Chen, M.Z. Anwar, M. Asif Khan, S.A. Nikishim, G.A. Seryogin, Applied Physics Letter, 69, 3566 (1996).

[50] Z.H. Wu, A.M. Fisher, F.A. Ponce, T. Yokogawa, S. Yoshida, R. Kato, Applied Physics Letter, 93, 011901 (2008),

[51] Z.H. Wu, A.M. Fisher, F.A. Ponce, B. Bastek, J. Christen, T. Wernicke, M. Weyers, M. Kneissl, Applied Physics Letter, 92 171904 (2008).

[52] R. Liu, J. Mei, S. Srinivasan, H. Omiya, F.A Ponce, D. Cherns, Y. Narukawa, T. Mukai, Jpn J. Applied Physics, 45, L549 (2006).

[53] E. Cho, D. Pavlidis, E. Sillero, Physica Status Solidi C4, 2764 (2007).

[54] E. Cho, S. Seo, C. Jin, D. Pavlidis, G. Fu, J. Tuerck, W. Jaegermann, J. Vaccum Science Technology B 27, 2079 (2009).

[55] V.M. Kaganer, O. Brandt, A.Trampert, K.H. Ploog, X-ray diffraction peak profiles from threading dislocations in GaN epitaxial films, Physics Review B, 72, 045423-045437 (2005)

[56] L.S. Chuah, Z. Hassan, S. Ng, H.A. Hassan, Structural properties of doped GaN on Si(111) studied by X-Ray Diffraction Techniques, J Nondestruct Eval, 28, 125-130, (2009).

[57] A. Stolz, Conception, Fabrication, et Caracterisation dôun modulateur optique à commande plasmonique sur nitride de gallium à une longueur dôonde de 1,55µm, Thèse de doctorat, Universite de Valenciennes (2011).

[58] A. Cai, ñWide band gap semiconductor optical waveguideò PhD thesis, North Carolina State University (2005).

[59] M. Born,E. Wolf, Principles of Optics (7th Ed), Pergamon Press, Oxford (1999)

[60] A. Vasicek, Optics of Thin Films, North-Holland, Amsterdam (1960)

[61] G. Witjaksono, I. Saraswati, ñDesign and Analysis of SEDFB Laser for Radio Over Fiberò, IJCNDS Vol 1, Issue 3, 330 (2008)

[62] Y. Enami , B. Yuan, M. Tanaka, J. Luo, A. K.- Y. Jen,ò Electro-optic polymer/TiO 2 multilayer slot waveguide modulatorsò, Appl. Phys. Lett. 101, 123509 (2012)

[63] S-H. Hsu, Y-T. Huang, ñDesign and analysis of Machï Zehnder interferometer sensors based on dual strip antiresonant reþecting optical waveguide structuresò, Optics Letters, Vol. 30, No. 21, 2897 (2005)

[64] P.K. Tien, R. Ulrich, R.J. Martin ñModes of propagating light waves in thin deposited semiconductor filmsò, Appl. Phys. Lett. 14, 291-294 (1969)

[65] R. Ulrich, R. Torge. ñMeasurement of thin film parameters with a prism couplerò, Appl. Opt. 12, 2901-2908 (1973)

[66] P. K. Tien, G. Smolinsky, R. J. Martin, Appl. Opt. 11, 1313 (1972).

[67] R. Ulrich, H. P. Weber, Appl. Opt. 11, 428 (1972).

[68] R. Ulrich, J. Opt. Soc. Am. 61, 1467 (1971).

[69] J. Rams, A. Tejeda, J. M. Cabrera, ñRefractive indices of rutile as a function of temperature and wavelengthò, J. Applied Physics 82(3), 994ï 997 (1997).

[70] E. Dogheche, X. Lansiaux, D. Remiens , ñm-line spectroscopy for optical analysis of thick LiNbO3 layers grown on sapphire substrates by radio-frequency multistep sputteringò, J. Appl. Phys. 93, 1165 (2003).

[71] A. Stolz, ñConception, Fabrication et caracterisation dôun moduateur optique a commande plasmonique sur nitrure de gallium à une longueur dôonde de 1,55µm, these de doctorat, Universite de Valenciennes, (2011).

[72] A. Stolz, E. Cho, E. Dogheche, Y. Androussi, D. Troadec, D. Pavlidis, D. Decoster, ñOptical waveguide loss minimized into gallium nitride based structures grown by metal organic vapour phase epitaxyò, Appl. Phys. Lett. 98, 161903 (2011)

[73] G. Li, ñWaveguides Produced by Ultra-short Laser Pulses inside Lithium Niobateò, Thesis, National University of Singapore, 2004.

[74] E. Bartholin, "An account of sundry experiments made and communicated by that learn'd mathematician," Philosophical Transactions of the Royal Society of London, **5** : 2041-2048 (1670).

[75] SK. Shevell, Science of Color, Optical Society of America, ISBN 0444512519, (2003).

[76] B.A. Saleh, M. Carl Teich,Fundamentals of Photonics, John Wiley & Sons Inc., (1991)

[77] K. D. Singer, M. G. Kuzyk, W. R. Holland, J. E. Sohn, S. J. Lalama, R. B. Comizzoli, H. E. Katz, M. L. Schilling, ñElectrooptic phase modulation and optical secondharmonic generation in coronapoled polymer filmsò, Appl. Phys. Lett. 53, 1800 (1988).

[78] P Tang, D. J. Towner, A. L. Meier, B.W. Wessels, Low-voltage, polarization-insensitive, electro-optic modulator based on a polydomain barium titanate thin film, Applied Physics Letters, 85, 20, 4615 (2004).

[79] D.Y. Wang, S. Li, H.L.W. Chan, C.L. Choy, Electro-optic characterization of epitaxial $Ba_{0.7}Sr_{0.3}TiO_3$ thin films using prism coupling technique, Current Applied Physics, 11, S52-S55, (2011).

[80] M. Cuniot-Ponsard, J. M. Desvignes, A. Bellemain, F. Bridou, ñSimultaneous characterization of the electrooptic, converse-piezoelectric, and electro-absorptive effects in epitaxial (Sr,Ba)Nb_2O_6 thin filmsò, J. Appl. Phys. 109, 014107 (2011).

[81] A Stolz, SM Ko, G Patriarche, E Dogheche, Y-H Cho, Surface plasmon modulation induced by a direct-current electric field into gallium nitride film grown on Si(111), Appl. Phys. Lett. 102, 021905 (2013).

[82] M Cuniot ï Ponsard, I Saraswati, SM Ko, M. Halbwax, YH Cho, E. Dogheche, Electro-optic and converse-piezoelectric properties, Appl. Phys. Lett. 104, 10 (2014) 101908

[83] X.C. long, R.A. Myers, S.R. J. Brueck, R. Ramer, K. Zheng, S.D. Hersee, J. Appl. Phys. Lett. 67 (10), 1349 (1995)

PUBLICATION

I. Journal:

[1] Irma Saraswati, Arnaud Stolz,S.Ko, Elhadj Dogheche, NR.Poespawati, Retno Wigajatri P, Didier Decoster (2014).
Optical Properties of Gallium Nitride Heterostructures Grown on Silicon for Waveguiding Application, ***Advanced Material Research Vol.980, pp 41-45.***
Online available since 2014/Jun/30 at www.scientific.net, @2014 Trans Tech Publications, Switzerland.
doi:10.4028/www.scientific.net/AMR.980.41

[2] R.W. Purnamaningsih, N.R. Poespawati, I. Saraswati, and E. Dogheche (2014).
Design of GaN-based Optical Modulator with Mach-Zehnder Interferometer Structure, ***WSEAS Trans. Communications, Vol.13, p.229-233, E-ISSN: 2224-2864***.

[3] R.W. Purnamaningsih, N.R. Poespawati, I. Saraswati, and E. Dogheche (2014).
Design of GaN-based Low-Loss Y-Branch Power Splitter, ***Makara Journal of Technology Vol.13, Number 3, pp 101-104***.

[4] M. Cuniot-Ponsard, I. Saraswati, S.-M. Ko, M. Halbwax, Y. H. Cho, and E. Dogheche (2014).
Electro-optic and converse-piezoelectric properties of epitaxial GaN grown on silicon by metal-organic chemical vapor deposition, ***Applied Physics Letters 104, 101908.***
doi: 10.1063/1.4868427.
View online: http://dx.doi.org/10.1063/1.4868427

II. International Conference:

[1] Irma Saraswati, Arnaud Stolz, NR.Poespawati, Retno Wigajatri P, Elhadj Dogheche, Didier Decoster, S.Ko, Y.H. Cho, L. Considine, D. Pavlidis (2012).
Investigation of structural, morphological and optical properties of GaN/AlGaN heterostructures on Si, ***Proceeding in PGC (Photonic Global Conference), 13-16 Dec 2012 Singapore, page 731***.
http://toc.proceedings.com/17279webtoc.pdf

[2] M. Cuniot-Ponsard, I. Saraswati, S.-M. Ko, M. Halbwax, Y. H. Cho, N.R. Poespawati, and E. Dogheche (2014)
Electro-optic and converse piezoelectric coefficients of highly polar epitaxial films: GaN grown on Si, and (Sr,Ba)Nb2O6 (SBN) grown on Pt coated MgO, ***Proceeding in European Conference on Application of Polar Dielectrics (ECAPD) 2014, July 7-11,2014 Vilnius, Lithuania. page.47.***
http://www.ecapd2014.ff.vu.lt/admin/js/ckeditor/filemanager/userfiles/ECAPD_2014_Abstract_Book.pdf

[3] M. Cuniot-Ponsard, I. Saraswati, S.-M. Ko, M. Halbwax, Y. H. Cho, and E. Dogheche (2014).
Electro-optic and converse piezoelectric coefficients of epitaxial thin films: GaN grown on Si, and (Sr,Ba)Nb2O6 (SBN) grown on Pt coated MgO, ***Poster in Conference on Lasers and Electro-Optics (CLEO 2014) San Jose, California, USA. 8-13 June 2014***.